Modelling of the Coupled Chemistry-Climate System:

Projections of Stratospheric Ozone in the 21st Century and Impact of Shipping on Atmospheric Composition and Climate

dem Fachbereich 1 Physik / Elektrotechnik der Universität Bremen
zur Habilitation in Umweltphysik vorgelegte wissenschaftliche Arbeit

(Department 1 Physics / Electrical Engineering of the University of Bremen
Habilitation in Environmental Physics)

Dr. rer. nat. Veronika Eyring

Deutsches Zentrum für Luft- und Raumfahrt
Institut für Physik der Atmosphäre
Oberpfaffenhofen, Germany

November 2007

Contents

Introduction

With the notable exception of carbon dioxide, the majority of human-produced radiatively active gases and aerosols are also chemically active in the atmosphere. An increase of greenhouse gas concentrations in the atmosphere leads to higher tropospheric temperatures and lower stratospheric temperatures, which affects the chemical composition of the atmosphere since many chemical reactions are temperature dependent. Changes of the temperature structure also modify the atmospheric circulation in the troposphere and stratosphere and therefore the transport of trace gases and particles. Therefore, a complete understanding of atmospheric composition changes requires the consideration of climate change and its feedback on chemistry. The focus of my research involves developing and using chemistry-climate models (CCMs), which consider the feedback of physical, dynamical, and chemical processes, in combination with atmospheric observations to understand better the key processes that determine chemistry-climate connections. My work evolves around two related areas.

The first area is stratospheric research, with the main goal to provide reliable projections of future changes in the stratosphere and their impacts on climate through a multi-model approach. To reach this goal, the Chemistry-Climate Model Validation (CCMVal) Activity for WCRP's SPARC[1] has been established. CCMVal helps coordinating and organizing CCM model efforts around the world. In this way, the CCM community can provide the maximum amount of useful scientific information for ozone and climate assessments. CCMVal is a response to the need for consistent evaluation of CCMs with detailed descriptions of the stratosphere. These CCMs provide valuable indications of how stratospheric ozone will evolve in the future as halogen concentrations decline in an atmosphere with a changing climate. The high complexity of CCMs requires a systematic process-oriented evaluation in order to demonstrate that the models are representative of the atmosphere and to quantify the uncertainty. A coherent framework for the evaluation of CCMs has been defined in [EY1]. In my role as CCMVal coordinator, I lead a multi-model intercomparison in support of the 2006 WMO/UNEP Scientific Assessment of Ozone Depletion. This study first assessed the capability of the participating CCMs to simulate key processes that determine stratospheric ozone [EY2], and second, it provided projections of the evolution of stratospheric ozone throughout the 21st century from the same CCMs [EY3]. This topic is discussed in Section 1.

My second research area is to study how gaseous and particulate emissions from international shipping contribute to radiative forcing[2] (RF), climate change and air quality degradation. As economic globalization continues, more goods move from factories throughout the world to major markets in other continents, generating increased domestic freight transport. Regulating transport emissions requires comprehensive knowledge of the present day fuel consumption and emissions, their potential future evolution, and mitigation options. To study the effects of ocean-going ships, the Helmholtz-University Young Investigators Group SeaKLIM[3] has been established. An entirely consistent set of emission inventories from 1950 to 2050 suitable as input for global chemistry models has been developed [EY4; EY5]. The impact of ship emissions on atmospheric composition, human health and climate is complex and has been assessed in a variety of studies using models on different scales combined with observations [EY6-12]. This topic is discussed in Section 2.

The work closes with a list of integrated references from the author, which are explicitly discussed in the manuscript [EY1-12] and a list of other cited publications.

---

[1] CCMVal Activity for WCRP's (World Climate Research Programme) SPARC (Stratospheric Processes and their Role in Climate project), see http://www.pa.op.dlr.de/CCMVal/.

[2] RF refers to the change in the earth-atmosphere energy balance since the pre-industrial period.
[3] Young Investigators Group SeaKLIM (Einfluss von Schiffsemissionen auf Atmosphäre und Klima) of the DLR-Institute of Atmospheric Physics (DLR-IPA) and the Institute of Environmental Physics of the University of Bremen (IUP).

1 Chemistry-Climate Modelling of the Stratosphere

1.1 Motivation

The stratospheric ozone layer has been depleted by anthropogenic emissions of halogenated species since the 1980s. Observations show that tropospheric halogen loading is now decreasing [*Montzka et al.*, 2003], which reflects the controls of ozone-depleting substances (ODSs) by the Montreal Protocol and its Amendments and Adjustments. Ozone is expected to continue to respond to these changes in ODSs but the timing and sensitivity of the response will depend on other changes in the atmosphere. Atmospheric concentrations of greenhouse gases (GHGs) have also increased and are expected to further increase in the future [*IPCC*, 2000] with consequences for the ozone layer. As a result of climate change, it is unlikely that the ozone layer will return to precisely its pre-1980 unperturbed state when the abundance of halogens returns to background levels. Furthermore, climate change complicates the attribution of ozone recovery to the decline of halogenated species.

For these reasons, considerable interest in the interaction between ozone recovery and climate change through the rest of this century exists. To predict the future evolution of stratospheric ozone and attribute its behaviour to the different forcings, models are required that can adequately represent both the chemistry of the ozone layer and the dynamics and energetics of the atmosphere, as well as their natural variability. Such models, known as coupled Chemistry-Climate Models (CCMs), are three-dimensional atmospheric circulation models with fully coupled chemistry, i.e. where chemical reactions drive changes in atmospheric composition which in turn change the atmospheric radiative balance and hence dynamics.

CCMs representing the stratospheric ozone layer are key tools for the detection, attribution and, especially, prediction of the response of stratospheric ozone to ozone-depleting substances and other factors (climate change, solar variability, volcanic erup-

tions, natural variability). In contrast to chemical transport models (CTMs), which specify the meteorological conditions, CCMs specify the chemical and dynamical forcings and predict the resulting change in the chemistry-climate system. They simulate a climate that bears a statistical relationship to the real atmosphere, and so a comparison of model results with measurements must be performed in a statistical manner. This is problematic, because it appears to take many decades of observations to define a robust stratospheric climatology, especially in the Arctic winter. While tropospheric climate models can be validated, in part, by their ability to reproduce the climate record over the 20th century, the paucity of stratospheric climate data prior to the satellite era (post-1979) limits such possibilities for model validation of stratospheric change.

Therefore, the evaluation of CCMs requires a process-oriented basis to complement the standard comparison of models with climatologies of observations. A schematic diagram showing the principal regions and processes in the stratosphere is displayed in Figure 1-1 and the key processes are briefly described in Box 1-1. By focusing on processes, models can be more directly compared with measurements. In this case, natural variability becomes an aid because it allows dependencies between model fields to be examined in a larger variable space and, thereby, make identifying cause and effect relationships within a model more reliable. The Chemistry-Climate Model Validation activity (CCMVal) for WCRP's SPARC is a response to the need for consistent evaluation of CCMs with detailed descriptions of the stratosphere. The goal of CCMVal is to improve understanding of CCMs and their underlying GCMs (General Circulation Models) through process-oriented evaluation, along with discussion and coordinated analysis of science results of the CCM community. Reducing the uncertainties in projections of the coupled chemistry-climate system by CCMs requires several important steps, which are detailed below.

In a first step, a coherent framework and benchmark for the process-oriented evaluation of CCMs has been developed [*EY1*]. This framework is described in Section 1.2.
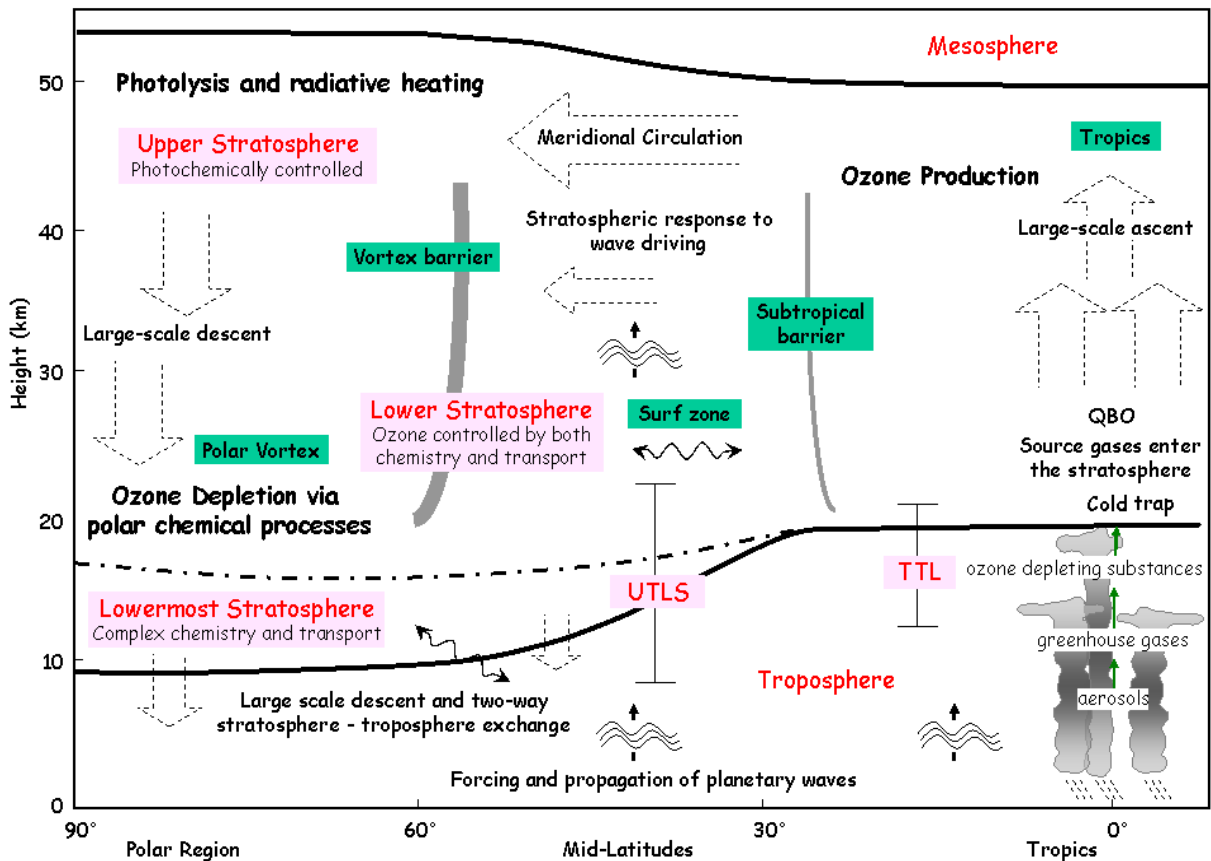
Figure 1-1. *Schematic diagram of the principal regions and processes in the winter hemispheric stratosphere.* Broad arrows denote diabatic circulation and wavy arrows denote transport along isentropic surfaces. The average position of the tropopause is shown by the lower thick black line, the average position of the stratopause by the upper thick black line, and the 380 K isentropic surface by the thick black dashed line. The vertical bars denote the range of the upper troposphere and lower stratosphere (UTLS) region and the tropical tropopause layer (TTL). The key processes are described in Box 1-1. From [*EY1*].

In a second step, a set of reference and sensitivity simulations has been defined [*EY2, EY3* and *Eyring et al.*, 2005]. The simulations were designed to answer the key question how well we can understand observed changes and to produce a best estimate of the future ozone-climate change in the 21st century. They are described in Section 1.3. Thirteen CCMs worldwide participated in the first CCMVal intercomparison and carried out the proposed simulations. Temperatures, trace species and ozone in the CCM simulations of the past from the current generation of these thirteen CCMs have been assessed in [*EY2*] and are described in Section 1.4. This assessment has guided the interpretation of the multi-model projections of stratospheric ozone in the 21st century from the same CCMs [*EY3*]. The projections are discussed in Section 1.5.

The results of the above mentioned work directly fed into the recent *WMO* [2007] report, in particular into Chapter 6 'The Ozone Layer in the 21st Century', and are summarised in Section 1.6. The next set of CCMVal model simulations in support of the next upcoming ozone and climate assessments and the planned SPARC CCMVal report on the evaluation of CCMs has already been defined [*Eyring et al.*, 2008a,b]. An outlook on this future work is given in Section 1.7.

1.2 Benchmark for Process-oriented Model Evaluation [EY1]

In the context of stratospheric GCMs (*i.e.*, models without chemistry), process-oriented validation represents the level II tasks within the GCM-Reality Intercomparison Project for SPARC (GRIPS) [*Pawson et al.*, 2000]. A first attempt at process-oriented validation of stratospheric CCMs is summarized in *Park et al.* [1999], *WMO* [2003], and *Austin et al.* [2003].

Box 1-1. *Key processes in the stratosphere.*

Stratospheric Transport

Transport in the stratosphere involves both meridional overturning (the residual circulation) and mixing, which together represent the Brewer-Dobson circulation. The most important aspects are the vertical (diabatic) mean motion and the horizontal mixing. Horizontal mixing is highly inhomogeneous, with transport barriers in the subtropics and at the edge of the wintertime polar vortex; mixing is most intense in the wintertime "surf zone", i.e. the region surrounding the polar vortex, and is comparatively weak in the summertime extratropics. Accurate representation of this structure in CCMs is important for the ozone distribution itself, as well as for the distribution of chemical families and species that affect ozone chemistry (NO_y, Cl_y, H_2O, CH_4). Within both the tropics and the polar vortex, the key physical quantities to represent are the degree of isolation and the diabatic ascent or descent, respectively. The impact of diabatic ascent or descent on the actual vertical motion of chemical species depends on the degree of isolation. Transport in the Upper Troposphere and Lower Stratosphere (UTLS) region is also complex. The extratropical tropopause 'break' is a barrier to quasi-horizontal mixing, causing significant contrasts in chemical species between the extratropical lowermost stratosphere and the tropical upper troposphere. The degree of isolation can be assessed by the sharpness of horizontal or isentropic gradients at the tropopause (because tropopause height changes with latitude), and with chemical correlations (e.g., O_3 vs. CO). The Tropical Tropopause Layer (TTL) is marked by changes in the vertical stability and in chemical species beginning below the tropical tropopause. Processes in this layer are important for setting chemical boundary conditions for the stratosphere. In addition, convective processes and microphysics affect water vapor and the chemistry of ozone and other minor species. These radiatively active gases can have large impacts on the climate of the UTLS.
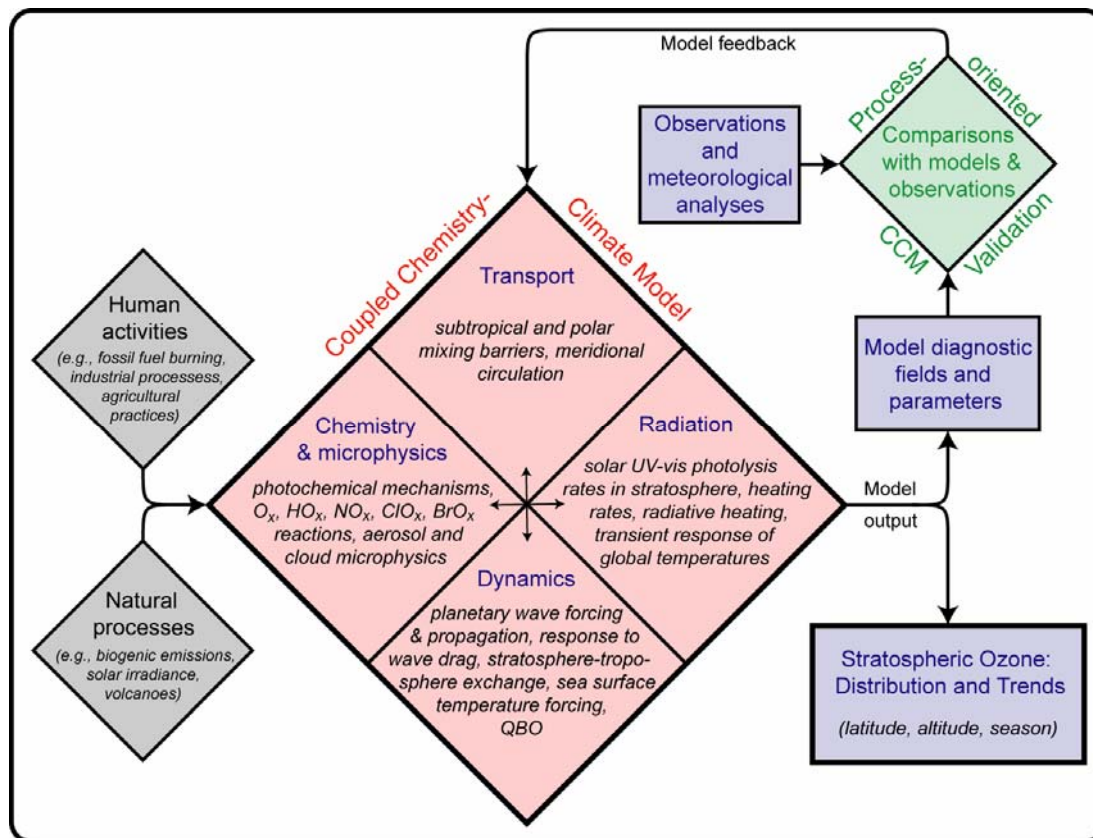
Dynamics

The basic dynamical state of the stratosphere within which transport takes place is determined by a number of physical processes. These include: the forcing mechanisms and propagation of planetary-scale Rossby and gravity waves, wave-mean-flow interaction, and the diabatic circulation. The Quasi-Biennial Oscillation (QBO) is an internal mode of variability of the atmosphere that dominates the inter-annual variability in wind in the tropical stratosphere and contributes to the variability in the extratropical dynamics. It is recognized that the QBO is important for understanding interannual variability in ozone and other constituents of the middle atmosphere, in the tropics and extratropics. Correct reproduction of the climatological mean state of the stratosphere by CCMs, including inter-hemispheric differences, inter-annual and intra-seasonal variability, is important but not sufficient: the basic dynamical mechanisms must be well represented in the underlying GCMs on which the CCMs are based if future changes are to be modeled credibly.

Radiation

Radiative calculations are used in CCMs to derive photolysis rates and heating rates. Photolysis rates in the stratosphere control the abundance of many chemical constituents that in turn control chemically active constituents, such as ozone. At the same time these trace gases feedback on temperature and, thus, circulation through the radiative heating rates. At present, most models calculate radiative heating rates and photolysis rates in an inconsistent manner. For example, the spherical geometry of the Earth might be included in the photolysis rate calculation, but not in the heating rate calculation. Also different radiation schemes are usually employed for the two calculations. Such inconsistencies should be avoided. There are currently not enough high quality measurements that can be used to validate the important radiative processes in global models. Presently, the best radiative models (currently not included in CCMs) provide an important complement to available measurements for CCM validation. Accordingly the approach taken here (unlike the other three categories) is to perform detailed model comparisons between the best radiative models and the radiation modules actually used in CCMs. The photolysis and radiative heating rate calculations are evaluated separately.

Stratospheric Chemistry and Microphysics

One of the ways in which chemistry and dynamics are coupled is the temperature dependence of many chemical reaction rates. The importance of local control of ozone by chemistry relative to transport varies substantially between various times and places. In the upper stratosphere transport plays a role by controlling the concentrations of long-lived tracers such as inorganic chlorine, but photochemical timescales are so short that transport has a minimal direct impact on ozone. However, in the lower stratosphere, the photochemical timescales are rather longer (typically of the order of months) and interactions with dynamics are complex and more challenging to model accurately. Aerosols have an important role on chemistry in the lower stratosphere, since reactions can take place within or on the particles. Consequently, even though the photochemical lifetime of ozone is typically many months in the lower stratosphere, rapid chemical loss of ozone occurs in the Antarctic lower stratosphere, following exposure of air to polar stratospheric clouds.

Figure 1-2. *Schematic diagram of the CCMVal approach to CCM evaluation.* The centrepiece is a CCM comprised of four basic ingredients: transport, dynamics, radiation, and stratospheric chemistry & microphysics. The four ingredients are fundamentally interdependent and interactive and require as inputs, knowledge of human activities and natural processes. The CCM output includes a wide array of parameters and diagnostics associated with the four different aspects. The distribution of stratospheric ozone is highlighted separately here because of the strong contemporary interest in halogen-based ozone depletion and the recovery of the ozone loss that has developed over recent decades. The comparisons of model diagnostics and other outputs with atmospheric observations and meteorological analyses are the key to process-oriented CCM validation. Finally, the results of the comparisons can be used to provide feedback to the representation of processes in CCMs in order to improve subsequent CCM validation comparisons. In this way, the uncertainties in future trends in stratospheric ozone and other key model outputs can be reduced. The key processes are described in Box 1-1. From [*EY1*].

A strategy for a more long-term comprehensive approach to CCM validation was developed at workshops on process-oriented validation of CCMs held in Grainau, Germany in November 2003 [*Eyring et al.*, 2004] and in Boulder, USA in October 2005 [*Eyring et al.*, 2006]. Members of the CCM and CTM communities have met with members of the measurement and data analysis communities to develop ideas on this issue. The role of the latter communities was crucial in order to understand both the opportunities and the limitations presented by the available data. The size of the task involved with a complete validation exercise quickly became apparent and so the approach taken was to develop a range of diagnostics which can be worked through as time and interest allow.

Although the focus was on defining a methodology for the evaluation of CCMs, it was recognized that observational uncertainties are a potentially important component of CCM evaluation. Observational uncertainties can influence the outcome of model-data consistency tests [e.g., *Santer et al.*, 2003a,b], and should be explicitly accounted for in any CCM evaluation strategy. A set of key processes has been defined and each process is associated with one or more model diagnostics and with relevant datasets that can be used for validation [*EY1*; see also Figure 1-2]. The key processes are structured around four major topics (transport, dynamics, radiation, and stratospheric chemistry & microphysics), see also Box 1-1.

Confidence in the performance of CCMs will increase as more model attributes become validated against the whole suite of diagnostics. Further, new models can be evaluated against an acknowledged, benchmark set of diagnostics as the models are developed. At the same time, the diagnostics themselves should develop as experience is gained and as new measurements become available allowing more processes to be diagnosed.

1.3 Definition of a common set of model simulations and forcings [EY2; EY3]

Limitations and deficiencies in models can be revealed through inter-model comparisons and through comparisons with observations. An intercomparison and assessment of CCMs was performed by *Austin et al.* [2003]. Since then a number of new CCMs with a focus on the middle atmosphere have been developed, and changes have also been made to the CCMs considered by *Austin et al.* [2003]. Some of the new and updated CCMs have been tested and compared to observations [*Austin et al.*, 2006; *Dameris et al.*, 2005; *Egorova et al.*, 2005; *Garcia et al.*, 2007; *Steinbrecht et al.*, 2006a,b; *Struthers et al.*, 2004; *Tian and Chipperfield*, 2005], but there was a need for a new multi-model assessment, in particular an assessment of simulations with a common focus and experimental set-up.

The proposed CCMVal reference and sensitivity simulations [*EY2*; *EY3; Eyring et al.*, 2005] were developed to address the following key question outlined by the Steering Committee of *WMO* [2007] to be of significance to the 2006 assessment: (1) How well do we understand the observed changes in stratospheric ozone (polar and extra-polar) over the past few decades during which stratospheric climate and constituents (including halogens, nitrogen oxides, water, and methane) were changing? (2) What does our best understanding of the climate and halogens, as well as the changing stratospheric composition, portend for the future?

In order to address these questions, two reference simulations (REF) and two sensitivity simulations (SCN) have been proposed. The forcings in these simulations are defined by natural and anthropogenic emissions based on existing scenarios, on atmospheric observations, and on the Kyoto and Montreal Protocols and Amendments. A summary of the CCMVal simulations is given in Table 2 of *Eyring et al.* [2005] and the simulations are briefly described in Box 1-2.

CCM groups were encouraged to run the proposed simulations with the same forcings. In order to facilitate the set-up of the reference simulations, a website has been established at DLR, where the forcings for the simulations can be downloaded (http://www.pa.op.dlr.de/CCMVal/Forcings/ CCMVal_Forcings.html). This web site was developed to serve the needs of the CCM community, and encourage consistency of anthropogenic and natural forcings in future model/model and model/observation intercomparisons. A set of standard diagnostics has been defined in addition and the output from the simulations has been collected in a common data format at the British Atmospheric Data Centre (BADC). This output has been analysed in [*EY2*; *EY3*], and is further investigated in several follow-up studies (see http://www.pa.op.dlr.de/CCMVal/List_CCM ValCollaborators.html).

1.4 Assessment of chemistry-climate model simulations of the recent past [EY2]

Thirteen CCMs have participated in the first CCMVal model intercomparison (AMTRAC, CCSRNIES, CMAM, E39C, GEOSCCM, LMDZrepro, MAECHAM4CHEM, MRI, SOCOL, ULAQ, UMETRAC, UMSLIMCAT, and WACCM (v.3)). Their main features are summarized in Table 1 of [*EY2*] and detailed descriptions of the CCMs are given in the cited literature. The CCMs examined have performed simulations of the past evolution of the stratosphere and have been used to predict the future evolution of stratospheric ozone in the 21st century in a follow up study [*EY3*, see Section 1.5] and in support of the 2006 WMO/UNEP Scientific Assessment of Ozone Depletion [*WMO*, 2007]. The primary objective of the [*EY2*] study was to evaluate the capabilities of the

Box 1-2. *CCMVal reference and sensitivity simulations in support of WMO [2007]*

REF1 is defined as a transient simulation from 1980 to the present to reproduce the well-observed period of the last 25 years during which ozone depletion is well recorded, and allows a more detailed investigation of the role of natural variability and other atmospheric changes important for ozone balance and trends. This transient simulation includes all anthropogenic and natural forcings based on changes in trace gases, solar variability, volcanic eruptions, quasi-biennial oscillation (QBO), and sea surface temperatures (SSTs). SSTs in this run are based on observations. Depending on computer resources some model groups might be able to start earlier and reporting results for REF1 between 1960 and 2004 is recommended to examine model variability. Forcings for the simulation are defined for the time period 1950 to 2004.

REF2 is defined as a transient run from 1980 to 2025 and is an internally consistent simulation from the past into the future. The proposed transient simulation uses the IPCC SRES scenario A1B(medium) [*IPCC*, 2000]. Changes in halogens are prescribed following the Ab scenario (*WMO* [2003], Table 4B-2). External natural forcings such as solar variability and volcanic eruptions are not considered, as they cannot be known in advance, and the QBO is not externally forced (also as it cannot be known in advance; furthermore it represents the internal dynamics of the model). To avoid introducing inhomogeneity into the time series, these natural forcings are not applied in the past either. SSTs in this run are based on coupled atmosphere-ocean model-derived SSTs. Depending on computer resources some model groups might be able to run longer and/or start earlier. It is recommended to report results for REF2 until at least 2050. The forcings are defined through 2100.

SCN1 (REF1 with enhanced Br$_y$): An additional simulation is being developed to represent the known lower stratospheric deficit in modelled inorganic bromine abundance. This simulation will be identical to REF1, with the exception of including source gases abundances that will increase the stratospheric burden of Br$_y$.

SCN2 (REF2 with natural forcings): A sensitivity simulation has been defined similar to REF1, with the inclusion of solar variability, volcanic activity, and the QBO in the past. Future forcings include a repeating solar cycle and QBO, under volcanically clean aerosol conditions. SSTs are based on REF2. Greenhouse gases and halogens will be the same as in REF2.

CCMs to simulate processes and fields that play an important role in determining the ozone distribution. Such an evaluation provides guidance for the interpretation of predictions of future ozone evolution made by the same CCMs.

To evaluate the CCM results the simulated distributions of temperature, ozone, and other trace gases have been compared with those derived from meteorological analyses and trace gas observations. The focus of the [*EY2*] study was on quantities that are important for the simulation of ozone distribution and that can be validated against observations. This includes temperature, water vapour, hydrogen chloride (a principal reservoir of inorganic chlorine), and observationally-based transport diagnostics. Both, the climatological mean distributions as well as decadal-scale variations and trends during the 1960 to 2004 period were examined.

The study of [*EY2*] extends both the *Austin et al.* [2003] assessment of CCMs and the *Pawson et al.* [2000] assessment of middle atmospheric GCMs. First, a larger number of CCMs was considered. Second, in contrast to these previous studies, the CCM simulations defined as part of CCMVal (*Eyring et al.* [2005], see also Section 1.3) and used in this study were all transient simulations and had almost identical forcings (e.g., sea surface temperatures (SSTs), long-lived GHGs, and halocarbons). This eliminates many of the uncertainties in the conclusions of the earlier assessments that resulted from the differences in experimental set-up of individual models. Finally, and perhaps most importantly, the [*EY2*] study was the first multi-CCM assessment to evaluate transport and distributions of important trace gases. This includes an evaluation of the simulations of inorganic chlorine, which is of particular importance for simulations of the evolution of ozone and ozone recovery. A detailed assessment of temperature, trace species and ozone in chemistry-climate model simulations of the recent past is given in [*EY2*], and a short summary is presented here.
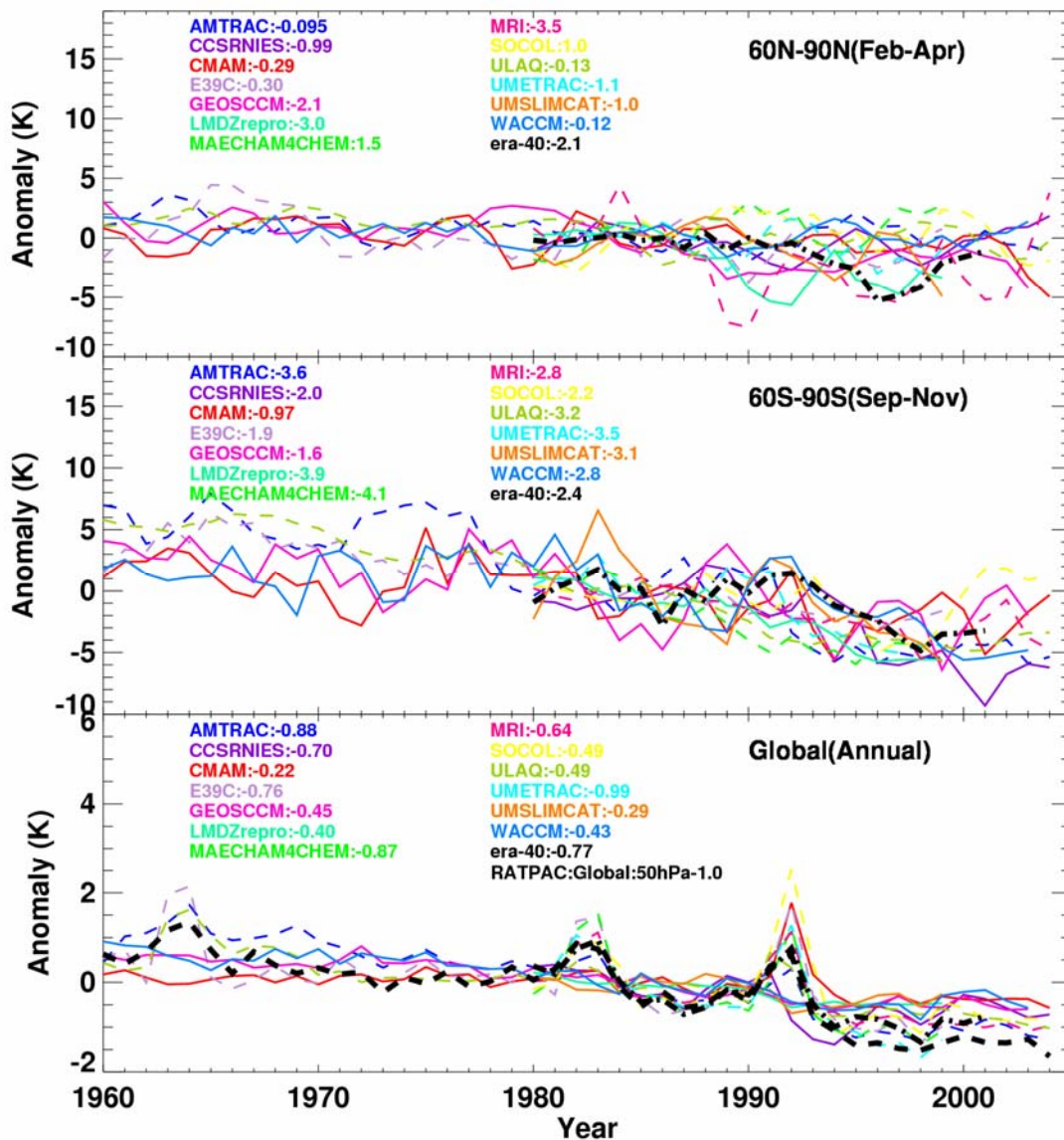
Figure 1-3. Modeled and observed time series of monthly-mean temperature anomalies at 50 hPa from the CCMs, ERA-40 re-analyses and the Radiosonde Atmospheric Temperature Products for Assessing Climate (RATPAC) climatology. The temperature anomalies are calculated with respect to a mean reference period between 1980 and 1989 using three-month averages for February to April in the polar northern hemisphere (60°-90°N, upper panel), September to November in the polar southern hemisphere (60°-90°S, middle panel) and annual averages for the global anomalies (lower panel). For the polar plots a three year smoothing window has been applied. AMTRAC, E39C, MAECHAM4CHEM, MRI, SOCOL, ULAQ and UMETRAC are shown with dashed lines, all others CCMs with solid lines. A linear temperature trend in K/decade is calculated for each model using data between 1980 and 1999. The temperature trend is given next to the name of each participating model. From [*EY2*].

1.4.1 Stratospheric Temperatures

Because of the temperature dependence of many of the chemical reactions determining the ozone distribution it is important to accurately model stratospheric temperatures. A measure of the accuracy of the underlying radiative heating in the models is given by the simulated global annual-mean temperatures. The thirteen CCMs considered in [*EY2*] reproduce the vertical profile of global

annual-mean temperature in the stratosphere fairly accurately. Overall a significant improvement on the persistent stratospheric problem of negative global, annual mean temperature biases found in most of the middle atmosphere GCMs evaluated by *Pawson et al.* [2000, Figure 1] could be reported.

The CCMs examined in [*EY2*] are able to reproduce the observed long-term global-mean lower stratospheric temperature trend resulting from GHG increases and strato-

spheric ozone depletion over the last two decades (Figure 1-3). All CCMs, except MRI (see discussion in Section 1.4.3), reproduce the stronger cooling trend in the Southern Hemisphere high latitudes compared to the North, which is expected due to the larger southern hemisphere polar ozone loss in spring. This gives us some confidence that the temperature feedback from changes in GHGs, and the ozone radiative-dynamical feedback, are well captured in the CCMs and suggests that CCMs are suitable tools for projecting stratospheric temperatures under a given GHG and halogen emission scenario, which is a prerequisite for predicting ozone.

Most models reproduce the observed phase of the annual cycle of equatorial temperatures at 100 hPa, but there are variations in the amplitude and, more importantly, the an-

nual mean value, which causes a large spread in the water vapour distributions in the CCMs.

1.4.2 Stratospheric Transport Characteristics

Transport in the stratosphere involves both meridional overturning (the residual circulation) and mixing. Horizontal mixing is highly inhomogeneous, with transport barriers in the subtropics and at the edge of the wintertime polar vortices [e.g. *Sankey and Shepherd*, 2003]. Possible errors in transport characteristics have important impacts on the distribution of chemical families and individual species that affect ozone chemistry (NO_y, Cl_y, H_2O, and CH_4) and consequently the ozone distribution itself. Useful information on transport characteristics can be
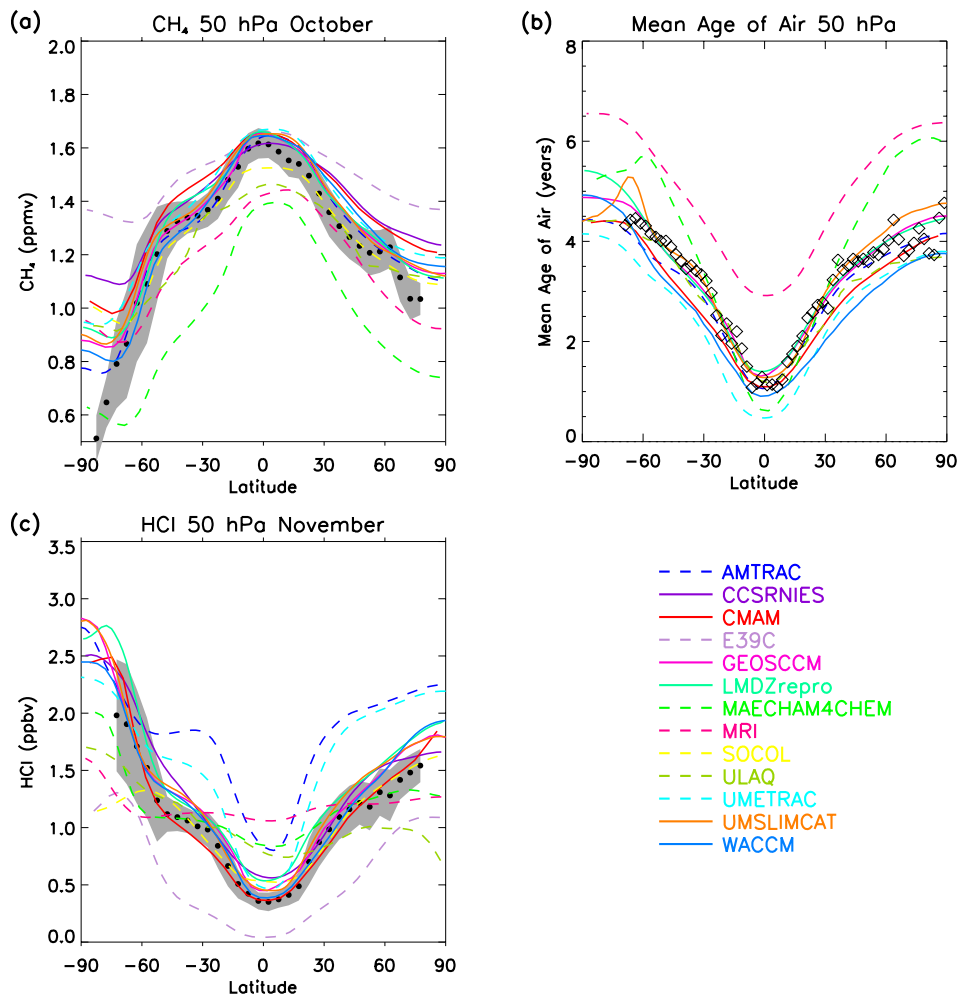
Figure 1-4. Comparison of climatological zonal-mean (a) methane in October, (b) annual mean of the mea age of air, and (c) HCl in November, at 50 hPa from CCMs and observations. Observations in (a) and (c) are from the Halogen Occultation Experiment (HALOE): Black dots are values averaged in latitudes (zonal means) and the grey area shows plus and minus 1 standard deviation about the climatological zonal mean HALOE. Observations in (b) are based on ER-2 aircraft measurements of CO_2 from many different years and months [*Andrews et al.*, 2001]. From *WMO* [2007], adapted from [*EY2*].
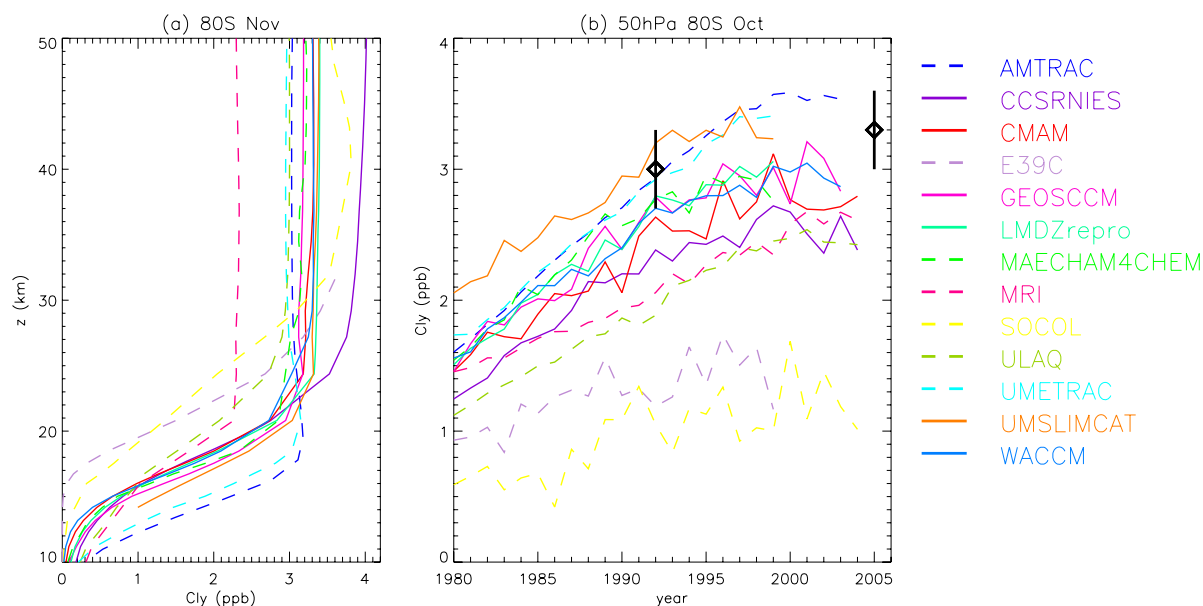
Figure 1-5. (a) Climatological mean vertical profiles (1990 to 1999) at 80°S in November for Cl_y in ppb. (b) Time series of October mean Antarctic Cl_y at 80°S from CCM model simulations. Estimates of Cl_y from the Halogen Occultation Experiment (HALOE) HCl measurements in 1992 [*Douglass et al.*, 1995; *Santee et al.*, 1996] and Aura MLS HCl in 2005 [*M. Santee*, pers. communication] are shown in addition. From [*EY2*].

obtained from examining the distribution of long-lived tracers, such as methane and nitrous oxide. Also, information on the tropical ascent, vertical diffusion and tropical-extratropical mixing can be obtained from the vertical propagation of the annual cycle in water vapour (the so-called "tape recorder", *Mote et al.* [1996]), while the mean age of air provides information on integrated transport within the stratosphere. The mean age of air is defined as the mean time that a stratospheric air mass has been out of contact with the well-mixed troposphere. This diagnostic can be inferred from observations of conserved tracers with an approximately linear increase in concentration with time (e.g., CO_2, SF_6, total chlorine), and has been used in previous model-data comparisons [e.g., *Hall et al.*, 1999; *Park et al.*, 1999].

There is in general a large spread in the simulated tracer fields among the models examined in [*EY2*], indicating large variations in model transport. However, for each diagnostic a large fraction of the spread is due to a subset of models (E39C, MAECHAM4CHEM, MRI, SOCOL, and ULAQ) where large deviations from observations are apparent in several of the transport diagnostics. This is illustrated for methane and mean age of air at 50 hPa in Figure

1-4(a) and (b), where the above models are shown as dashed curves. The cause of significant biases in the tracer fields in these models is generally not known, but in some cases it can be attributed to specific model features, e.g., very low horizontal resolution (ULAQ) or a low upper boundary (E39C). For the remaining CCMs there is a much smaller spread for all tracers and the tracer fields are in general in good agreement with observations. Previous model-data comparisons have identified serious model deficiencies in simulating the mean age of air and propagation of the water vapour tape recorder signal [*Hall et al.*, 1999], but better agreement is found for many of the CCMs examined here.

1.4.3 Hydrogen Chloride (HCl) and Inorganic Chlorine (Cl_y)

The ability of CCMs to reproduce past stratospheric chlorine and bromine concentrations clearly affects the confidence that we can place in their projections of future ozone changes, particularly in the Antarctic.

There are substantial quantitative differences and large deviations from observations in the simulated HCl and Cl_y fields, see Figure 1-4(c) and Figure 1-5(b). The differences are most pronounced in the polar lower strato-
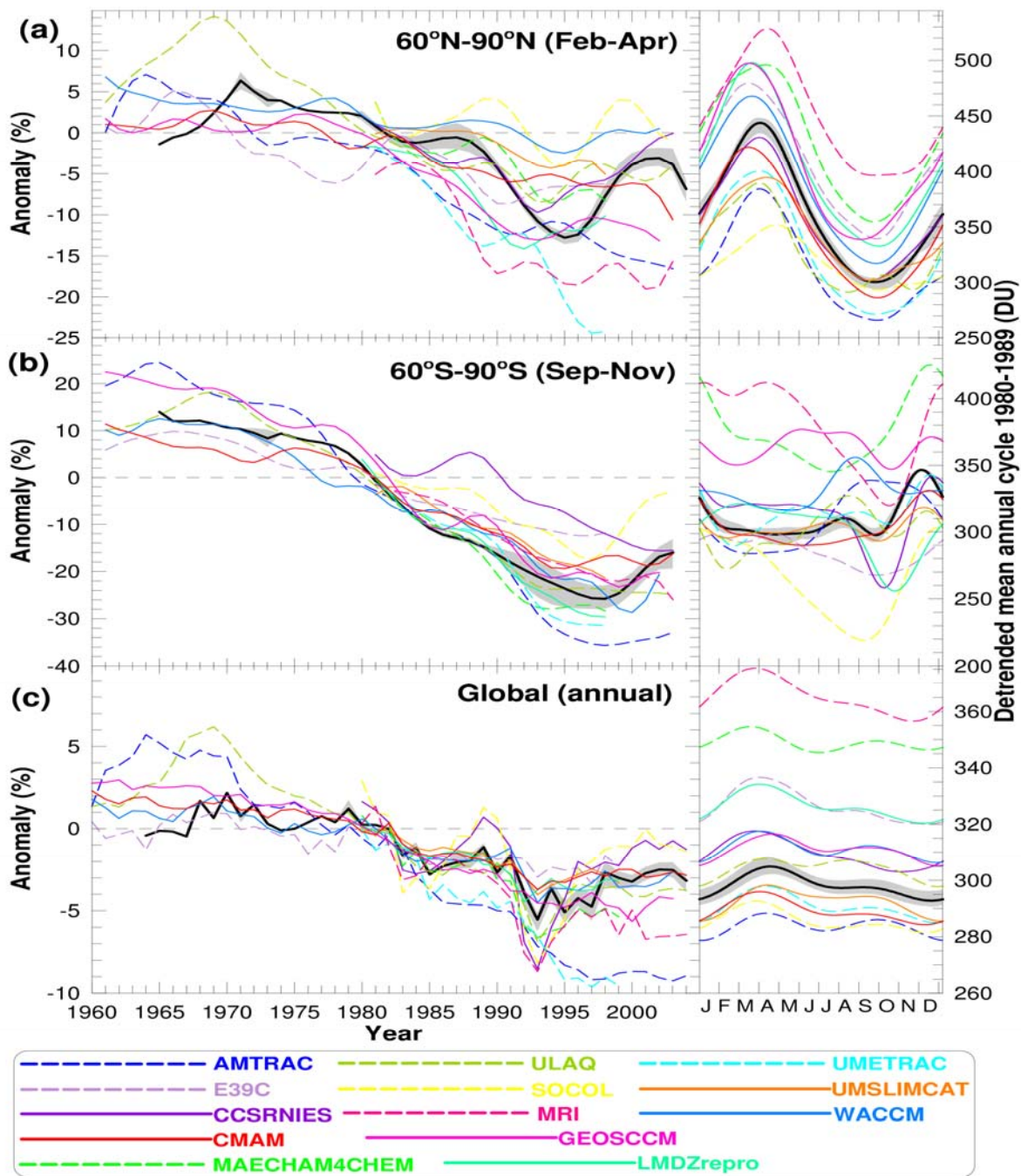
Figure 1-6. *Total column ozone trends in the past and detrended mean annual cycles as simulated by 13 CCMs.* **Left panels:** (a) seasonal (February to April) total column ozone anomalies for the Arctic (60°N-90°N), (b) seasonal (September to November) total column ozone anomalies for the Antarctic (90°S-60°S), and (c) annual total column ozone anomalies sets for the whole globe (90°S-90°N) from CCMs and four observational data sets. The CCM results are shown with colored lines while the mean and range of the four observational data sets are shown as a thick black line and grey shaded area respectively. The anomalies are calculated with the method described in Appendix A of [*EY2*]. The seasonal anomaly time series shown in panel (a) and (b) have been smoothed by applying a 1:2:1 filter iteratively five times. The filter width is reduced to one at the ends of the time series. The annual global anomalies shown in panel (c) are unsmoothed. **Right panels:** detrended mean annual cycles for each model (1980 to 2003) and the mean and range of the observations. From [*EY2*].

sphere where peak Cl_y varies from around 1 ppb to over 3.5 ppb. Measurements of Cl_y in the Antarctic lower stratosphere (symbols in Figure 1-5(b)) clearly show that peak values of Cl_y close to or less than 2.5 ppb, as simulated by several CCMs, are unrealistic.

Transport deficiencies are a major contributor to deficiencies in the simulated HCl and Cl_y, and the models discussed above that did not perform well for transport diagnostics also showed differences from observed HCl and Cl_y.

In MRI the age of air decreases significantly with time and, unlike in all other models and observations, Cl_y does not peak around 2000 but continues to increase until after 2015. The very slow Cl_y increase in MRI comes from the combined effect of the diffusive nature of the transport scheme and a weak Brewer-Dobson circulation. The continued increase of Cl_y and Cl_{tot} is unrealistic, as observations show upper stratospheric Cl_{tot} has peaked and is currently decreasing [*Anderson* et al., 2000; *Waugh et al.*, 2001; *Froidevaux et al.*, 2006]. This unrealistic continued increase of Cl_y lowers the confidence that can be placed in the long-term ozone projections given by the MRI simulation.

In the polar southern hemisphere lower stratosphere most CCMs underestimate peak Cl_y, but two models simulate values that are much too low (SOCOL and E39C). A likely cause of these differences is transport and, consistent with this, the CCMs that have problems simulating the CH_4 distribution also generally have problems simulating Cl_y and HCl. However, transport differences cannot explain all the model-model differences, and other factors play a role in determining the model-model differences in Cl_y. For example, higher than observed Cl_y in the extra-polar lower stratosphere in AMTRAC and UMETRAC results from photolysis rates of organic chlorine species being artificially increased by about 25% so that the Cl_y in the upper stratosphere is in close agreement with observed Cl_y.

1.4.4 Ozone

Differences between observations and some of the models as outlined in the previous sections affect the capability of the models to simulate realistic ozone distributions. Temperature biases affect the temperature dependent chemical reaction rates globally and lead to significant differences in simulated PSCs in polar regions [*Austin et al.*, 2003].

Deficiencies in transport lead to errors in ozone transport as well as in transport of the chemical species that react with ozone. The ability of CCMs to reproduce past stratospheric chlorine concentration is important to track observed ozone evolution globally, but is of particular importance in the Antarctic.

Overall, the CCMs are generally able to reproduce the observed amplitude and phasing of the mean annual cycle in total column ozone in different latitude bands, except in southern high latitudes (see Figure 1-6). However, most models exhibit large annual-mean biases, with the majority overestimating total ozone (most severe in MAECHAM4CHEM). Related to this, the simulated ozone hole is too small in terms of both the maximum Antarctic ozone hole area between September and October defined by the 220 DU contour, and the ozone mass deficit calculated as the mean of daily values between September and October based on a 220 DU threshold.

Most CCMs show reasonable agreement with observed total ozone trends and variability on a global scale, but a greater spread in the ozone trends in polar regions in spring, especially in the Arctic (Figure 1-6). Although it is not possible to trace all these differences in the simulated ozone fields to deficiencies in the simulated temperature and tracers, in some cases a link can be made. For example, the models with low climatological mean extra-polar methane values have high ozone there (MAECHAM4CHEM, MRI, and SOCOL), and the model with the largest cold bias in the Antarctic lower stratosphere in spring (LMDZrepro) simulates very low ozone. In the Antarctic, the models with the largest (AMTRAC and UMETRAC) and smallest (SOCOL and E39C) Cl_y trends exhibit respectively too-strong and too-weak ozone trends.

1.5 Multi-model projections of stratospheric ozone in the 21st century [EY3]

Projections of ozone recovery in the 21st century from the current generation of CCMs have been examined in [*EY3*]. This

study extends the previous multi-model as-
sessment [*Austin et al.*, 2003] by comparing
only transient simulations with nearly identi-
cal forcings from a larger number of CCMs.
The future simulations of the eleven partici-
pating CCMs follow the IPCC (In-
tergovernmental Panel on Climate Change)

SRES (Special Report on Emission Scenar-
ios) greenhouse gas (GHG) scenario A1B
[*IPCC*, 2000] and the surface halogens are
prescribed according to the Ab scenario of
WMO [2003]. Only a small number of the
CCMs performed ensembles of simulations,
and only one of those used different SSTs
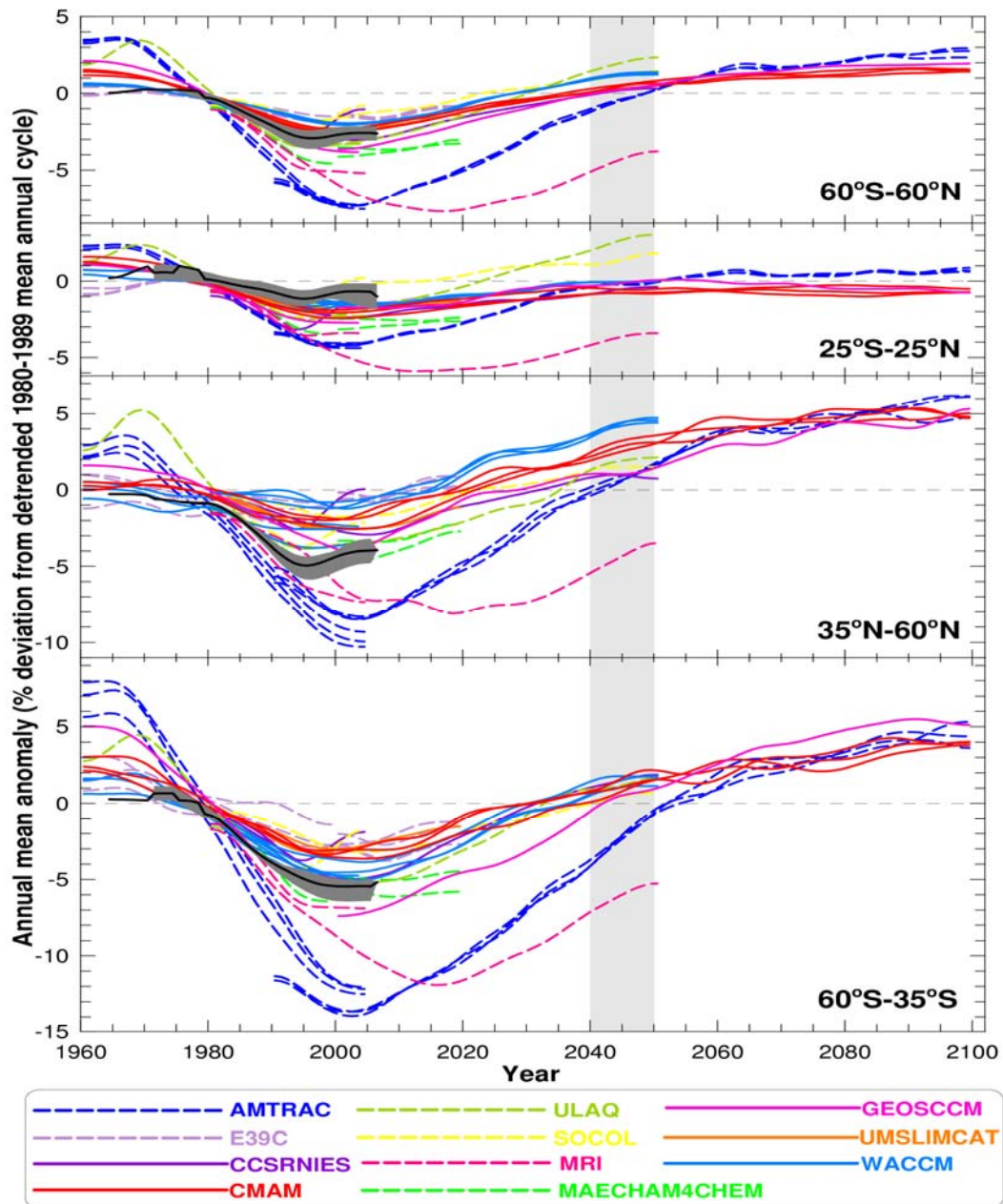
Figure 1-7. Annual mean zonal mean total column ozone anomalies from CCMs (colored lines) and
from four observational data sets (thick black line and grey shaded area show the mean and range of
observed anomalies). The four observational data sets are taken from ground-based measurements
(updated from *Fioletov et al.* [2002]), merged satellite data [*Stolarski and Frith*, 2006], the National Insti-
tute of Water and Atmospheric Research (NIWA) assimilated data base [*Bodeker et al.*, 2005] and from
Solar Backscatter Ultraviolet (SBUV, SBUV/2) retrievals (updated from *Miller et al.* [2002]). Area
weighted zonal mean time series are shown for the extra-polar region (60°S to 60°N), the equatorial re-
gion (25°S to 25°N), the northern mid-latitude region (35°N to 60°N), and the southern mid-latitude re-
gion (60°S to 35°S). The light grey shading between 2040 and 2050 shows the period when strato-
spheric concentrations of halogens are expected to return to their 1980 values. Monthly anomalies were
calculated by subtracting a detrended mean annual cycle, calculated over the period 1980-1989, from
each time series. The annual cycle was detrended as in [*EY2*]. From [*EY3*].

from different realizations of the same coupled GCM. However, the ensemble spreads were generally much smaller than the inter-model differences.

Before the projected ozone evolution from the CCMs were examined, the simulated changes in quantities that influence ozone recovery have been investigated, with a focus on the simulated stratospheric halogens, temperature, water vapour, and NO_y. The CCMs show large differences in peak Cl_y and timing of when future values have returned to modelled 1980 values, which is a major cause of the differences in simulated ozone recovery, in particular in the Antarctic. In contrast, the model-to-model agreement in projected temperature trends is good, and all CCMs predict continued, global-mean cooling of the stratosphere over the next five decades, increasing from around 0.25 K/decade at 50 hPa to values of around 1 K/decade at 1 hPa. The magnitude of simulated changes in stratospheric water vapour and total reactive nitrogen (NO_y) suggests that they play only a minor role in simulated ozone recovery in the CCMs.

While the CCMs project similar long-term (1960-2100) evolution in ozone, there is a wide spread in the magnitude of past decreases in ozone and in future rates of ozone increases (Figure 1-7 and 1-8). However, there is sufficient agreement among the CCMs on the underlying causes of the ozone changes that general conclusions can be drawn and some confidence can be placed in their projections. In general, the future evolution of stratospheric ozone in the CCMs is mainly determined by decreases in halogen amounts and continued cooling of the global stratosphere due to increases in GHGs.

1.5.5   Mid-latitudes and Global

All CCMs project extra-polar (60°S to 60°N) total column ozone to increase between 2000 and 2020, with most of the increase of 1% to 2.5% occurring after 2010 (Figure 1-7). Over mid-latitudes, the majority of the CCMs predict an increase of 1.5% to 3.5% between 2000 and 2020. As a result of ozone increases in the middle and upper stratosphere due to GHG induced cooling, mid-latitude, extra-polar, and global total ozone is pro-

jected to increase to 1980 values before lower stratospheric halogen amounts decrease to 1980 values. Most CCMs predict northern mid-latitude ozone returning to 1980 values before southern mid-latitude ozone. After 2050 the ozone changes primarily reflect changes in GHGs and by 2100, ozone is projected to be above 1980 values.

Simulated past ozone column changes over the tropics (25°S-25°N) are small compared to other regions but slightly overestimated compared to observations that show essentially no changes in this region over the period 1980-2004. Between 2000 and 2020 total column ozone increases of less than 2% are projected. The majority of the CCMs predict ozone columns that are similar or lower than 1980 values between 2040 and 2050 as a result of small decreases in tropical lower stratospheric ozone. The negative trends in this region are likely related to increases in tropical upwelling. Another possible factor might be that increasing ozone in the upper stratosphere reduces the penetration of UV to the lower stratosphere reducing ozone production there (a reverse of the 'self-healing' effect). Two out of three CCMs that were run to 2100 predict that tropical ozone is still below 1980 values by 2100.

1.5.6   Spring-time Polar Ozone

Maximum spring-time ozone losses over the Antarctic (60°-90°S) occur between 2000 and 2010, and total column ozone is projected to increase by 5% to 10% between 2000 and 2020 because of decreases of stratospheric halogen concentrations (Figure 1-8). In the polar lower stratosphere in midwinter the CCMs simulate only small cooling trends in the first and second half of the 21st century, and large increases of the Antarctic ozone hole due to increased heterogeneous chemical ozone loss as a result of GHG induced cooling in the lower stratosphere are not projected. Column ozone returns to 1980 values later than in midlatitudes due to the delay associated with transport of stratospheric air to polar regions. In most CCMs that time is around 2050, but as most models underestimate peak Cl_y near 2000, ozone recovery may occur even later, between 2060 and 2070.
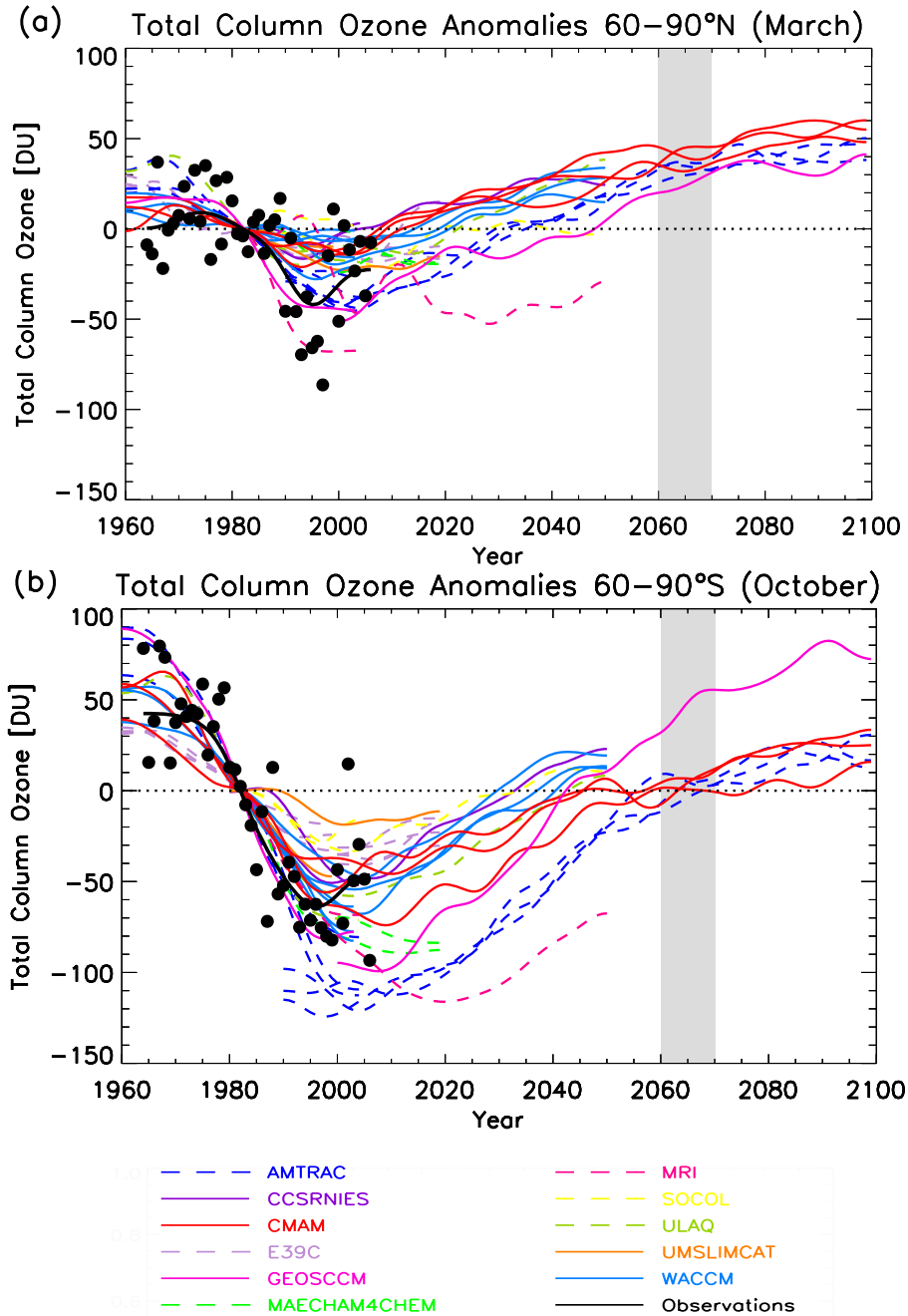
Figure 1-8: **(a)** March Arctic (60°N to 90°N) total column ozone anomalies from CCMs (coloured lines) and the mean from four observational data sets (thick black line for smoothed curve and black dots for individual years). **(b)** as for (a) but October Antarctic (90°S to 60°S) total column ozone anomalies. The anomalies have been calculated by subtracting the 1980-1984 mean from the smoothed time series. The light grey shading between 2060 and 2070 shows the period when stratospheric concentrations of halogens in the polar lower stratosphere are expected to return to their 1980 values. From [EY3].

Arctic (60°-90°N) spring-time ozone is projected to increase by 0% to 10% between 2000 and 2020. While the large interannual variability in projected Arctic ozone obscures the date when the ozone turnaround due to decreasing halogens occurs, this is projected to occur before 2020. Increase in ozone does not follow halogen decreases as closely as in the Antarctic, reaching 1980 values before Arctic halogen amounts decrease to 1980 values and before the Antarctic. There is no indication of future large decreases in the Arctic column ozone in any of the models simulations and simulated temperature trends in the Arctic lower stratosphere in the 21st century are small. By 2100, Arctic ozone is projected to be substantially above 1980 values.

1.6 Summary

The CCM assessment shown in [*EY2*] provides insight into the ability of the different CCMs to model key processes and the observed state of the stratosphere. This in turn provides guidance on how to interpret CCM predictions of the future atmosphere. The CCMs vary in their skill in representing different processes and characteristics of the atmosphere. The importance placed on the models ability to represent a particular process or characteristic depend, to some degree, on the objective of a model prediction. For predicting the recovery of ozone due to declining concentrations of ozone depleting substances, a realistic simulation of the evolution of chlorine (and bromine) in the stratosphere is important. Thus, the evaluation of the abilities of CCMs to simulate stratospheric inorganic chlorine is valuable for interpreting their predictions of ozone recovery. Furthermore, as temperatures and ozone are closely coupled, the temperature biases in the southern lower stratosphere in spring and associated late break up of the vortex in many of the models will need to be considered when interpreting the CCM future predictions of polar ozone evolution. The evaluation of the CCMs in [*EY2*] has been guided by the CCMVal evaluation table of [*EY1*].

In a follow up study, the simulations from the same CCMs have been used to project the evolution of stratospheric ozone throughout the 21st century, employing nearly identical forcings [*EY3*]. The model-to-model agreement in projected temperature trends is good, and all CCMs predict continued, global-mean cooling of the stratosphere over the next five decades, increasing from around 0.25 K/decade at 50 hPa to around 1 K/decade at 1 hPa under the IPCC SRES A1B scenario. In general, the simulated ozone evolution is mainly determined by decreases in halogen concentrations and continued cooling of the global stratosphere due to increases in greenhouse gases (GHGs). Column ozone is projected to increase as stratospheric halogen concentrations return to 1980s levels. Because of ozone increases in the middle and upper stratosphere due to GHG induced cooling, total ozone averaged over mid-latitudes, outside the polar regions, and globally is projected to increase to 1980 values between 2035 and 2050 and before lower stratospheric halogen amounts decrease to 1980 values. In the polar regions, the CCMs simulate small temperature trends in the first and second half of the 21st century in mid-winter. Differences in stratospheric inorganic chlorine (Cl_y) among the CCMs are the key to diagnosing the inter-model differences in simulated ozone recovery, in particular in the Antarctic. It has been found that there are substantial quantitative differences in the simulated Cl_y, with the October mean Antarctic Cl_y peak value varying from less than 2 ppb to over 3.5 ppb in the CCMs, and the date at which the Cl_y returns to 1980 values varying from before 2030 to after 2050. There is a similar variation in the timing of recovery of Antarctic spring-time column ozone back to 1980 values. As most models underestimate peak Cl_y near 2000, ozone recovery in the Antarctic could occur even later, between 2060 and 2070. In the Arctic, the column ozone increase in spring does not follow halogen decreases as closely as in the Antarctic, reaching 1980 values before Arctic halogen amounts decrease to 1980 values and before the Antarctic. None of the CCMs predict future large decreases in the Arctic column ozone. By 2100, total column ozone is projected to be substantially above 1980 values in all regions except in the tropics.

The projected ozone in 2100 is sensitive to future levels of GHGs. Different scenarios of future emissions of GHGs will, in addition to radiative effects, result in a different chemical composition of the stratosphere through the production of radicals which catalytically destroy ozone [e.g., *Chipperfield and Feng*, 2003]. In the simulations presented in [*EY3*], only a single GHG scenario has been used.

1.7 Conclusions and Outlook

The coupling of stratospheric chemical models with climate models has led to a new generation of models far more complex than those available when the Montreal Protocol was signed twenty years ago. This increased complexity allows questions about future stratospheric ozone and UV radiation levels

to be studied in much more detail than could be done at that time. However, the workings of these CCMs themselves are also much harder to fully understand.

With the studies discussed in Section 1 [*EY1-3*], the advantage of a multi-model evaluation strategy could be demonstrated. The CCM assessment of [*EY2; EY3*] directly fed into the 2006 WMO/UNEP Scientific Assessments of Ozone Depletion [*WMO*, 2007]. The model comparison has allowed some groups to identify and correct previously unrecognized model errors, a prerequisite for a better representation of these processes in future model configurations. Important examples are the underestimation of Cl_y and too weak transport barriers (see schematic diagram in Figure 1-1) in several models [*EY2* and Section 1.4]. The multi-model approach also indicates a range of model uncertainties and missing or falsely modelled processes (e.g. 'cold bias') in the case of a systematic bias of all models.

Nevertheless, the multi-CCM assessment of [*EY2*] has focused only on a subset of key processes defined in the CCMVal evaluation standard [*EY1*]. Further analysis is needed to better understand the causes of the differences in future ozone projection in polar regions, and relative contribution of differences in dynamics and chemistry. This could include analysis of chemical ozone loss in the models, using artificial passive ozone tracers or tracer-ozone relations [*Chipperfield et al.*, 2005; *Douglass et al.*, 2006; *Lemmen et al.*, 2006] or improved measures of the ozone mass deficit [*Huck et al.*, 2007]. In addition, the frequency of occurrence of polar stratospheric clouds (PSCs) and the partitioning of the chemical families are important diagnostics to assess how well the chemistry is represented. Future research also needs to focus on the representation of the dynamics and variability in the CCMs. This includes the representation of vortex barriers and the frequency and timing of major mid-winter stratospheric sudden warmings as a basic unit of stratospheric variability [*Charlton and Polvani*, 2007]. If the models have problems to simulate correctly the size of the vortex, the break up date of the vortex, or the strength of the transport barrier at the edge of the polar vortex, this

will have implications on quantities like total column ozone anomalies poleward of 60° [e.g., *WMO*, 2007]. In addition, several other considerations suggest that the ozone projections must be used with caution. First, uncertainties exist that are directly related to parameterized processes in the CCMs themselves. For example, sub-grid scale processes like gravity-wave propagation and breaking or convection are parameterized in a way that is tuned to past and present conditions and assumed to be the same in the future. There are also uncertainties in the simulated future chemistry-climate feedbacks [Chapter 5 of *WMO*, 2007]. Changes in the generation and propagation of planetary-scale waves may affect stratospheric ozone [e.g., *Stolarski et al.*, 2006]. These changes and those in the sub-grid scale momentum deposition presumably give rise to the projected increase in the Brewer-Dobson circulation [*Butchart et al.*, 2006; *Rind et al.*, 1998; *Sigmond et al.*, 2004]. While the increase in the Brewer-Dobson circulation appears to be a robust feature of climate model simulations, the rate of change of the circulation varies substantially from one model to the next and the reasons for the change are not well understood.

Therefore, CCMVal is undertaking to prepare a Report on the Evaluation of Chemistry Climate Models by 2009 [see *Eyring et al.*, 2008a for details] in time for consideration in the anticipated WMO/ UNEP Ozone Assessment in 2010. The SPARC CCMVal report itself has two major aims: 1) provide valuable base material for that Assessment, and 2) improve the understanding of the strengths and weaknesses of CCMs and thus increase their integrity and credibility. The report will be based on the diagnostic metrics developed within CCMVal [*EY1*] and will be completed in time to provide useful and timely information for the expected WMO/UNEP Scientific Assessment of Ozone Depletion: 2010, as well as for the expected IPCC 5th Assessment Report. With the SPARC report it is hoped that some of the key open questions arising from the 2006 Ozone Assessment [*Shepherd and Randel, 2007*] can be answered. An important next step is to ask whether stratospheric ozone and surface UV radiation are responding as

expected to the controls imposed by the Montreal Protocol [Executive Summary of *WMO*, 2007]. Objectives also include the identification and quantification of causes for climate-change related changes of stratospheric circulation and their impact on the troposphere, in particular on weather, using satellite data and models, and the effects of an ozone super-recovery on the lower stratosphere and troposphere.

The outcome of the extensive evaluation of the SPARC CCMVal Report should provide the authors of the next WMO/UNEP Ozone Assessment with a sound basis to make objective judgements of the uncertainties associated with future ozone projections from the participating CCMs. In addition, CCMVal will establish closer links with the tropospheric chemistry and climate community, partly through the IGBP-IGAC / WCRP-SPARC Atmospheric Chemistry and Climate Initiative (AC&C)[4] and the WCRP/ CLIVAR Working Group on Coupled Mod-

elling (WGCM)[5]. Until present, detailed tropospheric and stratospheric chemistry has been treated separately. In general, sea surface temperatures in the CCM simulations are prescribed from observations or climate model simulations, which hinder the feedback between chemistry-climate interactions, especially in the troposphere. In addition to that, chemical models are evolving towards Earth-System Models (ESMs), which include the interaction between the atmosphere and the biosphere. The emission of greenhouse gases, aerosols and ozone precursors by vegetation and soils and the response of these emissions to a changing climate are now recognized as key issues in the interaction of chemistry and climate. A detailed ESM evaluation would provide means to identify possible model weaknesses and increase our level of understanding of uncertainties affecting climate predictions. An improved understanding of the key processes and feedback mechanisms is needed if credible ESM projections of climate change and its implications on human activities are to be made.

---

[4] IGBP-IGAC (International Geosphere-Biosphere Programme-International Global Atmospheric Chemistry) / WCRP-SPARC Atmospheric Chemistry and Climate Initiative (AC&C).
http://www.igac.noaa.gov/ACandC.php

---

[5] WCRP/ Climate Variability and Predictability (CLIVAR) Working Group on Coupled Modelling.
http://wcrp.wmo.int/AP_Modelling_WGCM.html

2   Impact of Shipping on Atmospheric Composition and Climate

2.1   Motivation

Emission of exhaust gases and particles from seagoing ships contribute significantly to the total emissions from the transportation sector [*EY4*; see Figure 2-1], thereby affecting the chemical composition of the atmosphere, climate as well as regional air quality and human health. Key compounds emitted are carbon dioxide (CO_2), nitrogen oxides (NO_x), carbon monoxide (CO), volatile organic compounds (VOC), sulphur dioxide (SO_2), black carbon (BC) and particulate organic matter (POM). NO_x emissions from shipping are relatively high because most marine engines operate at high temperatures and pressures without effective reduction technologies. SO_2 emissions are high because of high average sulphur content (2.4%-2.7%) in marine fuels used by most ocean-going ships [*EPA*, 2006]. Importantly, future scenarios demonstrate that significant reductions are needed to offset increased emissions due to the predicted growth in seaborne trade [*EY5*].

The chain of impact from ship emissions on atmospheric composition and climate is complex. This is schematically illustrated in Figure 2-2. To study the relevant processes from the exhaust of vessels to climate change (see Box 2-1), a variety of studies using models on different scales combined with observations are needed.

Emissions of NO_x and other ozone precursors from shipping lead to tropospheric ozone (O_3) formation and perturb the hydroxyl radical (OH) concentrations, and hence the lifetime of methane (CH_4). The dominant aerosol component resulting from ship emissions is sulphate, which is formed by the oxidation of SO_2. For some of the compounds (CO_2, O_3 and BC) the radiative forcing (RF) is positive while for others the forcing is negative (direct effect of sulphate particles [*Haywood and Shine*, 1995], reduced methane). The particles can also have an indirect effect on climate through their ability to act as cloud condensation nuclei (CCN) or by dissolving in the cloud drops and so change their surface tension [*Conover*, 1966; *Twomey et al.*, 1968]. The indirect aerosol effect contributes with a negative forcing.

In addition to impacts on the global scale, local and regional air quality problems in coastal areas and harbours with heavy traffic are of concern because of their impact on human health. The addition of CO_2 and SO_2 from ships into the ocean also contributes to acidification of the ocean, which poses a threat to marine biota [*Doney et al.*, 2007]. It is therefore a major challenge to improve our understanding of the impact of international shipping on atmospheric composition and climate and come up with suggestions for mitigation options.
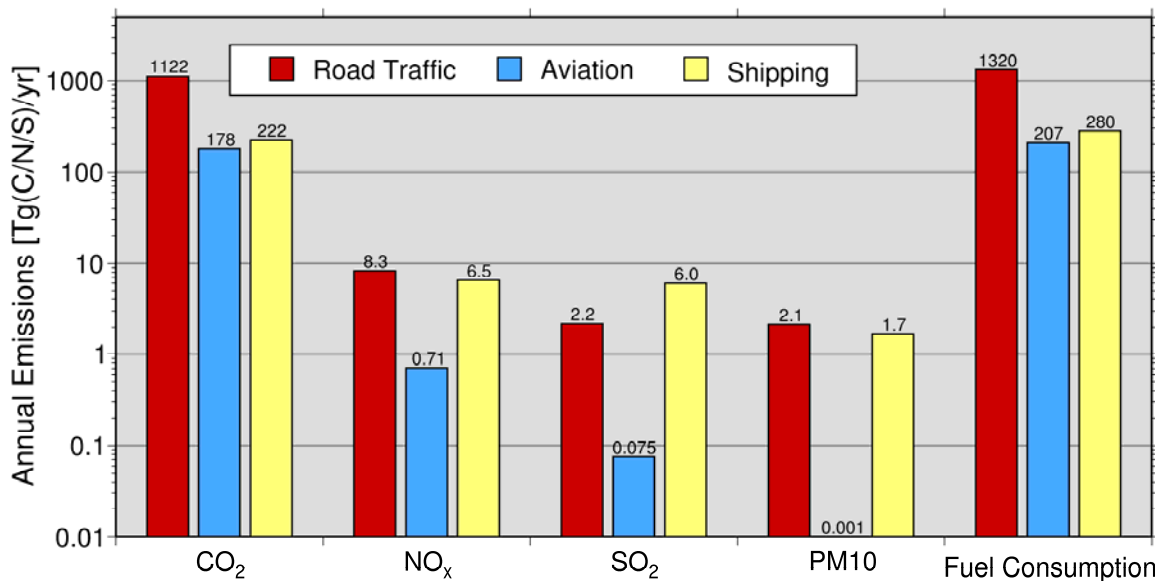
Figure 2-1: Transport-related annual emissions of CO_2 in Tg (C), NO_x in Tg (N), SO_2 in Tg (S) and PM_{10} in Tg (PM < 10 μm) and the fuel consumption in Mt estimated for the year 2000. From [*EY4*].
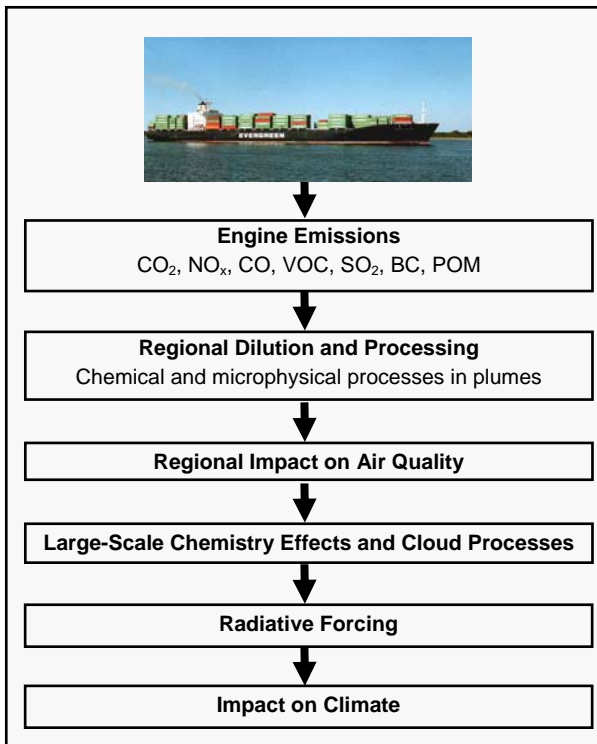
Figure 2-2. Schematic chain of impact from ship emissions on atmospheric composition and climate.

Since ship exhaust gases contribute to the worldwide pollution of air and sea, ships are facing an increasing number of rules and regulations as well as voluntary appeals from international, national and local legislators. Merchant ships in international traffic are subject to International Maritime Organisation (IMO) regulations. Emissions from ships in international trade are regulated by ANNEX VI of MARPOL 73/78 (International Convention for the Prevention of Pollution from Ships). Annex VI entered into force in May 2005, and sets limits on sulphur oxide and nitrogen oxide emissions from ship exhausts. In addition, the first sulphur emission control area (SECA, with a maximum fuel sulphur content of 1.5%) in the Baltic Sea entered into force in May 2006, while the North Sea and English Channel SECAs entered into force between August and November 2007. IMO has declared the goal of a 30% NO_x reduction from internationally operating vessels and introduced NO_x limits in Annex VI which depend on engine speed [*IMO*, 1998]. Since 1st January 2000, all new marine diesel engines delivered for new vessels comply with this regulation (NO_x-optimised engines).

Because of the increased air pollution in harbour cities, the EU has agreed on the Directive 2005/33/EC, to limit the sulphur content to 0.1% in marine fuels for harbour regions in 2010. The United States' Environmental Protection Agency (EPA) has adopted ship emissions standards for NO_x, CO and HC for all US ships with engines manufactured on or after 1 January 2004. Most industrial countries have made commitments under the Kyoto Protocol to reduce their GHG emissions, in particular CO_2. The Kyoto Protocol entered into force in February 2005. However, international shipping is currently excluded from emission targets under the Kyoto protocol and no decision has yet been taken on how to allocate the international GHG emissions from ships to the individual countries. Since no legislative action in this respect was agreed by the IMO in 2003, the EU is required to identify and take action to reduce the GHG emissions from shipping and is now discussing whether shipping is going to be included into the EU emission trading scheme (EU ETS).

This section provides a summary of the results that have been achieved by the Helmholtz-University Young Investigators Group SeaKLIM. SeaKLIM has been established in January 2004 and is a group of four scientists (1 research scientist, 1 post-doc and 2 PhD students) working in this field in close collaboration with other national and international scientists. The SeaKLIM results contributed significantly to the increasing attention of shipping over the past few years. Shipping has now been recognized as a growing problem and an intense dialogue on how to best reduce emissions from ships has started between policymakers, industry, and scientists. SeaKLIM studies on past, present-day and future ship emissions are discussed in Section 2.2 [*EY4; EY5*] and their impact on atmospheric composition [*EY6; EY7; EY8; EY9*] and human health [*EY10*] are discussed in Section 2.3 and 2.4, respectively. Radiative forcing due to ship emissions is discussed in Section 2.4 [*EY7; EY9; EY11; EY12*]. A summary, conclusions and an outlook on this topic are presented in Sections 2.6 and 2.7.

Box 2-1. Chain of impact from ship emissions on atmospheric composition, RF and climate.

Regional dilution and processing

Ship emissions occur locally at relatively high concentrations in relation to the atmospheric background concentrations. The emissions are diluted by mixing with the ambient air. During the dilution process the emitted species are chemically transformed, secondary species (e.g., ozone) are formed and they are already partially removed from the atmosphere by wet and dry deposition. These processes non-linearly depend on the concentrations of the primary emissions, the atmospheric background concentrations and on the actual meteorological state of the atmosphere such as height and stability of the marine boundary layer, vertical wind profile or the presence of clouds. Other important factors involve the insolation depending on latitude and time of the day.

Regional impact on air quality and large-scale chemistry effects

At a local and regional-scale, ocean-going ships impact on air quality in particular through the formation and transport of ground-level ozone, sulphur emissions and particulate matter. The main reaction pathways of relevance for the climate active compounds (e.g. CH_4, O_3 and sulphate particles) are the NO_x-catalysed formation of ozone, the gaseous and aqueous oxidation of SO_2 to sulphate aerosol, and the destruction of methane by OH. The main oxidising agent in the troposphere is the OH radical, which is produced through the ultra-violet photolysis of ozone followed by reaction of the $O(^1D)$ radical with water vapour and through conversion of the HO_2 radical to OH by NO. Thus NO_x emissions from shipping increase the OH radical through two routes, directly by reaction with HO_2, and indirectly by generating ozone. This extra OH removes methane and other hydrocarbons from the atmosphere. The formation of ozone is initiated by the reaction of OH with species such as CO and CH_4 forming HO_2 and CH_3O_2, respectively. OH reactions with more complex hydrocarbons are analogous to CH_4, generating the related organic peroxy radicals. In the presence of NO_x, reactions of peroxy radicals with NO lead to formation of NO_2 which photolyses and produces ozone. However, at low concentrations of NO_x, peroxy radicals primarily react through peroxy-peroxy self- and cross reactions yielding hydrogen and organic peroxides (H_2O_2 and CH_3OOH). Ozone is mainly destroyed by photolysis, reaction with HO_2 and deposition to the ocean surface. Net ozone formation in the MBL is then a result of competition between ozone formation and sink reaction cycles. Ozone chemistry in the MBL is thus very sensitive to changes in concentrations of NO_x. As a water soluble gas, ozone also partitions in the aqueous phase in the presence of clouds.

Cloud processes

Besides gaseous pollutants ships also emit aerosols and their gaseous precursors. The dominant aerosol component resulting from shipping is sulphate, which is formed by the oxidation of SO_2 by the hydroxyl radical (OH) in the gas phase or by O_3 and hydrogen peroxide (H_2O_2) in the aqueous phase of cloud droplets. The aerosol impacts the Earth's radiation budget directly by scattering and absorbing incoming solar radiation and indirectly by changing cloud properties. Particles and their precursors from ship emissions are able to act as cloud condensation nuclei (CCN) in the water-vapour saturated environment of the maritime cloud or can change the surface tension due to their solubility. Amount and size of these particles depend on the fuel and also the kind of combustion, but can possibly result in a higher cloud droplet concentration. The increase in cloud droplet number concentration can lead to an increased cloud reflectivity, known as indirect aerosol effect. This mechanism can also cause anomalous cloud lines, so-called ship tracks, which have often been observed in satellite data. In addition, aerosols from shipping might also change cloud cover and precipitation formation efficiency as well as the average cloud lifetime.

Radiative Forcing

A common metric to quantify climate impacts from different sources is radiative forcing (RF) in units of W/m^2, which is defined as a change in the earth-atmosphere energy balance at the tropopause due to a perturbation. There is an approximately linear relationship between global mean radiative forcing related to the concentration change of a species and change in global mean surface temperature [*Forster et al.*, 2007]. The RF represents the stratospherically adjusted radiative flux change evaluated at the tropopause. Positive RFs lead to a global mean surface warming and negative RFs to a global mean surface cooling. The radiative forcing drives a surface temperature change (ΔT_s): $\Delta T_s = \lambda \cdot RF$, where λ is a climate sensitivity, which indicates the equilibrium surface temperature change per unit radiative forcing. Low values of λ indicate an insensitive climate and high values indicate a sensitive climate. The value of λ is uncertain, mainly due to poorly understood cloud feedbacks. *Forster et al.* [2007] report that λ is likely to lie in the range from about 0.54 to 1.2 K $(W/m^2)^{-1}$. Both changes in atmospheric composition and in cloudiness due to ship emissions perturb the radiative energy flow in the atmosphere, resulting in a RF and a related temperature change.

2.2 Emissions [EY4; EY5]

2.2.1 Present-day Fuel Consumption and Emissions

2.2.1.1 Methodologies

Before the impact of ship emissions on atmospheric composition and climate can be studied, emission inventories have to be developed. The principal existing approaches to produce spatially resolved ship emissions inventories for the key compounds can be characterised as either bottom-up or top-down [*Wang et al.*, 2007].

In a bottom-up approach emissions are directly estimated within a spatial context so that spatially-resolved emissions inventories are developed based on detailed activities associated to locations. Bottom-up approaches estimate ship- and route-specific emissions based on ship movements, ship attributes, and ship emissions factors. The locations of emissions are determined by the locations of the most probable navigation routes, often simplified to straight lines between ports or on predefined trades. Bottom-up approaches to date have been limited to smaller scale or regional emissions inventories due to the significant efforts associated with routing.

In a top-down approach emissions are calculated without respect to location by means of quantifying the fuel consumption by power production first and then multiplying the consumption by average emission factors. The resulting emission totals are distributed over the globe by using spatial proxies. There are mainly two different top-down approaches to calculate the fuel consumption.

One approach uses total fuel consumption from world-wide sales of bunker by summing up per country. Bunker sales figures require combination of fuels reported under different categories (e.g. national bunker, international bunker). This can be challenging at a global scale because most energy inventories follow accounting methodologies intended to conform to International Energy Agency (IEA) energy allocation criteria [*Thomas et al.*, 2002] and because not all statistical sources for marine fuels define international marine fuels the same way [*Olivier and Peters*, 1999].

Therefore in [*EY4*] the other top-down approach was chosen, which models fleet activity and estimates fuel consumption resulting from this activity, summing up per ship or ship class. The fuel consumption calculation is based on installed engine power for a ship, number of hours at sea, fuel consumed per power unit (kW), and an assumed average engine load in each of the 132 ship classes. Global ship emission totals are derived by combining the modelled fuel consumption with specific emission factors. Detailed input data to the modelling is based on measurement data from the diesel engine manufacturers [*Köhler*, 2003].

Detailed activity-based modelling has been defined as best practices for port and regional inventories [*ICF Consulting*, 2005], usually separating on different ship types and size categories, to establish categories with mostly the same characteristic of the input variables. On the global scale activity-based modelling is also challenging, because of the uncertainties in input parameters.

2.2.1.2 Fuel Consumption and Emissions in 2001

The results of [*EY4*] suggest a fuel consumption of approximately 280 million metric tons (Mt) for the year 2001. This corresponds to annual emissions of 813 Tg CO_2, 21.4 Tg NO_2, 12.03 Tg SO_2, 1.31 Tg CO,

Table 2-1: Relative contribution of road traffic, shipping [*EY4*] and aircraft to total annual anthropogenic emissions for the year 2000 [*EDGAR 32FT2000, Olivier et al.*, 2005].

	CO_2	CH_4	CO	NO_x	NMVOC	SO_2
Road Traffic	14.1%	0.3%	17.2%	20.6%	17.8%	2.4%
Shipping	2.7%	16.1%	12.2%	15.4%	1.8%	7.8%
Aircraft	2.2%	0.0%	16.4%	1.7%	0.3%	0.1%

1.67 Tg PM and 1.96 Tg hydrocarbons in 2001. In addition, 1.959 Tg hydrocarbons from crude oil transport evaporate yearly during loading, transport, and unloading [*Endresen et al.*, 2003].

Although shipping contributes only about 16% to the total fuel consumption of all traffic related sources (Aviation: 207 Mt, International Shipping: 280 Mt, Road Traffic: 1320 Mt), ship emissions significantly contribute to emissions of pollutants from all transport modes (see Figure 2-1), particularly because there have been no strict international emission regulations in the past. Table 2-1 gives an overview of the relative contribution of the three individual transport modes to the total anthropogenic emissions.

Uncertainties in the calculated emission totals in the activity-based approach arise from the use of average input parameters in the selected ship type classes, for example, marine engine load factor, time in operation, fuel consumption rate, and emission factors, which vary by size and age of the ship, fuel type, and market situation.

2.2.1.3 Comparison to other ship emission inventories

Several studies have calculated global emissions from ocean-going civil ships by combining estimates for marine fuel sales with their respective fuel based emissions factors. These estimates based on energy statistics result in a total fuel consumption below 200 Mt for the year 2000 [e.g., *Skjølsvik et al.*, 2000; *Endresen et al.*, 2003, 2007; *Dentener et al.*, 2006].

Although emissions estimates and fuel consumption are related to the energy used by ships, recent studies, including the [*EY4*] study discussed above, call into question the validity of statistics of marine fuel sales. These studies have focused on activity-based estimation of energy and power demands from fundamental principles [*Corbett and Köhler*, 2003; *EY4*; *ICF*, 2005]. These approaches estimate fuel consumption for the world fleet of around 280 Mt in 2001 and have shown that fuel allocated to international fuel statistics is insufficient to describe total estimated energy demand of international shipping. *Corbett and Köhler* [2004]

considered alternative input parameters in their activity-based fuel consumption and emission model. They conclude that alternative assumptions in the input parameters could reduce their fuel consumption estimate, but not more than 14% to 16%. However, other activity-based studies have reported lower estimates, considering alternative operation profile. They claim that the main reason for the large deviation between activity based fuel consumption estimates is the number of days assumed at sea and that better activity data (per ship type and size categories) on a yearly basis is required when fleet modelling is used to determine the actual fuel consumption for the entire world fleet [*Endresen et al.*, 2004, 2007].

Convergence is emerging on baseline estimates at least in terms of major insights, through a dialogue about uncertainty ranges in ocean-going fuel consumption and emissions. While it remains challenging to quantify ship emission totals, greater uncertainty may be related to the technological and economic performance of strategies to implement effective regulations and incentives.

2.2.1.4 Spatial Proxies of Global Ship Traffic

Global inventory estimates for fuel use or emissions derived from a top-down approach are distributed according to a calculated ship traffic intensity proxy per grid cell, referring to the relative ship reporting frequency or relative ship reporting frequency weighted by the ship size.

The spatial distribution of emissions used in EDGAR (Environmental Database for Global Atmospheric Research; *Dentener et al.* [2006]) was derived from the world's main shipping routes and their traffic intensity [*Times Books*, 1992; Figure 2-3 upper panel] and was one of the first top-down shipping inventories. However, more comprehensive inventories have replaced EDGAR as the primary choice by introducing more realistic shipping patterns. *Corbett et al.* [1999] produced one of the first global spatial representations of ship emissions using a shipping traffic intensity proxy derived from the Comprehensive Ocean-Atmosphere Data Set (COADS), a data set of voluntarily
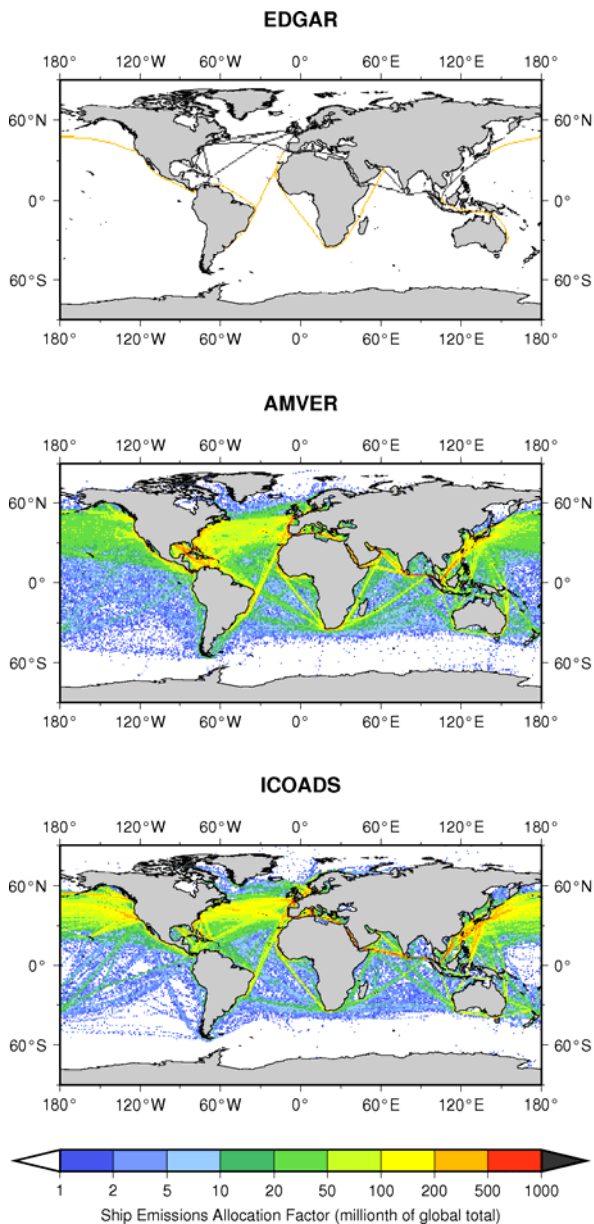
Figure 2-3. Ship Emissions Allocation Factors (SEAF) from EDGAR [*Dentener et al.*, 2006], AMVER [*Endresen et al.*, 2003], and ICOADS [*Wang et al.*, 2007]. SEAF in each grid cell is defined as the fraction of ship emissions in that grid cell of the global total (expressed in millionth of the global total).

reported ocean and atmosphere observations with ship locations which is freely available. *Endresen et al.* [2003] improved the global spatial representation of ship emissions by using ship size (gross tonnage) weighted reporting frequencies from the Automated Mutual-assistance Vessel Rescue system (AMVER) data set (Figure 2-3, middle panel). AMVER, sponsored by the United Coast States Guard (USCG), holds detailed voyage information based on daily reports for differ-

ent ship types. Participation in AMVER was, until very recently, limited to merchant ships over 1000 GT on a voyage for 24 or more hours and data are strictly confidential. The participation in AMVER is 12,550 ships but only around 7,100 ships have actually reported. *Endresen et al.* [2003] found that COADS and AMVER lead to highly different regional distributions.

Wang et al. [2007] addressed the potential statistical and geographical sampling bias of the International Comprehensive Ocean-Atmosphere Data Set (ICOADS, current version of COADS; Figure 2-3 lower panel) and AMVER data sets, the two "best" global ship traffic intensity proxies, and made four advancements to improve the accuracy of the top-down approach using ICOADS as spatial proxy: i) trimming over-reporting vessels to mitigate geographic and statistical sampling bias; ii) increasing sample size by using multiple-year ICOADS data; iii) weighting ship observations with installed ship power to reflect emissions variability among different sizes and types of vessels; and iv) smoothing the inventory with GIS[6] tools.

The three different shipping traffic intensity proxies are shown in Figure 2-3. It should be noted, that each of them only covers part of the total world fleet movements. In [*EY4*] AMVER from *Endresen et al.* [2003] has been used to distribute the emission over the globe.

2.2.2 Historical Fuel Consumption and Emissions

Over the last 100 years the fleet expanded by 72,000 motor ships to a total of 88,000, with a corresponding increase in total tonnage from 22.4 to 553 million gross tonnage (GT) [*Lloyd's*, 2002]. This growth has been driven by increased demand for passenger and cargo transport, with 300 Mt cargo transported in 1920 [*Stopford*, 1997] and 5,400 Mt in 2000 [*Fearnresearch*, 2003]. In 1950 the civilian fleet consisted of 30,844 vessels of 100 GT and above with a total of 84.6 million GT [*ISL*, 1994]. Starting around 1960, the world merchant fleet increased rapidly and the ship number more than doubled in the period between 1960 and 1980.

---

[6] GIS = Geographic Information System

Part of this ship boom was the tanker business, which reached its peak around 1973-1975, and the introduction of a new type of cargo ship, the container vessel. In general, little information on the historical development of fuel consumption is available, with little data published pre-1950 and large deviations reported for estimates covering the last three decades.

[*EY4*] produced one of the first estimates for fuel usage over a historical period from 1950 to 2001. They have reported simplified activity-based inventories from 1950 up to 1995 using ship number statistics and average engine statistics, while the estimate for 2001 is based on detailed fleet-modelling. The results suggest that fuel consumption from ocean-going ships has increased by a factor of 4.3 from 1950 (64.5 Mt) to 2001 (280 Mt). Uncertainties in this estimate arise from the fact that reliable input data such as detailed shipping and engine as well as engine performance statistics, activity data and the detailed fleet structures before 1976 are not available. *Endresen et al.* [2007] reported more detailed activity estimates from 1970 to 2000.
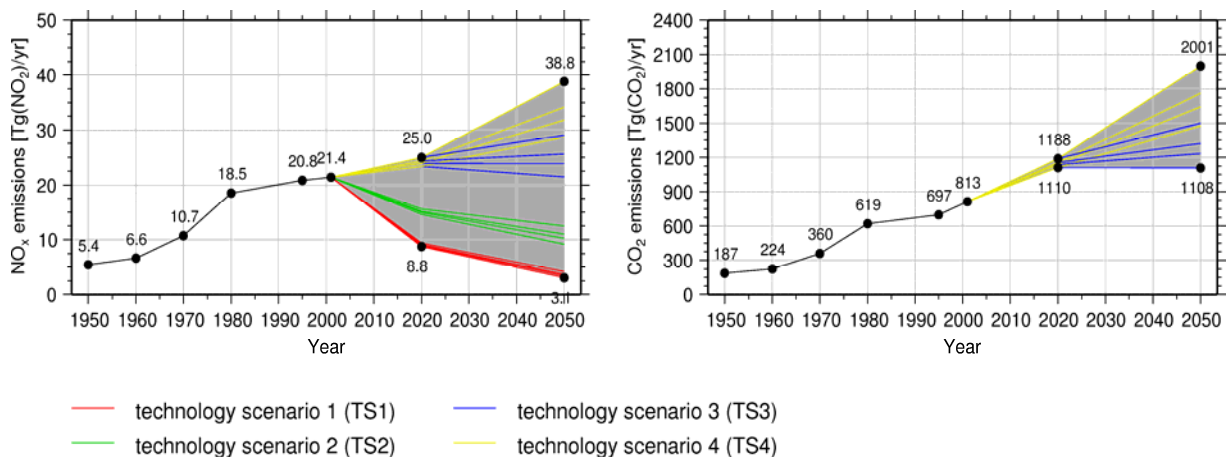
2.2.3   Future Emission Scenarios

To address possible future development, several scenarios until 2050 have been investigated by [*EY5*]. The scenarios are based on some very strict assumptions on future ship traffic demands and technological improvements.

The four future ship traffic demand scenarios are mainly determined by the economic growth, which follows the IPCC SRES storylines [*IPCC*, 2000]. The resulting fuel consumption is projected through extrapolations of historical trends in economic growth, total seaborne trade and number of ships, as well as the average installed engine power per ship. The scenario calculations indicate that the demand for ship transport will continue to increase in the future. For the future technology scenarios a diesel-only fleet in 2020 is assumed, resulting in fuel consumption between 382 and 409 Mt. For 2050, one technology scenario assumes that 25% of the fuel consumed by a diesel-only fleet can be saved by applying future alternative propulsion plants, resulting in a fuel consumption that varies between 402 and 543 Mt. The other scenario is a business-as-usual scenario for a diesel-only fleet even in 2050 and gives an estimate between 536 and 725 Mt.

The today's fleet-average emission factors of the most important ship exhausts from [*EY4*] are used to calculate emission scenarios for the future through 2050 in [*EY5*]. These calculations show that if no control measures are taken beyond existing IMO regulations, NO_x emissions could exceed those from present-day global road transport in 2050. If the

Figure 2-4. Possible range of future NO_x and CO_2 emissions according to the four different technology scenarios (TS1-4) and the four different ship traffic demand scenarios (DS1-4). Results for the technology scenario 1 (TS1) are shown for different ship traffic demand scenarios (DS1-4) with red lines, those for TS2 with green lines, for TS3 with blue lines, and for TS4 with yellow lines. From [*EY5*].

sulphur content remains at present day levels, a doubling of SO_2 emissions can be expected by then. However, given the air quality issue of shipping emissions, further emission reductions of NO_x and SO_2 are to be expected. Applying technologies for an aggressive NO_x emission reduction a significant decrease up to 85% of today's NO_x emissions can be reached until 2050, in spite of the larger fleet. CO_2 emissions are suggested to further increase by about 35% under the same "clean" scenario due to the direct connection between fuel consumption and CO_2 emissions. Figure 2-4 shows the possible range of future NO_x and CO_2 emissions.

As a result, an entirely consistent set of emission inventories from 1950 to 2050 suitable as input for global chemistry models has been provided by the SeaKLIM group [*EY4; EY5*].

2.3   Impact on Atmospheric Composition [EY6; EY7; EY8; EY9]

To a large extent the chemistry of the Marine Boundary Layer (MBL), as with the rest of the troposphere, is determined by the oxidation of primary emitted species and their subsequent reactions. The main reaction pathways of relevance for the climate active compounds (e.g. CH_4, O_3 and sulphate particles) are the NO_x-catalysed formation of ozone, the gaseous and aqueous oxidation of SO_2 to sulphate aerosol, and the destruction of methane by OH (see Box 2-1). The efficiency of ozone production from NO_x emissions is much greater in cleaner environments [*Lin et al.*, 1988; *Seinfeld and Pandis*, 1998].

2.3.1   Near-Field Processes

The majority of emissions from shipping are injected into the atmosphere in form of coherent plumes, often in relatively pristine parts of the atmosphere. For modelling studies, the emission totals (see Section 2.2) are distributed over the globe with the help of spatial proxies of global ship traffic derived in various ways and are instantaneously spread onto large inventory grid boxes, usually 1° longitude x 1° degree latitude, without accounting for dispersion, transformation

and loss processes on the sub-grid scale. Emissions are further distributed within grid boxes of a few hundreds of kilometres horizontal resolution for use in global modelling simulations to study the impact of ship emissions on the composition of the atmosphere (see Section 2.3.2).

The effects of plume processes in photochemical transformation of ship emissions were addressed in several studies, some based on measurements in ship plumes [*Sinha et al.*, 2003; *Chen et al.*, 2005; *Schlager et. al.*, 2007], some based on theoretical model simulations [*Song et al.*, 2003; v*on Glasow et. al.*, 2003]. In-plume processes that need to be considered include oxidation of NO_x, deposition of NO_2 and SO_2, scavenging of HNO_3, oxidation and heterogeneous removal of SO_2, and impact of ship-emitted and background particles on chemistry.

In SeaKLIM, the dispersion and chemical conversion of emissions in the near-field of a single ship has been studied with two different box modelling approaches to explore the differences between gradual dispersion and instantaneous dilution into a box with a size comparable to the large grid boxes of global scale models or satellite data [*EY6*]. While both techniques use the same photochemical mechanism to solve the chemical equations, the parameterisation of the dilution of the exhaust into the background air is different. One approach uses a Gaussian plume model and accounts for the expansion phase of a plume (hereafter: 'Plume Dispersion' (PD)). The other one instantaneously disperses the emissions over a large gridbox, a technique commonly used by large scale models (hereafter: 'Instantaneous Dilution' (ID)). In a case study both approaches are applied to ship emissions of 145 mol(NO_x)/s, which where emitted at noon of May 8. The ship emissions were calculated from the fuel consumption of a large container ship, the Clifford Maersk [*Schlager et al.*, 2007]. Background concentrations and the meteorological parameters were taken from measurements during the ITCT 2k2 ship plume experiment, about 100 km off the coast of California [*Chen et al.*, 2005].

The calculations were performed until the time t_{ref} when the PD-box has grown to the size of the ID box. The maximum height was limited by the height of the marine boundary layer. 60 km was chosen as maximum width of horizontal plume expansion and size of the ID box. Comparison of both approaches show significant differences in ship induced ozone production. The different box sizes lead to different NO_x-concentrations. The small PD box with high concentrations of NO_x lies in a regime where ozone production is hydrocarbon limited and additional NO_x results in ozone destruction. On the other hand in the ID box the ozone chemistry is in the NO_x-limited regime where additional NO_x produces ozone. The resulting ozone development can be seen in Figure 2-5. For the PD case at the reference time t_{ref} a total of 3 mol ozone has been produced, while in the ID box about 1 mol is produced. Therefore, for this particular case with emissions from a large container ship, global models would overestimate the ozone response by a factor of three.
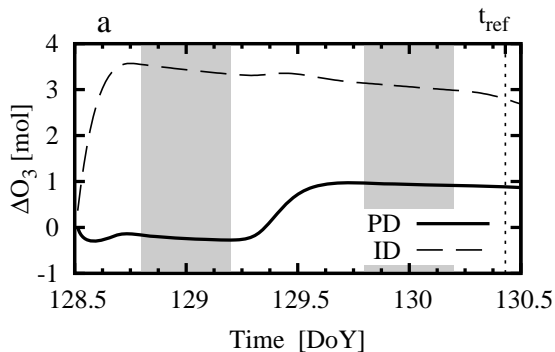
Figure 2-5. Temporal development of ship induced ozone change. Shown is the ozone change integrated over the boxes of one calculation with plume dispersion (PD) and one with instantaneous dispersion (ID). From [*EY6*].

One possibility to account for these sub-grid processes in global models is the use of effective emissions, i.e. actual emissions are changed and emissions of additional compounds like ozone are introduced in a way that they take sub-grid processes into account. In a second step, this method to correct for the overestimation in global models has been tested. The method follows *Petry et al.* [1998], who investigated the same problem for aircraft emissions. The core idea of

this approach is to adjust the emissions for the ID approach in a way that at the reference time t_{ref} the calculations end up at values approximately that of a corresponding PD simulation. For the above described situation of emissions at noon it is possible to correct the ozone production for an ID calculation. This can be seen in Figure 2-6 (12 local time (LT)).

The differences in ozone production and therefore the effective emissions are expected to depend on a variety of parameters, e.g. background conditions, time of release, and emission strength. To study these dependences, sensitivity studies have been conducted. Figure 2-6 shows ship induced ozone concentration changes in the different boxes ID and PD as a function of time of the emissions released into the MBL.

A dependence of ozone production on release time can be seen for both the PD and the ID calculations. However, while the ozone produced for the PD calculations reaches its maximum at 3 LT in the morning with 0.82 ppb and the minimum at noon with 0.46 ppb, the ozone production calculated with the ID model reaches its maximum at noon with 1.5 ppb and minimum at 6 in the evening with 0.63 ppb. This is due to the different times after emission when ozone production takes place. In the ID case ozone production directly starts after the emissions while in PD calculations the production of ozone occurs mainly on the second day. The relative difference between the approaches is highest at noon, when in the ID box 3.2 times as much ozone as in the PD box is simulated. It is smallest at 21 LT, when ID simulates 1.2 times ozone than PD. Additionally, for all calculations shown the capability to correct the ID cases with effective emissions was tested. It can be seen that these calculations (EF) give approximately the same ozone production as the PD runs (Figure 2-6).

A similar study was made for the dependence on emission strength. Here the emissions from the first run (emissions of 145 mol/s at noon) are varied in ten steps from 14.5 mol/s up to 145 mol/s. For the ID case the ozone production at t_{ref} is nearly linear in respect to emission strength. It ranges
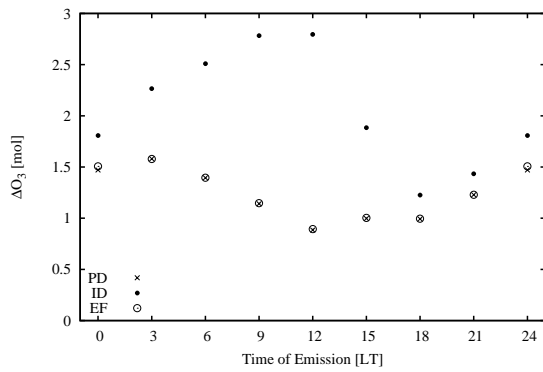
Figure 2-6. Ship induced ozone change at reference time t_{ref} as a function of time of the emissions release into the MBL. Shown are results for three calculations: with plume dispersion (PD), instantaneous dispersion without effective emissions (ID) and instantaneous dispersion with effective emissions (EF). From [*EY6*].

from 0.17 ppb for an emission of 14.5mol/s up to 1.5 ppb at 145 mol/s. In the PD case the ship induced change in ozone concentration ranges from 0.11 ppb at 14.5 mol/s to 0.46 ppb at 145 mol/s and shows no linear dependence on emission strength. The relative difference between the two approaches also increases with increasing emission strength. At 14.5 mol/s 1.6 times as much ozone is produced in the ID case as in the PD case, at 145 mol/s it is 3.2 times as much. Overall the results highlight the importance of plume chemistry but also the complexity of near-field processes. More research is required to develop a suitable method to parameterise subgrid-scale processes in global models.

2.3.2 Large-Scale Effects on Atmospheric Composition

Large scale effects on chemistry are evaluated with the help of coupled chemistry-climate models (CCMs) and chemistry-transport models (CTMs). In contrast to the CCMs used to project stratospheric ozone discussed in Section 1, the global models used here all have sophisticated tropospheric chemistry, but they do not include detailed stratospheric chemistry (see *Stevenson et al.* [2006] and [*EY7*] for details).

2.3.2.1 Large-Scale Effects of Ozone and Aerosol Precursor Emissions

The global impact of shipping on atmospheric chemistry and radiative forcing as well as the associated uncertainties have been quantified in [*EY7*] using an ensemble of ten state-of-the-art atmospheric chemistry models and a pre-defined set of emission data. The analysis is performed for present-day conditions (year 2000) and for two future ship emission scenarios (year 2030). The main characteristics of the participating models (CHASER-CTM, FRSGC/UCI, GMI/CCM3, GMI/DAO, LMDz/ INCA, MATCH-MPIC, STOCHEM-HadAM3, STOCHEM- HadGEM, TM4, and UIO_CTM2) are summarised in Table 1 of [*EY7*], and are described in detail in the cited literature.

Two of the five simulations have been defined as part of the wider PHOTOCOMP-ACCENT-IPCC study (*Stevenson et al.* [2006] and references therein): a year 2000 base case (S1) and a year 2030 emissions case (S4) where all other anthropogenic sources (except biomass burning emissions, which remain fixed at year 2000 levels) vary according to IPCC SRES A2 broadly representing a 'pessimistic' future situation. All models used the same anthropogenic and biomass burning emissions. To retain consistency with all other emissions, ship emissions in the year 2000 (S1) are based on the EDGAR3.2 dataset [see upper panel in Figure 2-3] at a spatial resolution of 1° latitude x 1° longitude. EDGAR3.2 includes data for 1995, which have been scaled to 2000 values assuming a growth rate of 1.5%/yr, resulting in annual NO_x and SO_2 emissions of 3.10 Tg(N) and 3.88 Tg(S), respectively, similar to the emission totals published by *Corbett et al.* [1999]. As noted in *Stevenson et al.* [2006] in the S4 simulation emissions from ships were included at year 2000 levels by mistake. For the shipping study of [*EY7*], an additional model simulation for 2030 (S4s) has been designed to assess the impact of shipping if emission growth remains unabated. Ship emissions in S4s are based on a 'Constant Growth Scenario' in which emission factors are unchanged and emissions increase with an annual growth rate of 2.2% between 2000 and 2030. In the S4s scenario

emissions from shipping increase to 5.95 Tg(N) for NO_x and 7.36 Tg(S) for SO_2 in 2030. In addition to the S1 and S4 simulations, two sensitivity simulations have been defined that use identical conditions to S1 or S4/S4s except that ship emissions are excluded. The year 2000 and 2030 experiments without ship emissions are denoted as S1w and S4w. The difference between the simulation with and without ship emissions are used to quantify the impact of shipping on NO_2, O_3, and sulphate distributions.

For present-day conditions [*EY7*] find the most pronounced changes in annual mean tropospheric NO_2 and sulphate columns over the Baltic and the North Sea, and also though smaller over the Atlantic, Gulf of Mexico, and along the main shipping lane from Europe to Asia. Maximum near-surface O_3 changes due to NO_x ship emissions are simulated over the North Atlantic in July (~12 ppbv) in agreement with previously reported results [*Lawrence and Crutzen*, 1999; *Endresen et al.*, 2003], see Figure 2-7. However, in contrast to *Endresen et al.* [2003], a decrease in O_3 in winter is found

over large areas in Europe (~3 ppbv) due to titration, which could be related to differences in the emission inventories. Overall NO_x emissions most effectively produce O_3 over the remote ocean, where background NO_x levels are small. The impact of CO, VOCs and direct methane from shipping on ozone is found to be very small, generally less than 0.1 ppb.

The amount of observational data available to compare to is very limited and comparisons are very sensitive to the choice of dataset. [*EY7*] found disagreement between their multi-model average NO_2 simulations and the observations used in *Davis et al.* [2001], but relatively good agreement with a larger observational dataset from *Emmons et al.* [2000], see Figure 2-8. An intercomparison of the model results with observations over the Northern Hemisphere (25°-60°N) oceanic regions in the lower troposphere showed that the models are capable to reproduce O_3 and NO_x reasonable well, whereas SO_2 in the marine boundary layer is significantly underestimated. However, evaluation of the models' response to ship emissions is
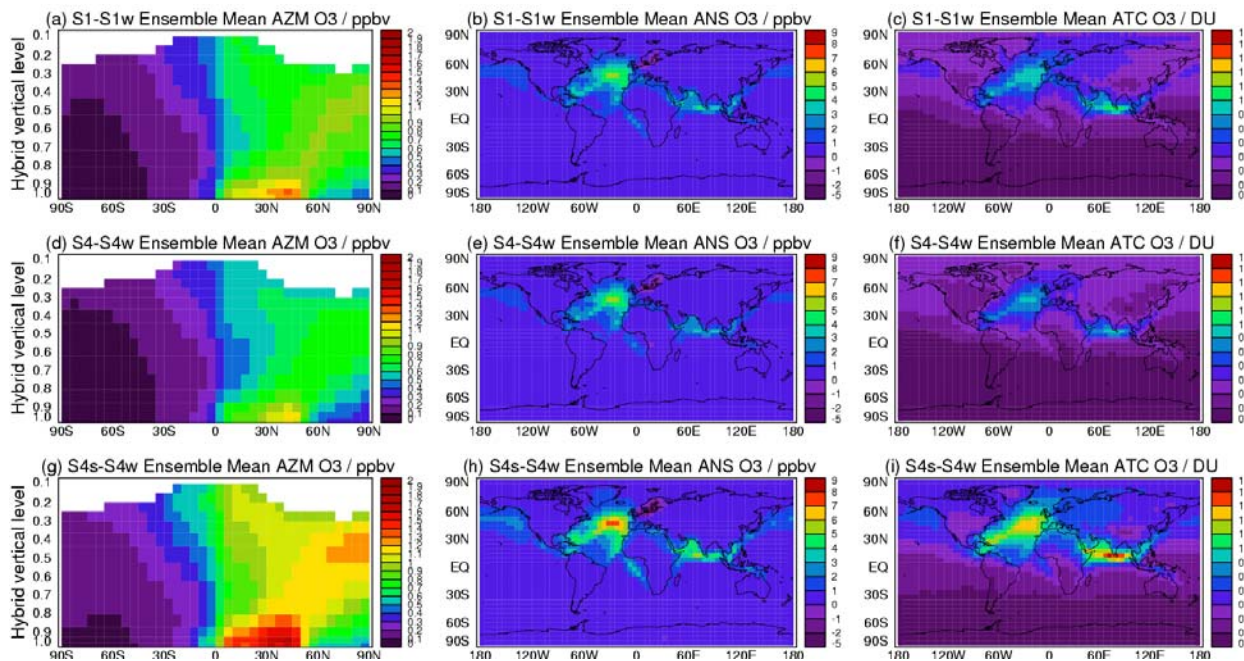

Figure 2-7: Modelled ensemble mean ozone change between (a-c) S1 (year 2000) and S1w (year 2000 without ship emissions), (d-f) S4 (year 2030) and S4w (year 2030 without ship emissions), and (g-i) S4s (year 2030) and S4w. Figure 2-7a, d, and g are zonal mean changes (ppb), Figures 2-7b, e, and h are near-surface ozone changes (ppb) and Figure 2-7c, f, and i are tropospheric ozone column changes (DU). From [*EY7*].

still at a preliminary stage and is currently limited by the coarse spatial resolution of the models, the uncertainty in the measurements, the lack of sufficient in situ measurements over the ocean, and the difficulty to separate ship emissions from other even stronger emission sources close to land.

Another approach to evaluate the shipping response in models is the use of satellite data. Unambiguous detection of ship emissions in satellite data is currently only available for the region of the Red Sea and the

Indian Ocean [*Beirle et al.*, 2004; *EY7*], where shipping routes are close to the coastal area. The satellite observations from SCIAMACHY aboard the European research satellite ENVISAT show enhanced tropospheric NO_2 concentrations along the major international shipping routes in the Red Sea and over the Indian Ocean [*EY8;* see Figure 2-9]. The pattern of the satellite data is in good agreement with the ship emission inventory, although it is worthwhile to point out that the inventory does not capture the slope of the lane between Sri Lanka and Su-
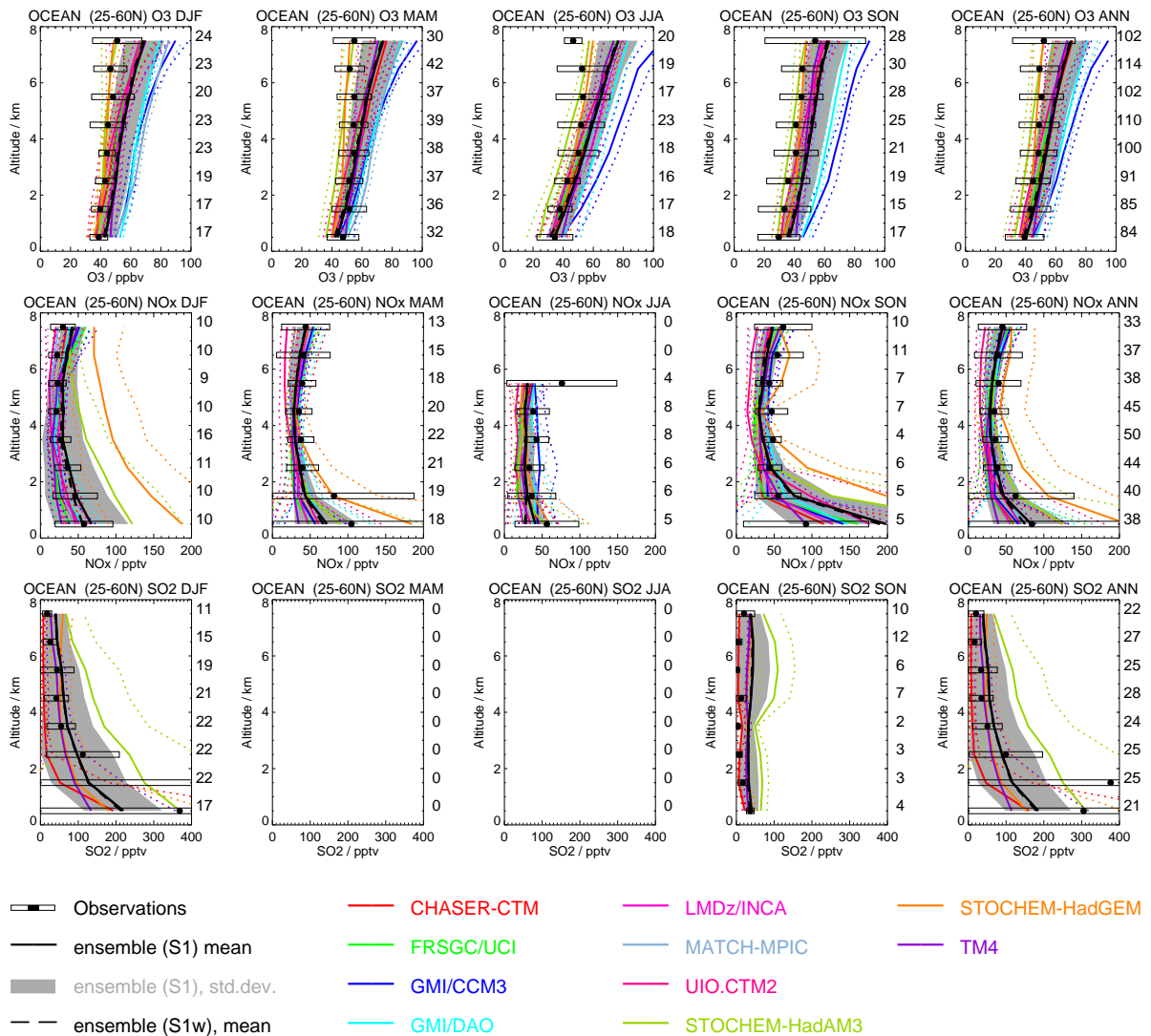
Figure 2-8. Seasonal and annual means of O_3 (upper row, ppbv), NO_x (middle row, pptv) and SO_2 (lower row, pptv) for the Northern Hemisphere (25°-60°N) oceanic regions obtained from a compilation of observations [*Emmons et al.*, 2000, plus updates] and calculated by models. The mean values of the 10 individual models are shown with solid coloured lines and the standard deviation with dotted coloured lines. The ensemble mean (all models) is drawn as dashed black line for the S1w simulation (without shipping) and as solid black line for the S1 simulation (all emissions included), the intermodel standard deviation for S1 as grey shaded areas, and the observations as filled black circles (mean) and white rectangles (standard deviation). From [*EY7*].
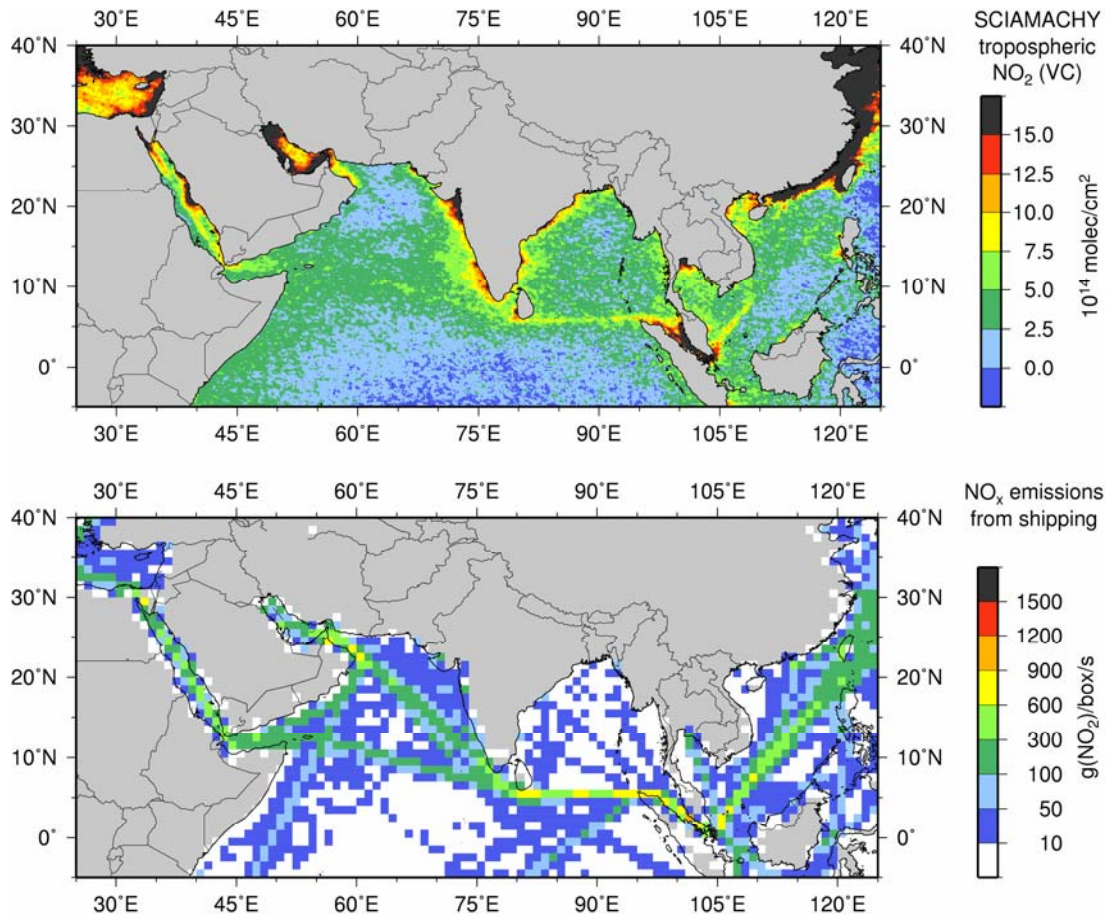
Figure 2-9. NO_x signatures of shipping in the Red Sea and Indian Ocean. Left: Tropospheric NO_2 columns derived from SCIAMACHY data from August 2002 to April 2004. Right: Estimated distribution of NO_x emissions by shipping in the same region. From [*EY8*].

matra and is too far east of the coast of Singapore.

To compare the model data to the satellite measurements, individual model results and SCIAMACHY data were interpolated to a common grid (0.5° x 0.5°). The models simulate similar tropospheric NO_2 columns over the remote ocean as observed by SCIAMACHY and also reproduce the overall pattern of the geographical distribution reasonably well. However, although the shipping signal is clearly visible in the satellite data it is not resolved by the models (see Figure 5 of [*EY7*]), because the intercomparison of modelled and observed NO_2 columns is complicated by several factors. First of all, the spatial resolution of the SCIAMACHY measurements (30 x 60 km²) is much higher than that of the global models (typically 5° x 5°) leading to higher NO_2 values in the localized plumes from ship emissions. Secondly, in the particular scene shown in Figure 2-9, shipping routes are

rather close to land. Given the low resolution of the models, the grid boxes close to the coast are dominated by NO_x emissions from land sources which are much stronger than emissions from shipping. Thus, the shipping signal cannot be identified in the coarse resolution model data in this region.

From this point of view, an intercomparison over the remote ocean (e.g. over the Atlantic) with satellite data far away from any land source would be preferable. However, up to now, no statistically significant satellite data on ship emissions are available for remote oceans. This is mainly due to the distributed nature of the emissions which leads to dilution and makes it difficult to distinguish the shipping signal from the effect of long-range transport from the US towards Europe. Increasing ship emission in the future should make detection possible, in particular if data from an instrument with good spatial coverage such as OMI or GOME-2 is used in combination with model calculations

of the contribution of long range transport. However, unambiguous identification and quantification will always be more difficult than in the special case between India and Indonesia with its unique emission pattern. Reduction in satellite measurement uncertainties through use of long-term averages and data from more instruments (e.g. OMI and GOME-2) combined with better constraints on land-based sources and higher spatial resolution in the models should facilitate such an intercomparison in the future.

The implications for the larger-scale of neglecting small-scale plume chemistry processes (see Section 2.3.1) depend on the resolution of the models. From the point of view of large-scale composition impacts, there is not enough observational data to confirm or refute the various emission datasets used by global models. There are sound chemical reasons why spreading shipping plumes over the size of grid squares used by global models should overestimate the NO_x, OH and ozone responses. Plume model studies have not yet come up with a simple reduction factor for the NO_x emissions that could be applied to global models. Thus global models tend to persist with the original NO_x emissions of the inventories, though preferring the ~3 Tg(N)yr^{-1} emission total over the ~6Tg(N)yr^{-1}, as in the study of [EY7].

Beside the evaluation of the present-day shipping signal in the model simulations, another key question addressed in the study of [EY7] was how NO_x and SO_2 emissions from international shipping might influence atmospheric chemistry in the next three decades if these emissions increase unabated. The models show future increases in NO_x and ozone burden which scale almost linearly with increases in NO_x emission totals. For the same ship emission totals but higher emissions from other sources a slightly smaller response is found. Changes in the annual mean near-surface level reach 5.5 ppb over the Atlantic (Figure 2-7b) and increase up to 7.4 ppb in the S4s scenario in 2030 (Figure 2-7h). Over Northern Europe where there are high levels of NO_x, and relatively low levels of insolation even in summer, the increase in NO_x from shipping decreases, rather than increases, ozone levels. This is due to reduction in oxidant levels as

OH is removed by the reaction $NO_2 + OH \rightarrow HNO_3$, and in winter to direct titration of ozone by NO_2. This effect can clearly be seen over the Baltic and the North Sea. The effect is stronger in the 2030 scenarios due to the increased background level of NO_x in Northern Europe, with shipping decreasing ozone by 3 ppb in the S4s scenario. The impact on the ozone decreases rapidly with height (Figure 2-7a,d,g). The most pronounced changes in tropospheric ozone columns are found over the Indian Ocean (1.16 DU in 2000 and 1.72 DU in 2030), related to the higher tropopause there and to more effective transport of ozone from the boundary into the upper troposphere. A second peak is simulated over the Atlantic. Over Europe, the increase in ship emissions under the 'Constant Growth Scenario' will enhance the positive trend in NO_2 over land up to 2030. In addition, efforts to lower European sulphate levels through reductions in SO_2 emissions from anthropogenic sources on land will be partly counteracted by the rise in ship emissions. The results discussed above are calculated under the assumption that all other emissions follow the IPCC SRES A2 scenario. However, if future ground based emissions follow a more stringent scenario, the relative importance of ship emissions becomes larger.

Another key issue of this work was to examine the range of results given by the individual models compared to the ensemble mean. Uncertainties in the different model approaches in the simulated ozone contributions from ships are found to be significantly smaller than estimated uncertainties stemming from the ship emission inventory, mainly the ship emission totals, the neglect of ship plume dispersion, and the distribution of the emissions over the globe.

2.3.2.2 Large-scale Effects on Aerosol Composition and Size-distribution

Emissions from shipping also impact on the chemical composition of aerosol particles, the aerosol size-distribution and thus aerosol optical thickness, direct aerosol forcing, and the ability of aerosol particles to act as cloud condensation nuclei. The dominant aerosol component resulting from ship emissions is sulphate, which is formed by the oxidation

of SO_2 by the hydroxyl radical (OH) in the gas phase or by O_3 and hydrogen peroxide (H_2O_2) in the aqueous phase of cloud droplets. The impacts of aerosols and their precursor emissions from ships have been studied with ECHAM5/MESSy1-MADE (hereafter referred to as E5/M1-MADE), a global climate model with detailed aerosol and cloud microphysics [*EY9*]. In E5/M1-MADE, an aerosol microphysics module (MADE) has been coupled to the global general circulation model ECHAM5 [*Roeckner et al.*, 2006], within the framework of the Modular Earth Submodel System MESSy [*Jöckel et al.*, 2005]. Aerosols are described by three log-normally distributed modes, the Aitken (typically smaller than 0.1 μm), the accumulation (typically 0.1 to 1 μm) and the coarse mode (typically larger than 1 μm). Aerosol components considered are sulphate, nitrate, ammonium, aerosol liquid water, mineral dust, sea salt, black carbon (BC) and particulate organic matter (POM). The simulations of the aerosol population take into account microphysical processes such as coagulation, condensation of sulphuric acid vapour and condensable organic compounds, particle formation by nucleation, size-dependent wet and dry deposition including gravitational settling, uptake of water and gas/-particle partitioning of trace constituents as well as liquid phase chemistry. Basic tropospheric background

chemistry (NO_x-HO_x-CH_4-CO-O_3) and the sulphur cycle are considered. Aerosol optical properties are calculated from the simulated aerosol size-distribution and chemical composition for the solar and thermal spectral bands considered by the GCM. These are used to drive the radiation module of the climate model. A detailed description of the model and the results of this study can be found in [*EY9*], and only a brief summary is given here.

The impact of shipping is estimated by calculating the differences between model experiments with and without taking shipping into account. In order to obtain significant differences with a reasonable number of model years, model dynamics have been nudged using operational analysis data from the European Centre for Medium-Range Weather Forecasts (ECMWF) from 1999 to 2004. The results have been averaged over all six years to reduce the effects of interannual variability.

To estimate uncertainties in present-day emission inventories (see Section 2.2), three model experiments under year 2000 conditions have been performed, using the ship emissions from [*EY4*] (hereafter "inventory A"), *Dentener et al.* [2006] (hereafter "inventory B") and *Wang et al.* [2007] (hereafter "inventory C"). In addition, a reference simulation was carried out neglecting ship

Table 2-2. Global burden of aerosol compounds considered in ECHAM5/MESSy1-MADE and the contribution from international shipping in the model simulations using the three emission inventories A [*EY4*], B [*Dentener et al.*, 2006], and C [*Wang et al.*, 2007]. From [*EY9*].

Compound	Inventory A		Inventory B		Inventory C	
	Atmospheric Burden (Tg)	Contribution of Shipping (%)	Atmospheric Burden (Tg)	Contribution of Shipping (%)	Atmospheric Burden (Tg)	Contribution of Shipping (%)
Sulphate	1.531	3.6	1.511	2.3	1.511	2.3
Ammonium	0.366	1.4	0.365	0.9	0.365	0.9
Nitrate	0.146	0.2	0.146	0.1	0.150	2.3
H₂O	17.881	1.0	17.784	0.4	17.841	0.6
BC	0.119	0.4	0.122	1.4	0.119	0.8
POM	1.040	0.1	1.047	0.1	1.050	1.1
Sea Salt	3.588	–	3.582	–	3.589	–
Mineral Dust	9.042	–	9.045	–	9.044	–

emissions.

In inventory A emissions are estimated from the fleet activity resulting into SO_2 emissions of 11.7 Tg for the world fleet in 2000. In inventory B emission estimates are based on fuel consumption statistics [*Dentener et al.*, 2006] with emission totals of 7.8 Tg SO_2 per year. Inventory C takes into account emissions from cargo and passenger vessels only, totalling 9.4 Tg SO_2 per year [*Corbett and Köhler*, 2003]. Inventories A and B provide annual average emissions whereas inventory C provides monthly averages. While the geographic distribution in inventory B considers the main shipping routes only, the geographic distribution in inventory A (AMVER) and inventory C (ICOADS) are based on shipping traffic intensity proxies. In all inventories, a major amount of SO_2 from shipping is emitted along the most frequented shipping routes between the eastern United States and Europe, as well as between Southeast Asia and the west coast of the USA. In general, the emissions in the first and third inventory are more widespread than those in the second.

Depending on the ship emission inventory used, 2.3% (inventory B,C) to 3.6% (inventory A) of the total annual sulphate burden stems from shipping. On average, 30-40% of the simulated sulphate mass concentration related to small particles (< 1 μm) near the surface above the main shipping routes originates from shipping. In contrast, contributions are smaller for black carbon emissions from shipping (0.4% in inventory A to 1.4% in inventory B) and particulate organic matter (0.1% in inventory A to 1.1% in inventory C), because the ship emission totals of both compounds are small compared to the contributions of fossil fuel combustion over the continents or to biomass burning. Despite high NO_x emissions from shipping, the global aerosol nitrate burden is only slightly increased by 0.1-0.2% using inventory A and B, but increased by 2.3% using inventory C. Due to the lower average SO_2 emissions in inventory C compared to inventory A, less ammonium is bound by sulphate and thus more ammonium-nitrate forms. This results in higher aerosol nitrate concentrations. Using inventory B, aerosol nitrate is lower than

using inventory C despite low SO_2 emissions. This is caused by the low NO_x emissions in inventory B compared to inventory C. The increase in the water soluble compounds sulphate, nitrate and associated ammonium causes an increase in the global burden of aerosol liquid water contained in the optically most active particles in the submicrometer size-range. This liquid water increase amounts to 4.3% (inventory A), 2.2% (inventory B), and 3.5% (inventory C). Table 2-2 summarizes the total burdens and the relative contribution of shipping for the aerosol compounds considered in E5/M1-MADE for all three ship emission inventories.

In addition to gaseous emissions, ship engines also release primary particles. Both emissions types affect the aerosol size-distribution. The model calculates a ship induced increase in the particle number concentration of the Aitken mode particles (typically smaller than 0.1 μm) of about 40% near the surface above the main shipping region in the Atlantic Ocean. Furthermore, the average geometric mean diameter of these particles decreases from 0.05 μm to 0.04 μm as the freshly emitted particles from shipping are smaller than the aged Aitken particles typically found above the oceans far away from any continental source. Subsequent processes such as condensation of sulphuric acid vapour enable some particles to grow into the next larger size-range, the accumulation mode (0.1 to 1 μm), increasing the number concentration in this mode. Accumulation mode particles act as efficient condensation nuclei for cloud formation. The model results indicate that the accumulation mode particle number concentration in the lowermost boundary layer above the main shipping routes in the Atlantic Ocean is increased by about 15%.

The changes in particle number concentration, particle composition and size-distribution result in an increase in aerosol optical thickness above the oceans of typically 2-3% (Figure 2-10). The direct aerosol effect from shipping is estimated to be –14 mW/m^2 in inventory A, –10 mW/m^2 in inventory B, and –9 mW/m^2 in inventory C.

Inventory A

Inventory B

Inventory C
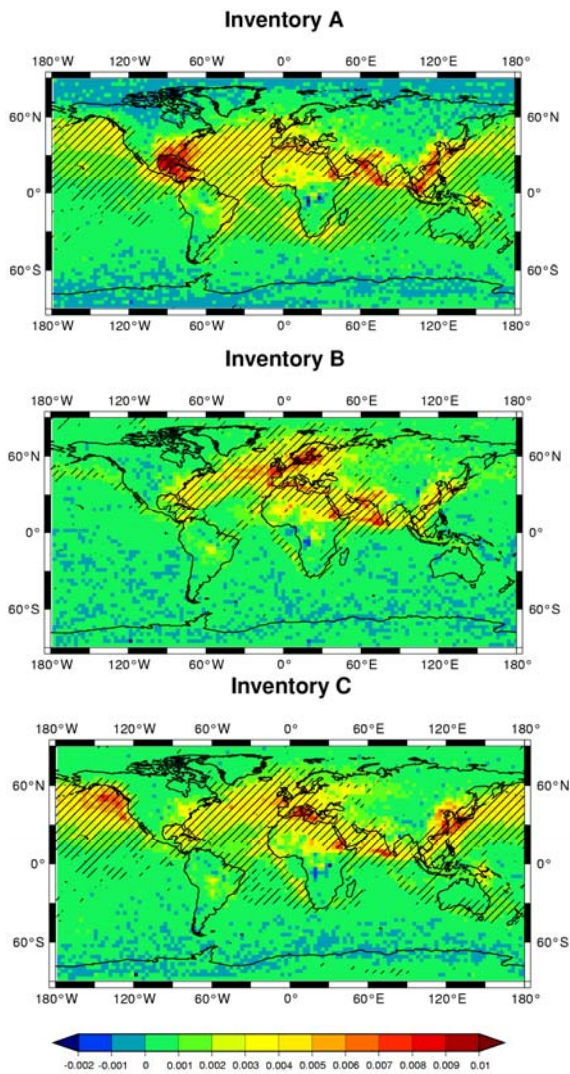
Figure 2-10. Climatological annual mean (1999-2004) of changes in total aerosol optical thickness at 550 nm due to shipping. Hatched areas show differences which are significant compared to the inter-annual variability. From [*EY9*].

2.4 Impact on Human Health [EY10]

At a local and regional-scale, ocean-going ships impact human health through the formation and transport of ground-level ozone, sulphur emissions and particulate matter [*EY10*]. In harbour cities, ship emissions are in many cases a dominant source of urban air pollution. Furthermore, emissions of NO_x, CO, VOCs, particles and sulphur (and their derivative species) from ships may be transported in the atmosphere over several hundreds of kilometres, and thus can contribute to air quality problems on land, even if they are emitted at sea [*EY7*]. This pathway is especially relevant for deposition of sulphur and nitrogen compounds, which cause acidi-

fication / eutrophication of natural ecosystems and freshwater bodies and threaten biodiversity through excessive nitrogen input. Therefore, control of emissions of NO_x, SO_2 and particles SO_2 emissions will have beneficial impacts on air quality, acidification and eutrophication.

Existing epidemiological studies consistently link ambient concentrations of particulate matter (PM) to adverse health effects, including asthma, heart attacks, hospital admissions, and premature mortality. In recent work, [*EY10*] demonstrate that PM emissions from ocean-going ships could cause numerous premature mortalities annually from cardiopulmonary disease and lung cancer. The following approach has been used to calculate the health impact due to shipping:

(1) *Determine pollutant emissions from ships:* Two different geospatial ship inventories were used, the International Comprehensive Ocean-Atmosphere Data Set (ICOADS) [*Wang et al.*, 2007; see lower panel in Figure 2-3], and the Automated Mutual-assistance Vessel Rescue system (AMVER) [*Endresen et al.*, 2003, see middle panel in Figure 2-3], to account for uncertainties in input data.

(2) *Apply global atmospheric chemistry models to estimate the increased concentrations due to ships:* Global-scale models may also model differently the $PM_{2.5}$ concentrations used in health-effects estimates. Therefore increased ambient $PM_{2.5}$ concentrations from marine shipping were compared by using two atmospheric models. The first, GEOS–Chem, is a global chemistry transport model driven by assimilated meteorological observations from the Goddard Earth Observing System (GEOS). GEOS-Chem output provided ambient dry concentrations of BC, POM, and sulphates from ocean-going ships separately from total $PM_{2.5}$ attributed to all other sources. The second model used was the global aerosol model E5/M1-MADE [*EY9*; see Section 2.3.2.2]. Along with global $PM_{2.5}$ concentrations attributed to non-ship sources, the E5/M1-MADE model provided ambient concentrations of BC, POM, and sulphates for direct comparison with GEOS-Chem results; separately the model produced concentrations of total

$PM_{2.5}$ constituents related to shipping (including nitrates and ammonium ions). Comparing results of each model with and without ship inventories of $PM_{2.5}$ components, the ambient concentrations of $PM_{2.5}$ due to marine shipping has been quantified.

(3) *Estimate increased risk to exposed population due to these additional concentrations:* The calculated annual $PM_{2.5}$ concentrations from (2) were used to assess annual mortality due to long-term PM exposure for various cases. This requires an estimate of exposed population. The 2005 global population estimates ($1^{o}x1^{o}$ resolution) from the Socioeconomic Data and Applications Center (SEDAC) at Columbia University have been used [*SEDAC*, 2007]. The atmospheric concentration output for each of the cases studied was interpolated to a $1^{o}x1^{o}$ resolution to conform to the population data resolution.

(4) *Calculate additional mortalities due to increased levels of $PM_{2.5}$:* The mortality estimates are based on cardiopulmonary and lung cancer causes of death for adults over 30 years of age. The *U.S. Census Bureau International Database* [2006] was applied to derive, by continent, the percentage of each grid cell's population over 30 years old. Incidence rates were estimated using World Health Organization (WHO) 2002 data aggregated to the WHO region level [*WHO*, 2004]. WHO cause of death by age estimates were used to derive incidence rates for the 30-99 age group for each of the six WHO regions. Similar to another assessment of global mortality from outdoor pollution, lung, tracheal and bronchial cancers were considered "lung cancers" [*Cohen et al.*, 2004]. These cancers are aggregated and non-distinguishable in WHO burden of disease estimates. United States cardiopulmonary incidence values obtained from *U.S. EPA* [2005] were used for North America. In calculating mortality effects Concentration-Response (C-R) functions derived from an American Cancer Society cohort study that examined the relationship between $PM_{2.5}$ and lung cancer and cardiopulmonary mortality in the US [*European Commission,* 2002] was used. Finally, a log-linear exposure function from *Pope et al.* [2002] was applied to estimate long-term mortality effects of $PM_{2.5}$.

The results indicate that shipping-related PM emissions are responsible for around 60,000 cardiopulmonary and lung cancer deaths annually, with most deaths occurring near coastlines in Europe, East Asia, and South Asia. This number is bounded by a range of 20,000 to 65,000 premature deaths when considering the uncertainties due to emission inventories and models as outlined above. Based on previous estimates of global $PM_{2.5}$-related mortalities [*Cohen et al.*, 2004], the [*EY10*] estimates indicate that 3% to 8% of these mortalities are attributable to marine shipping. *Cohen et al.* [2004] estimate that approximately 712,000 cardiopulmonary deaths are attributable to urban outdoor $PM_{2.5}$ pollution annually. Thus, the relationship between concentrations and mortality behaves proportionally within reasonable percentage uncertainty bounds. Uncertainties of the results are detailed in the Supporting Information of [*EY10*].

2.5 Radiative Forcing [EY7; EY9; EY11; EY12]

In addition to the impact on atmospheric composition and health, ship emissions have an impact on climate. A common metric to quantify climate impacts from different sources is radiative forcing in units of W/m^2, since there is an approximately linear relationship between global mean radiative forcing and change in global mean surface temperature [*Forster et al.*, 2007]. A positive RF implies warming whereas negative RF implies cooling to present-day climate. The changes in atmospheric composition due to ozone precursor emissions from ships have been discussed in Section 2.3. Section 2.5.1 gives a summary of the relevant SeaKLIM studies on the impact of ship emissions on clouds, while the radiative forcing from all key components emitted by ships is discussed in Section 2.5.2. The climate impact beyond radiative forcing in the form of temperature changes has been discussed by *Lee et al.* [2007].

2.5.1 Radiative Forcing due to Changes in Cloud Properties

Particles and their precursors from ship emissions are able to act as cloud condensa-

tion nuclei (CCN) in the water-vapour saturated environment of the maritime cloud or can change the surface tension due to their solubility. Amount and size of these particles depend on the fuel and also the kind of combustion, but can possibly result in a higher cloud droplet concentration. The perturbation of a cloud layer by ship-generated aerosol potentially changes the cloud reflectivity. This can be identified by elongated structures in satellite images known as ship tracks [*EY11*, *EY12*; see Section 2.5.1.1]. In addition to ship tracks, aerosol emissions from shipping can also affect clouds on a larger scale after dispersion [*EY9*]. The impact of shipping on large-scale clouds is discussed in Section 2.5.1.2.

2.5.1.1 Ship Tracks

The increase in cloud droplet number concentration can lead to an increased cloud reflectivity, known as indirect aerosol effect. Of all anthropogenic sources, ship-stack effluents provide the clearest demonstration of the indirect aerosol effect on cloud albedo. Curves of larger reflectance in cloud fields are frequently observed in satellite imagery and identified as ship tracks. Such perturbations of the marine stratiform cloud field are characterised as long-lived, narrow, curvilinear regions of enhanced cloud reflectivity which occur downwind of ships. An example of ship tracks appearing as bright features is given in Figure 2-11.

The first observations of ship tracks were presented by *Conover* [1966]. *Twomey et al.* [1968] concluded that the observations were consistent with the addition of CCN to a cloud layer with drop concentrations of about 1 to 10 cm^{-3}, i.e. a clean maritime boundary layer. *Twomey* [1974] later presented a link between cloud reflectance, droplet size and concentration, and CCN concentrations.

Several studies have shown that the droplet concentration in the ship tracks was enhanced significantly over the ambient cloud and that the effective radius was reduced [*Albrecht et al.,* 1988; *Radke et al.,* 1989; *Durkee et al.,* 2000; *Ferek et al.,* 2000].
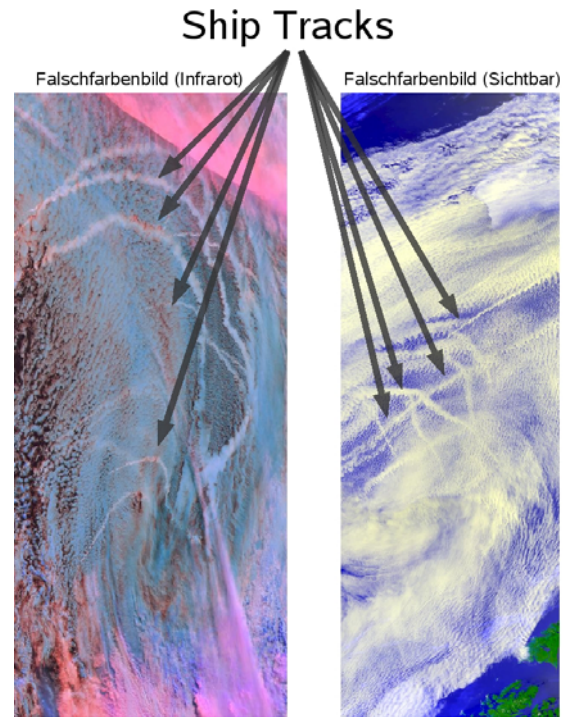
Figure 2-11. Ship tracks in a long strip of a 512-km swath observed by AATSR over the North Pacific (Graphic: M. Schreier, SeaKLIM Group). Shown are false-coloured plots for infrared (left) and visible (right) radiation.

To estimate the effect of ship emissions on the radiation budget of clouds, a case study for a satellite scene from MODIS (MODerate resolution Imaging Spectrometer) on the satellite Terra was performed over the west coast of North America [*EY11*]. The cloud optical thickness (Figure 2-12a) and the effective radius (Figure 2-12b) were calculated for a satellite scene via a semi-analytical approach [*Kokhanovsky et al.*, 2003] combined with a look-up-table-approach derived by libRadtran [*Mayer and Kylling*, 2005], to estimate the changes of the cloud optical properties. These values can also be used to calculate secondary cloud properties, e.g. the droplet number concentration (Figure 2-12c) and to compute the local radiative forcing via radiative transfer calculations.

In agreement with previous studies, the results of [*EY11*] show that ship emissions of aerosols and their precursors result in an increase of the droplet number concentration and a decrease in the effective radius in the cloud. A larger number of smaller droplets for fixed liquid water content results in the observed increase in the cloud optical thickness compared to the ambient cloud (Figure
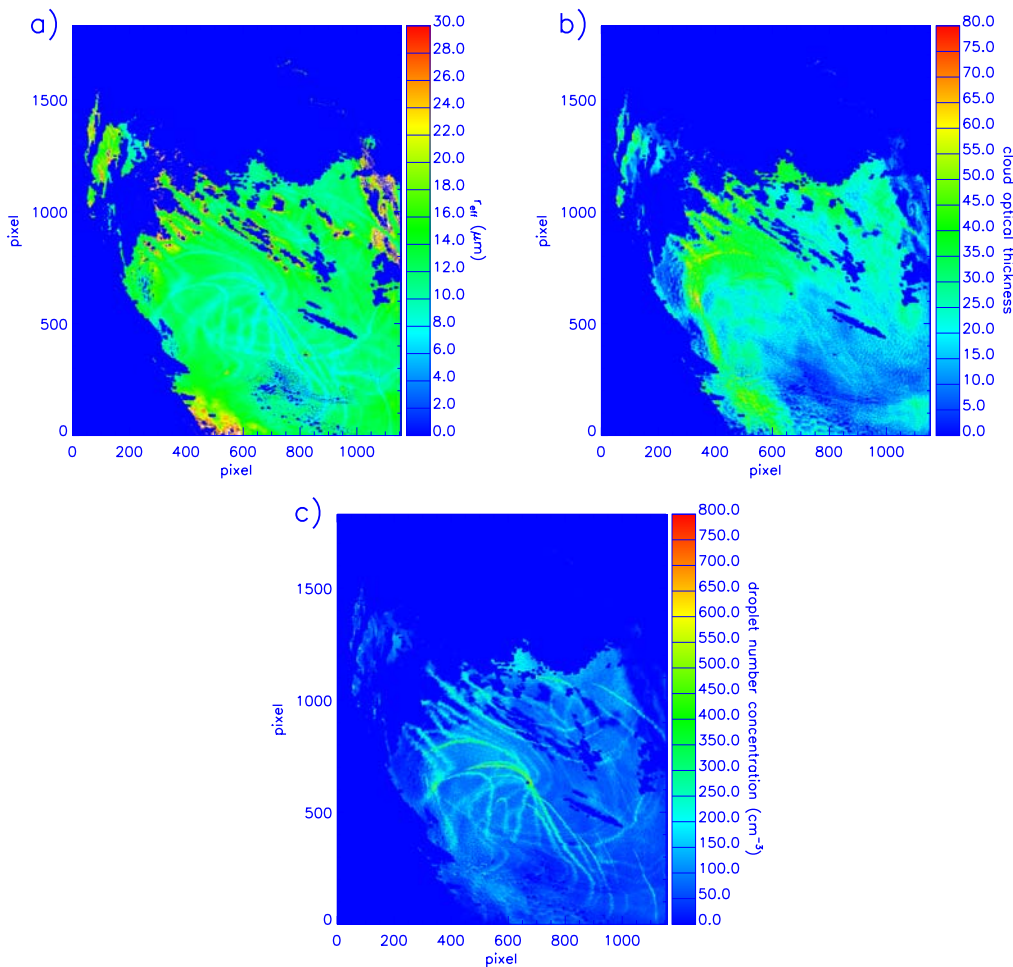
Figure 2-12. Cloud properties from a MODIS scene from 10th February 2003 on the west coast of North America. a) effective radius, b) cloud optical thickness, c) droplet number concentration. From [*EY11*].

2-12). The resulting cloud properties are used to calculate the radiation budget below and above the cloud. Assuming a mean solar zenith angle of 63° for the selected scene, the mean solar surface radiation below the ship track is decreased by 43.2 W/m^2 and the mean reflectance at top of atmosphere (ToA) is increased by 40.8 W/m^2. For the entire analysed scene the ship emission decreases the solar radiation at the surface by 2.1 W/m^2 and increases the backscattered solar radiation at ToA by 2.0 W/m^2, whereas no significant effect on thermal radiation was detected. With this study it could be shown that ship tracks change the radiation budget on a local scale. Thus, there was considerable interest to estimate their radiative impact on global scale.

In a follow up study, one year of ENVISAT-AATSR (Advanced Along Track Scanning Radiometer) satellite data for the year 2004 was analyzed to derive a global distribution of ship tracks and their radiative forcing [*EY12*]. An algorithm was developed and applied that extracts scenes dominated by marine low clouds susceptible for ship emissions and development of ship tracks. Ship tracks covered by higher clouds do not affect the net solar radiation by increased backscattering. The remaining relevant ship tracks are usually either embedded in low clouds or can be found in the vicinity of them. Therefore a three-step approach to identify ship tracks in satellite data was used in [*EY12*]. First, scenes with at least 20% coverage of very low clouds in the marine boundary layer (VLC) are automatically detected out of 4161 scenes which are selected as VLC scenes over the ocean in 2004. This reduced the data amount by 98%. Second, those scenes without ship tracks (3830 scenes) were sorted out and the remaining scenes (331 scenes) were analyzed for possible ship tracks. And third, the cloud optical proper-
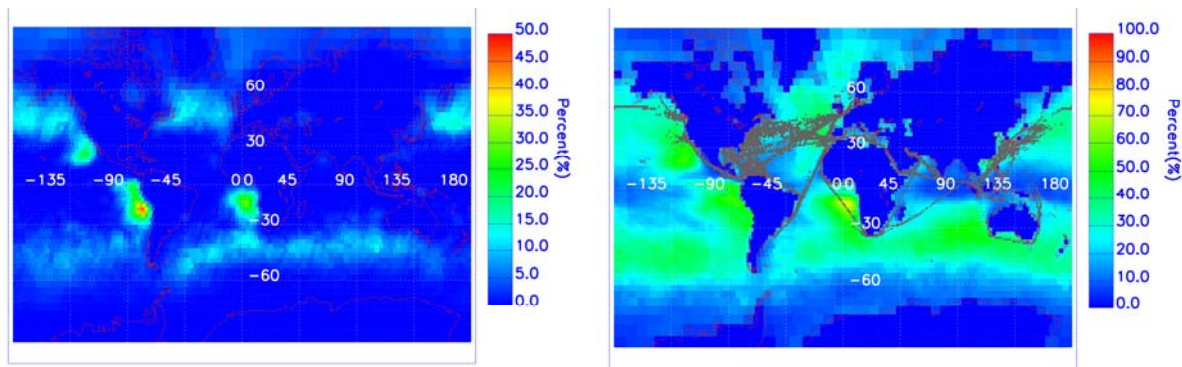
Figure 2-13.   *Left:* Annual mean global cover of very low clouds over the ocean in % derived from AATSR data. *Right:* Clouds below 680 hPa over the ocean derived from ISCCP data in 2004. Grey areas indicate high vessel densities. Note that the scale goes to 50% in the upper panel and to 100% in the lower panel. From [*EY12*].

ties of the ship tracks and the surrounding area within the selected scenes were used to estimate radiative forcing due to ship tracks.

To select scenes with low clouds over the ocean the following criteria have been applied: (1) reflectance for 0.87 μm larger than 0.2, and (2) temperature for 11 μm less than 4 K colder than local sea surface brightness temperature (approximated by the maximum temperatures of each image line). Criterion 1 is applied to distinguish clouds from cloud-free ocean. Criterion 2 is needed to estimate the cloud top height. It uses a temperature difference of 4 K between the cloud and the maximum temperature, which usually corresponds to the sea surface temperature. Clouds susceptible for ship tracks are very low [*Durkee et al.*, 2000; *Platnick et al.*, 2000] and assuming a wet adiabatic lapse rate of -0.6 K/100 m, a maximum temperature difference of about 4 K between cloud top temperature and sea surface temperature results in a cloud top height of around 700 m. If 256 successive lines fulfil criteria 1 and 2 by more than 20%, this part of the orbit (plus additional 256 lines on both ends) was selected as VLC scene for further analysis. The automated selection of scenes was verified by a thorough analysis of 1% of the complete satellite data (4 days, one for each season), showing a ship track detection efficiency of 70% when reducing the original data by 98%.

To validate the algorithm, the global coverage pattern of VLC that result from this analysis has been compared to the ISCCP

(International Satellite Cloud Climatology Project, *Rossow and Schiffer* [1991]) data base. ISCCP low clouds are defined within the altitude range from 1000 to 680 hPa, a much wider range than represented by VLC, leading to higher cloud coverage. The maxima in VLC coverage derived from AATSR data in 2004 are found in the subtropical latitudes at the west coasts of southern Africa, South America, and North America (Figure 2-13, left panel). In these regions cold upwelling ocean currents lead to a stable atmospheric boundary layer in combination with a low coverage by higher level clouds. In both hemispheres there is also a broad belt of increased coverage between 30° and 60°, resulting from the global Hadley circulation. A very similar pattern is found in the low cloud fraction of ISCCP data from the year 2004 (Figure 2-13, right panel). But, as expected, the amount of VLC in the AATSR data is much smaller than in ISCCP, as the temperature criterion selects clouds below 900 hPa whereas the boundary pressure level for the ISCCP low clouds is 680 hPa.

To derive a global distribution, ship tracks were analysed visually from a visible-infrared colour composite and a near-infrared combination of the VLC scenes. Figure 2-14 shows the percent coverage of ship tracks derived from AATSR measurements in 2004 on the left. It shows the predominant area for ship track occurrence is a latitude band between 30º – 60º N in both the North Atlantic and the Pacific Ocean. In the Southern Hemisphere ship tracks are
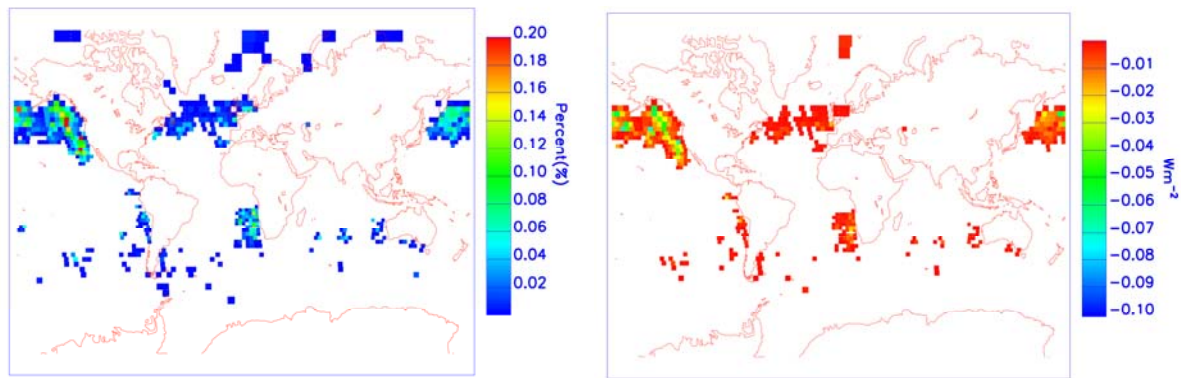
Figure 2-14. Annual mean coverage distribution of ship tracks (left) and resulting radiative forcing in W/m^2 (right). From [*EY12*].

much less frequent and are concentrated between 10º – 30º S off the west coasts of southern Africa and Australia. In these areas high amount of low clouds coincide with high ship emissions (compare Figure 2-13 and 2-14). The reduced effective radius and the higher cloud-optical thickness increased the backscattering ability of the ship tracks compared to the surrounding clouds (Figure 2-14, right panel). The global analysis of ship tracks by [*EY12*] showed that the change in backscattered radiation at ToA between ship track and surrounding cloud is highly variable and can reach between 10 and 100 W/m^2. For particular regions on the west coast of North America, the annual mean RF due to ship tracks estimated by the changes in backscattered radiation at ToA can be up to -50 W/m^2. The global annual mean RF due to ship tracks is small (-0.4 to -0.6 m/Wm^2) and negligible compared to global model estimates on the total indirect aerosol effect and RF contributions of other ship emissions, see Sections 2.5.1.2 and 2.5.2.

2.5.1.2 Large-scale Impact on Clouds

Ship plumes mix with the ambient air and are able to affect the surrounding clouds on a larger scale than visible ship tracks. To quantify the overall effect, global aerosol model studies or satellite trend analyses are needed.

In addition to the changes in chemical composition discussed in Section 2.3, the second important effect is a modification of cloud microphysical and optical properties. In par-

ticular, accumulation mode particles act as efficient condensation nuclei for cloud formation.

In [*EY9*] three different ship inventories under year 2000 conditions with different emission totals and global distributions were applied to study uncertainties in the radiative forcing due to the prescribed ship emissions inventory (see also Section 2.3.2.2). As an example, annual emissions of SO_2 from international shipping in the three different emission inventories are displayed in Figure 2-14, upper row.

The model simulations by [*EY9*] reveal that the effect of changes in particle number concentration, aerosol size-distribution and particle composition due to ship emissions on clouds is mainly confined to the lower troposphere, from the surface up to about 1.5 km. This implies that regions with a frequent high amount of low clouds above the oceans are most susceptible to ship emissions. Such regions coincide with dense ship traffic over the Pacific Ocean west of North America, the Atlantic Ocean west of southern Africa, and the North eastern Atlantic Ocean. Figure 2-15 shows the geographical distribution of 6-year annual average changes in ToA shortwave cloud forcing and the corresponding zonal means for the three ship emission inventories A, B, and C.

The indirect aerosol effect of ships is found to be far larger (–190 or –600 mW/m^2, depending on the inventory) than the direct aerosol effect, contributing 17% or 39% to the total indirect effect of anthropogenic
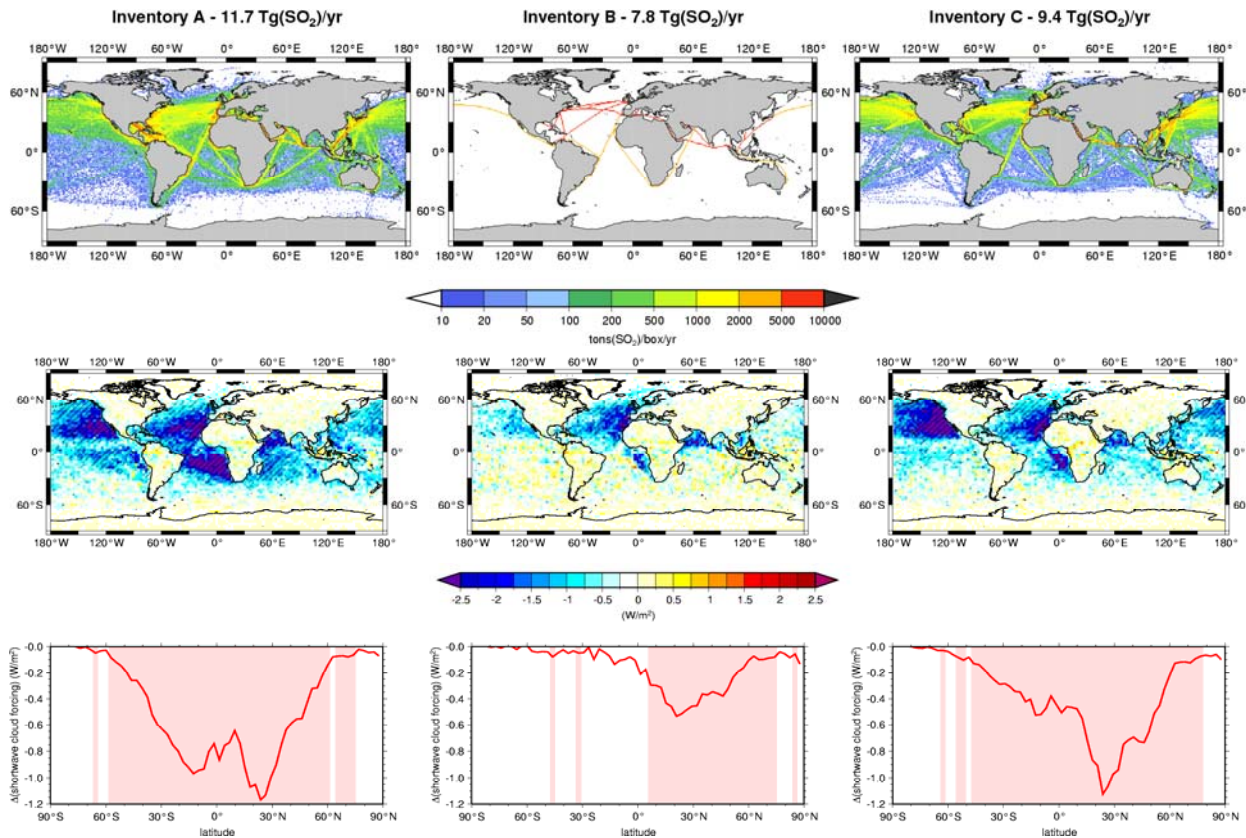
Figure 2-15. *Upper Row:* Annual emissions of SO_2 from international shipping in tons per 1°×1° box. *Middle and Lower Row:* Multi-year average of simulated changes in zonal mean shortwave cloud forcing due to shipping at the top of the atmosphere (ToA) in W/m^2. Middle row shows the geographical distribution, lower row zonal averages. Hatched areas (upper row) and light-red shaded areas (lower row) show differences which are significant at the 99% confidence level compared to the inter-annual variability. From [*EY9*].

aerosols. This contribution is high because ship emissions are released in regions with frequent low marine clouds in an otherwise clean environment. In addition, the potential impact of particulate matter emissions on the radiation budget is larger over the dark ocean surface than in polluted regions over land. A simple extrapolation from the contribution of shipping to the total aerosol burden to its radiative effects is therefore not appropriate and underestimates the indirect aerosol effect from shipping. Local changes in the Pacific and Atlantic can reach up to –2 to –5 W/m^2. In contrast, changes above the Indian Ocean are smaller despite the high ship traffic density. This is related to the fact that the low cloud amount susceptible to ship emissions is rather low in this region.

2.5.2   Net Radiative Forcing from Shipping

Ship emissions of CO_2, SO_2, NO_x and other O_3 precursors perturb atmospheric concen-trations of greenhouse gases (CO_2, CH_4 and O_3), and aerosols (mainly sulphate), causing both positive and negative contributions to direct radiative forcing of climate. In addition, sulphate causes a significant indirect radiative forcing, via changes in cloud microphysics. As CO_2 is a well-mixed greenhouse gas, its atmospheric lifetime (>100 yr) is much longer than global atmospheric mixing timescales, so ship CO_2 emissions generate a radiative forcing in just the same way as any other CO_2 source. SO_2 and NO_x are reactive species with much shorter lifetimes (days). Emissions of these species generate sulphate and O_3, which themselves have lifetimes of days to weeks in the troposphere. Perturbations to sulphate and O_3, and hence their radiative forcings, have regional-scale structure, and are closely related to their precursor source distributions. Emissions of NO_x, and the O_3 they form, lead to enhanced levels of the hydroxyl radical (OH), increasing removal rates of CH_4, generating a nega-

tive radiative forcing [*Wild et al.,* 2001; *Derwent et al.,* 2001]. Because of the decadal CH_4 lifetime, this forcing has a global signature.

The indirect aerosol effect of shipping on climate discussed in Section 2.5.1 results in a negative RF which is, in absolute numbers, much higher than the negative RF caused by the scattering and absorption of solar radiation by aerosol particles (direct aerosol effect) or the positive RF due to greenhouse gases, mainly carbon dioxide and ozone. NO_x and other ozone precursor emissions from shipping also increase removal rates of CH_4, thus generate a negative radiative forcing. These estimated forcings are all in the range of ±15 to 50 mW/m^2 [*Endresen et al.,* 2003; *EY7*].

RF due to direct CH_4 from shipping (0.52 Tg CH_4 from fuel and tanker loading [*EY4*]) has

not been estimated so far. However, because of the small contribution ($< 0.2\%$) to total anthropogenic CH_4 emissions [*Olivier et al.,* 2005], the resulting forcings are expected to be negligible compared to the other components. Figure 2-16 shows the RF due to shipping from CO_2, O_3, CH_4, and the direct effect of sulphate particles from *Endresen et al.* [2003] and [*EY7*] as well as the radiative forcing due to ship tracks [*EY12*] in comparison to the estimated direct and indirect aerosol effect from [*EY9*] for the three ship emission inventories A, B, and C.

[*EY11*] showed that ship tracks can change the radiation budget on a local scale, but are short lived and cover a very small fraction of the globe so that their radiative effect on the global scale is negligible (–0.4 to –0.6 mW/m^2 $\pm40\%$ [*EY12*]). The contribution of water vapour emissions from shipping is also negligible. Also shown is a previous esti-

Ship RF
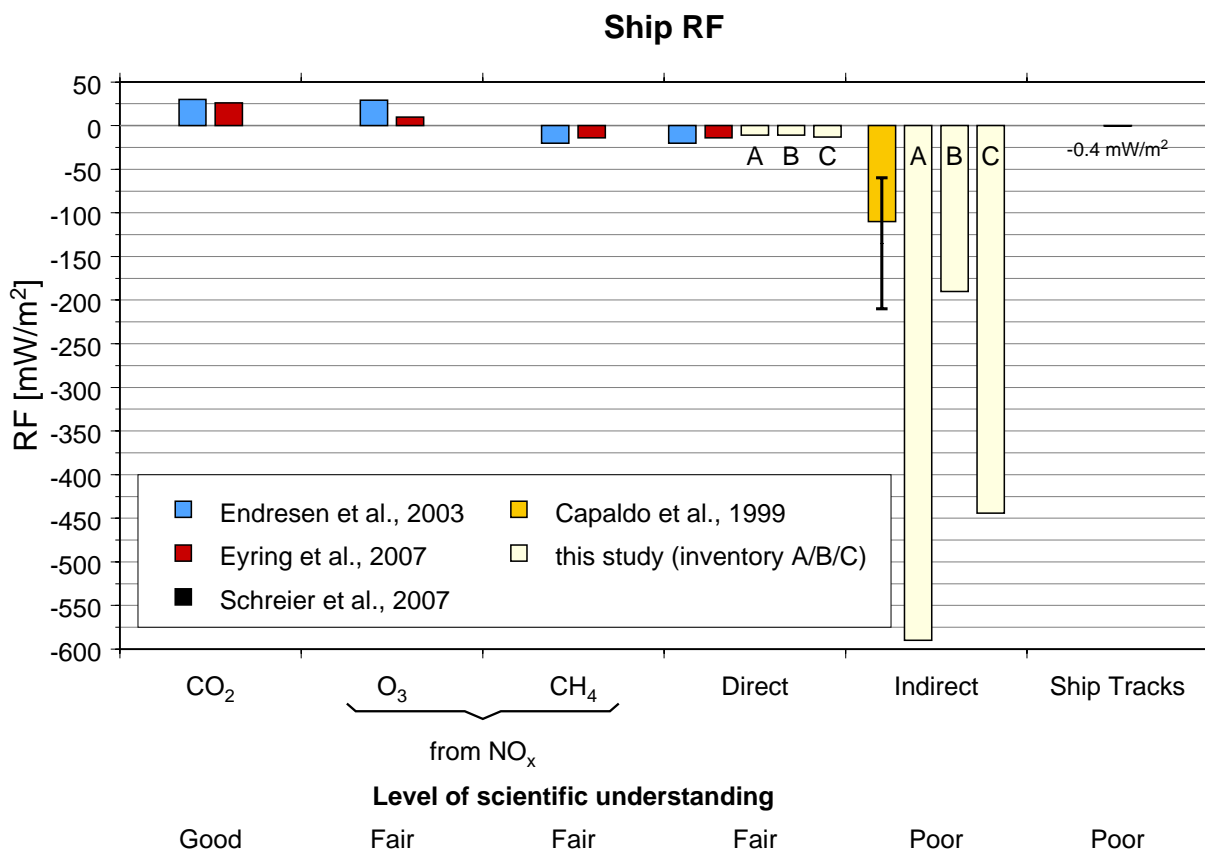
Figure 2-16. Annual mean radiative forcing (RF) due to emissions from international shipping in mW/m^2. Values for CO_2, O_3, CH_4, and sulphate (direct aerosol effect) are taken from different modeling studies. The indirect aerosol effect displayed with the orange bar includes the first indirect effect of sulfate aerosols only. The error bar depicts the range spanned by additional sensitivity studies. The estimated direct and indirect aerosol effect calculated for various emission inventories (yellow bars A, B, and C) also includes changes due to black carbon, particulate organic matter, ammonium, nitrate, and H_2O from shipping in addition to sulphate and refers to the changes in all-sky shortwave radiation fluxes and net cloud forcing at the top of the atmosphere. From [*EY9*].

mate by *Capaldo et al.* [1999], who used a global model without detailed aerosol microphysics and aerosol-cloud interaction and assessed the first indirect effect of sulphate plus organic material particles (–110 mW/m^2).

The model results on the indirect aerosol effect discussed in Section 2.5.1.2 and shown in Figure 2-15 also indicate that the geographical distribution of emissions over the globe plays a key role determining the global impact of shipping. The large differences in the model results obtained with three different ship emission inventories [*EY4*; *Dentener et al.*, 2006; *Wang et al.*, 2007] imply a high uncertainty, but on the other hand the main conclusions of [*EY9*] hold for all three inventories. For all inventories used, the present-day net RF from ocean-going ships is strongly negative, in contrast to, for instance, estimates of RF from aircraft [*Sausen et al.*, 2005]. In addition, the direct aerosol effect due to scattering and absorption of solar light by particles from shipping is only of minor importance compared to the indirect aerosol effect.

Additional sensitivity simulations with sulphur free fuel with E5/M1-MADE revealed that about 75% of the direct and indirect aerosol effect from shipping is related to the fuel sulphur content, which is currently about 2.4% [*EPA*, 2006]. Thus, a simple upscaling of the results from *Capaldo et al.* [1999] to the total indirect effect considering all relevant aerosol compounds from shipping results in about –150 mW/m^2. This value is comparable to the indirect aerosol effect calculated by [*EY9*] using inventory B (–190 mW/m^2). Inventory B has similar emission totals for SO_2 (7.8 Tg yr^{-1}) as the ship emission inventory used by *Capaldo et al.* [1999] totalling 8.4 Tg yr^{-1}.

2.6   Summary

With emissions of international shipping taking place both in coastal areas and open oceans their impact on the atmosphere and contribution to climate, health and environmental impacts can be significant.

Over the past decades, the world merchant fleet, fuel consumption and emissions from international shipping have substantially increased. The results of [*EY4*] suggest a fuel consumption increase from 64.5 million metric tons (Mt) in 1950 to 280 Mt in the year 2001. They reveal that shipping emitted around 800 Mt CO_2 and contributed around 2.7% to all anthropogenic CO_2 emissions in 2000. For comparison, aviation and road transport contributed around 2.2% and 14%, respectively. Other comparisons suggest that shipping accounts for around 15% of all global anthropogenic nitrogen oxide (NO_x) emissions and for around 8% of sulfur dioxide (SO_2) emissions. These relatively high contributions result because most marine engines operate at high temperatures and pressures without effective NO_x emission reduction technologies and because of high average sulfur content (2.4%-2.7%) in marine fuels. Emission scenario calculations up to the year 2050 show that if no control measures are taken beyond existing national and international regulations, NO_x emissions might increase up to a value higher than present day global road transport by 2050 (38.8 Tg (NO_2)/yr). If the sulphur content remains at present day levels a doubling of ship SO_2 emissions can be expected. However, given the air quality issue of shipping emissions, further emission reductions of total NO_x and SO_2 emissions are likely. It could be shown that using aggressive NO_x emission reduction technologies, a significant decrease down to 15% of today's NO_x emissions could be reached until 2050 despite a growing fleet [*EY5*].

Box model studies with emission data from a large container ship imply that large scale models with a horizontal resolution of several hundred kilometres might overestimate the ship-induced ozone production because emissions are instantaneously diluted into large grid-boxes [*EY6*]. This shows the importance to parameterise subgrid processes in global models. At noon, the differences between the plume and the global model approach in the ship induced ozone changes are largest. The global model approach overestimates the plume model results by up to a factor of three, depending on emission time and source strength. A method to derive effective ship emissions has been developed for a particular case. It has been shown that

this method is able to account for the neglect of subgrid processes for different emission times, emission strength and sizes of the large scale box, which cannot be resolved by global models. Overall the results highlight the importance of plume chemistry but also the complexity of near-field processes. More research is required to develop a suitable method to parameterise subgrid-scale processes in global models.

Evidence for the importance of ship emissions comes from satellite observations by SCIAMACHY that clearly show enhanced tropospheric NO_2 columns along the major international shipping routes in the Red Sea and over the Indian Ocean [EY8]. The global impact of shipping on chemistry as well as associated uncertainties have been quantified from an ensemble of state-of-the-art atmospheric chemistry models for present-day conditions and for two future ship emission scenarios for the year 2030 [EY7]. Large increases in tropospheric ozone column are found over the Atlantic and even stronger over the Indian Ocean (1 DU in 2000 and up to 1.8 DU in 2030). If all other emissions vary according to the IPCC SRES A2 scenario, shipping contributes with 3% to increases in ozone burden until 2030 and with 4.5% to increases in sulphate. However, if land-based emissions decrease but ship emissions continue to grow, shipping will significantly counteract the benefits derived from land-based emission reductions.

At a local and regional-scale, ocean-going ships impact human health through the formation and transport of ground-level ozone, sulphur emissions and particulate matter [EY10]. In harbour cities, ship emissions are in many cases a dominant source of urban air pollution. Furthermore, emissions of NO_x, CO, VOCs, particles and sulphur (and their derivative species) from ships may be transported in the atmosphere over several hundreds of kilometres, and thus can contribute to air quality problems on land, even if they are emitted at sea [EY7; EY10]. In [EY10] it has been demonstrated that PM emissions from ocean-going ships could cause between 20,000 to 65,000 premature mortalities annually from cardiopulmonary disease and lung cancer. These health impacts are par-

ticularly concentrated in areas of Southeast Asia and Europe.

In addition to the impact on atmospheric composition and health, ship emissions have an impact on climate. A common metric to quantify climate impacts from different sources is radiative gorcing' (RF) in units of W/m^2. The perturbation of a cloud layer by ship-generated aerosol changes the cloud reflectivity and is identified by elongated structures in satellite images, known as ship tracks. Compared to the surrounding cloud a significant increase in droplet number concentration and optical thickness as well as a decrease in effective radius is found within the ship tracks [EY11]. Ship tracks can change the radiation budget on a local scale, but are short lived and cover a very small fraction of the globe so that their radiative effect on the global scale is negligible (–0.4 to –0.6 mW/m^2 ±40% [EY12]).

Simulations with the global model system ECHAM5/MESSy1-MADE show a high impact of gaseous and particulate emissions from ocean-going ships on maritime clouds [EY9]. The additional aerosol particles brighten the clouds above the oceans, which then are able to reflect more sunlight back into space. Although the uncertainties associated with this study are still high, the model results clearly indicate that the cooling due to altered clouds far outweighs the warming effects from greenhouse gases such as carbon dioxide (CO_2) or ozone from shipping, overall causing a negative radiative forcing today. The indirect aerosol effect of ships on climate is found to be far larger than previously estimated contributing up to 39% to the total indirect effect of anthropogenic aerosols. This contribution is high because ship emissions are released in regions with frequent low marine clouds in an otherwise clean environment and the potential impact of particulate matter on the radiation budget is larger over the dark ocean surface than over polluted regions over land.

As these studies indicate, reductions in sulphur emissions could result in regional reductions in its resultant negative radiative forcing. The climatic trade-off between positive and negative radiative forcing is still a topic of scientific research, but from what is

currently known, a simple cancellation of global means is potentially inappropriate and a more comprehensive assessment metric is required. It is emphasized, that CO_2 remains in the atmosphere for a long-time and will continue to have a warming effect long after its emission. In contrast, sulphate has a residence time in the atmosphere of approximately one week, and the climate response from sulphate is of the order decades whilst that of CO_2 is of the order of centuries.

While the control of NO_x, SO_2 and particle emissions from ships will have beneficial impacts on air quality, acidification and eutrophication, CO_2 reductions from all sources, including ships and other freight modes, are urgently required to reduce global warming.

2.7   Conclusions and Outlook

With the work summarised in Section 2 [*EY4-12*], a variety of important results have been achieved. For example, the importance of ship emissions and the projected future increases were brought to the attention of the international community [*EY4; EY5*]. One of the major findings was that the potential of particle emissions or their precursors from shipping to modify the microphysical and optical properties of clouds (the so-called "indirect aerosol effect") is significant and more important than previously recognised [*EY9*]. The studies also showed that a large fraction of ship emissions occurs within 400 km of coastlines, and cause air quality problems in coastal areas and harbours with heavy traffic [*EY7; EY10*]. The long range transport of ship emissions motivated the Task Force on Hemispheric Transport of Air Pollution (TF HTAP) working under the UNECE Convention on Long-range Transboundary Air Pollution (CLRTAP) to include ship emissions among sources relevant for the intercontinental transport of air pollution.

Nevertheless, further work is needed to reach a complete synthesis of the results. A more thorough comparison of the impacts of shipping to impacts from aviation and road traffic is planned in the future and some processes need to be further investigated.

Uncertainties in the simulated ozone contributions from ships for different model approaches are found to be significantly smaller than estimated uncertainties stemming from the ship emission inventory and the neglect of plume processes. This reflects that the net ozone change from ship emissions under relatively clean conditions in global models is rather similar and suggests that the atmospheric models used in [*EY7*] are suitable tools to study these effects.

However, there is considerable uncertainty in the ship emission inventories, which has to be further explored. One approach is to develop bottom-up inventories based on ship movement data and compare them with the activity-based top-down approach used in [*EY4*]. In a bottom-up approach emissions are directly estimated within a spatial context so that spatially-resolved emissions inventories are developed based on detailed activities associated to locations. Although bottom-up approaches can be more precise, large-scale bottom-up inventories are also uncertain because they estimate engine workload, ship speed, and most importantly, the locations of the routes determining the spatial distribution of emissions. Both emission totals and the geographical distribution are key to simulate atmospheric impacts. For example, [*EY9*] showed that the geographical distribution of ship emissions over the globe plays a key role determining the global impact of shipping. The large differences in the model results obtained with three different ship emission inventories imply a high uncertainty in the input data.

From the point of view of large-scale composition impacts, there is not enough observational data to confirm or refute the various emission datasets used by global models [*EY7*]. There are sound chemical reasons why spreading shipping plumes over the size of grid squares used by global models should overestimate the NO_x, OH and ozone responses [*EY6*]. Plume model studies have not yet come up with a simple reduction factor for the NO_x emissions that could be applied to global models. So far the results are based on one given background environment. The step from a case study [*EY6*] to a suitable parameterisation of subgrid-scale processes in global models has to be made

for both gaseous and particulate emissions. To reach this, more measurements and model studies are needed to understand plume processes. The models studies also need to include different approaches than the one applied in [*EY6*]. More work is needed on the thermodynamical MBL parameters that control transport of ship effluent into the cloud layer, including large-eddy simulations of the MBL stability, ship track buoyancy affected by fuel burning, and subcloud saturation conditions.

Evaluation of the global models' response to ship emissions is still at a preliminary stage and is currently limited by the coarse spatial resolution of the models, the uncertainty in the measurements, the lack of sufficient in situ measurements over the ocean, and the difficulty to separate ship emissions from other even stronger emission sources close to land [*EY7*]. Additional in situ measurements inside single ship plumes, but also in the corridor of the shipping lanes are needed and the set up of a measurement network onboard ships similar to MOZAIC (Measurements of OZone and water vapour by in-service AIrbus airCraft; *Marenco et al.* [1998]) or CARIBIC (Civil Aircraft for Global Measurement of Trace Gases and Aerosols in the Tropopause Region; *Brenninkmeijer et al.* [2007]) onboard civil aircrafts would be desirable. Unambiguous detection of ship emissions in satellite data is currently only available for the region of the Red Sea and the Indian Ocean [*Beirle et al.*, 2004; *EY8*], where shipping routes are close to the coastal area. Reduction in measurement uncertainties through use of long-term averages and data from more instruments (e.g. OMI and GOME-2) combined with better constraints on land-based sources and higher spatial resolution in the models should facilitate such an intercomparison in the future.

Current uncertainties of global modelling studies on the effects of emissions from shipping on aerosols and clouds are expected to be much higher than in the case of the ozone change studies. In particular the indirect aerosol effect [*EY9*] depends crucially on simulated key properties such as the aerosol size-distribution and the activation of aerosol particles in clouds. Minor changes of these properties can have a significant impact on the simulated indirect effect. Furthermore, changes in cloud properties such as cloud liquid water content, cloud cover and precipitation formation due to ship emissions impact on atmospheric chemistry via wet deposition and changes in scavenging efficiency. Changes in atmospheric chemistry such as ozone or OH concentrations result in a feedback on aerosols e.g. via modified oxidation rates of SO_2. Further model development in particular on the representation of aerosol size-distribution, aerosol activation, aerosol-cloud interaction and extension of feedback mechanisms is needed in addition to extended measurement data e.g. of the size-distribution and composition of particles emitted by ships to reduce current uncertainties in global model studies.

Ship tracks are only the obvious stage of the indirect aerosol effect. An analysis of the global distribution of ship tracks and an estimation of their influence on the radiation budget has been derived from AATSR data [*EY12*]. However, the polar orbit of ENVISAT limits the knowledge about the development of ship tracks over time. An investigation via geostationary satellites like Meteosat-8 offers the opportunity to analyse the temporal and spatial development of ship tracks for a better estimate of the influence on marine boundary layer clouds. In addition, satellite data of marine boundary layer clouds offer the possibility to compare the cloud optical properties of different areas with low vessel traffic density with areas of high vessel traffic density or high ship track density. If there is a high influence from ship emissions, a clear difference should be observable. This can be used to estimate the radiative effect.

The European Assessment of Transport Impacts on Climate Change and Ozone Depletion will provide an up-to-date assessment of the impact of shipping on atmospheric composition and climate (ATTICA, see http://www.pa.op.dlr.de/attica/). This assessment and other ongoing research efforts will continue to inform policymakers and will help to further implementation of needed emission reduction and mitigation strategies.

Acknowledgements

References

The Section 'Integrated Author's References' lists the author's publications which are explicitly discussed in the manuscript. The Section 'Selected Author's References' contains a selection of references which are cited in addition in the manuscript. The last Section 'External references' lists other publications.

Integrated Author's References

[EY1]   **Eyring, V.**, N. R. P. Harris, M. Rex, T. G. Shepherd, D. W. Fahey, G. T. Amanatidis, J. Austin, M. P. Chipperfield, M. Dameris, P. M. De F. Forster, A. Gettelman, H. F. Graf, T. Nagashima, P.A. Newman, S. Pawson, M. J. Prather, J. A. Pyle, R. J. Salawitch, B. D. Santer, and D. W. Waugh (2005), A strategy for process-oriented validation of coupled chemistry-climate models, *Bull. Am. Meteorol. Soc.*, 86, 1117–1133.

[EY2]   **Eyring, V.,** N. Butchart, D. W. Waugh, H. Akiyoshi, J. Austin, S. Bekki, G. E. Bodeker, B. A. Boville, C. Brühl, M. P. Chipperfield, E. Cordero, M. Dameris, M. Deushi, V. E. Fioletov, S. M. Frith, R. R. Garcia, A. Gettelman, M. A. Giorgetta, V. Grewe, L. Jourdain, D. E. Kinnison, E. Mancini, E. Manzini, M. Marchand, D. R. Marsh, T. Nagashima, P. A. Newman, J. E. Nielsen, S. Pawson, G. Pitari, D. A. Plummer, E. Rozanov, M. Schraner, T. G. Shepherd, K. Shibata, R. S. Stolarski, H. Struthers, W. Tian, and M. Yoshiki (2006), Assessment of temperature, trace species and ozone in chemistry-climate model simulations of the recent past, *J. Geophys. Res.*, 111, D22308, doi:10.1029/2006JD007327.

[EY3]   **Eyring, V.**, D. W. Waugh, G. E. Bodeker, H. Akiyoshi, J. Austin, B. Boville, P. Braesicke, C. Brühl, N. Butchart, M. P. Chipperfield, E. Cordero, M. Dameris, R. Deckert, M. Deushi, S. M. Frith, R. R. Garcia, A. Gettelman, M. Giorgetta, D. E. Kinnison, E. Mancini, E. Manzini, D. R. Marsh, S. Matthes, T. Nagashima, P. A. Newman, J. E. Nielsen, S. Pawson, D. A. Plummer, G. Pitari, E. Rozanov, M. Schraner, T. G. Shepherd, K. Shibata, B. Steil, R. Stolarski, W. Tian, and M. Yoshiki (2007), Multimodel projections of ozone recovery in the 21st century, *J.*

Geophys. Res., 112, 112, D16303, doi:10.1029/2006JD008332.

[EY4]   **Eyring, V.**, H. W. Köhler, J. van Aardenne, and A. Lauer (2005), Emissions from International Shipping: 1. The last 50 Years, *J. Geophys. Res.*, D17305, doi:10.1029/2004JD005619.

[EY5]   **Eyring, V.**, H. W. Köhler, A. Lauer, and B. Lemper (2005), Emissions From International Shipping: 2. Impact of Future Technologies on Scenarios Until 2050, *J. Geophys. Res.*, 110, D17306, doi:10.1029/2004JD005620.

[EY6]   Franke, K., **V. Eyring**, R. Sander, J. Hendricks, A. Lauer, and R. Sausen (2007), Toward Effective Emissions of Ships in Global Models, *Meteorol. Z.*, 17, 2, 117-129(13), 2008.

[EY7]   **Eyring, V.**, D. S. Stevenson, A. Lauer, F. J. Dentener, T. Butler, W. J. Collins, K. Ellingsen, M. Gauss, D. A. Hauglustaine, I. S. A. Isaksen, M. G. Lawrence, A. Richter, J. M. Rodriguez, M. Sanderson, S. E. Strahan, K. Sudo, S. Szopa, T. P. C. van Noije, and O. Wild (2007), Multi-model simulations of the impact of international shipping on atmospheric chemistry and climate in 2000 and 2030, *Atmos. Chem. Phys.*, 7, 757-780.

[EY8]   Richter, A., **V. Eyring**, J. P. Burrows, H. Bovensmann, A. Lauer, B. Sierk, and P. J. Crutzen (2004), Satellite measurements of NO_2 from international shipping emissions, *Geophys. Res. Lett.*, 31, L23110, doi:10.1029/2004GL020822.

[EY9]   Lauer, A., **V. Eyring**, J. Hendricks, P. Jöckel, and U. Lohmann (2007), Global model simulations of the impact of ocean-going ships on aerosols, clouds, and the radiation budget, *Atmos. Chem. Phys.*, 7, 5061-5079.

[EY10]   Corbett, J. J., J. J. Winebrake, E. H. Green, P. Kasibhatla, **V. Eyring**, and A. Lauer (2007), Mortality from Ship Emissions: A Global Assessment, *Environ. Sci. Technol.*, 41, doi: 10.1021/es071686z.

[EY11]   Schreier, M., A. A. Kokhanovsky, **V. Eyring**, L. Bugliaro, H. Mannstein, B. Mayer, H. Bovensmann, and J. P. Burrows (2006), Impact of ship emissions on the microphysical, optical and radiative properties of marine stratus: a case study, *Atmos. Chem. Phys.*, 6, 4925-4942.

[EY12] Schreier, M., H. Mannstein, **V. Eyring**, and H. Bovensmann (2007), Global ship track distribution and radiative forcing from 1 year of AATSR data, *Geophys. Res. Lett.*, 34, L17814, doi:10.1029/2007GL030664.

Selected Author's References

Dameris, M., V. Grewe, M. Ponater, R. Deckert, **V. Eyring**, F. Mager, S. Matthes, C. Schnadt, A. Stenke, B. Steil, C. Brühl, and M. Giorgetta (2005), Long-term changes and variability in a transient simulation with a chemistry-climate model employing realistic forcings, *Atmos. Chem. Phys.*, 5, 2121-2145.

Eyring, V., N. R. P. Harris, M. Rex, T. G. Shepherd, D. W. Fahey, G. T. Amanatidis, J. Austin, M. P. Chipperfield, M. Dameris, P. M. de F. Forster, A. Gettelman, H. F. Graf, T. Nagashima, P. A. Newman, M. J. Prather, J. A. Pyle, R. J. Salawitch, B. D. Santer, and D. W. Waugh (2004), Comprehensive Summary on the Workshop on "Process-Oriented Validation of Coupled Chemistry-Climate Models", *SPARC Newsletter No. 23*, 5-11.

Eyring, V., D. E. Kinnison, and T. G. Shepherd (2005), Overview of planned coupled chemistry-climate simulations to support upcoming ozone and climate assessments, *SPARC Newsletter No. 25*, 11-17.

Eyring, V., A. Gettelman, N. R. P. Harris, S. Pawson, T. G. Shepherd, N. Butchart, M. P. Chipperfield, M. Dameris, D. W. Fahey, P. M. de F. Forster, P. A. Newman, R. J. Salawitch, B. D. Santer, and D. W. Waugh (2006), Summary of the CCMVal 2005 Workshop on "Process-Oriented Validation of Coupled Chemistry-Climate Models, *SPARC Newsletter No. 26*, p. 28-29.

Eyring, V., A. Gettelman, N. R. P. Harris, S. Pawson, T. G. Shepherd, D. W. Waugh, H. Akiyoshi, N. Butchart, M. P. Chipperfield, M. Dameris, D. W. Fahey, P. M. de F. Forster, P. A. Newman, M. Rex, R. J. Salawitch, and B. D. Santer (2008a), Report on the Third SPARC CCMVal Workshop, *SPARC Newsletter No. 30*, p.17-19, 2008.

Eyring, V., M. P. Chipperfield, M. A. Giorgetta, D. E. Kinnison, E. Manzini, K. Matthes, P. A. Newman, S. Pawson, T. G. Shepherd, and D. W. Waugh (2008b), Overview of the New CCMVal Reference and Sensitivity Simulations in Support of Upcoming Ozone and Climate Assessments and the Planned SPARC CCMVal, *SPARC Newsletter No. 30*, p.20-26, 2008.

Lee, D. S., L. L. Lim, **V. Eyring**, R. Sausen, Ø. Endresen, and H.-L. Behrens (2007), Radiative forcing and temperature response from shipping, In: *Proceedings of the International Conference on Transport*, Atmosphere and Climate (TAC), Oxford, UK, 208-213.

External References

Albrecht, B. A. (1989), Aerosols, cloud microphysics, and fractional cloudiness, Science, 245, 1227-1230.

Anderson, J., J. M. Russell III, S. Solomon, and L. E. Deaver (2000), Halogen Occultation Experiment confirmation of stratospheric chlorine decreases in accordance with the Montreal Protocol, *J. Geophys. Res.*, *105*, 4483-4490.

Austin, J., D. Shindell, S. R. Beagley, C. Brühl, M. Dameris, E. Manzini, T. Nagashima, P. Newman, S. Pawson, G. Pitari, E. Rozanov, C. Schnadt, and T. G. Shepherd (2003), Uncertainties and assessments of chemistry-climate models of the stratosphere, *Atmos. Chem. Phys.*, 3, 1-27.

Austin, J., R. J. Wilson, F. Li, and H. Vömel (2006), Evolution of water vapor concentrations and stratospheric age of air in coupled chemistry-climate model simulations, *J. Atmos. Sci.*, 64 (3), 905–921.

Beirle, S., U. Platt, R. von Glasow, M. Wenig, and T. Wagner (2004), Estimate of nitrogen oxide emissions from shipping by satellite remote sensing, *Geophys. Res. Lett.*, 31, L18102, doi:10.1029/2004GL020312.

Bodeker, G. E., H. Shiona, and H. Eskes (2005), Indicators of Antarctic ozone depletion, *Atmos. Chem. Phys.*, 5, 2603-2615.

Brenninkmeijer, C. A. M., P. Crutzen, F. Boumard, T. Dauer, B. Dix, R. Ebinghaus, D. Filippi, H. Fischer, H. Franke, U. Frieß, J. Heintzenberg, F. Helleis, M. Hermann, H. H. Kock, C. Koeppel, J. Lelieveld, M. Leuenberger, B. G. Martinsson, S. Miemczyk, H. P. Moret, H. N. Nguyen, P. Nyfeler, D. Oram, D. O'Sullivan, S. Penkett, U. Platt, M. Pupek, M. Ramonet, B. Randa, M. Reichelt, T. S. Rhee, J. Rohwer, K. Rosenfeld, D. Scharffe, H. Schlager, U. Schumann, F. Slemr, D. Sprung, P. Stock, R. Thaler, F. Valentino, P. van Velthoven, A. Waibel, A. Wandel, K. Waschitschek, A. Wiedensohler, I. Xueref-Remy, A. Zahn, U. Zech, and H. Ziereis (2007), Civil Aircraft for the Regular Investigation of the atmosphere Based on an Instrumented Container: The new CARIBIC system, *Atmos. Chem. Phys.*, 7, 4953–4976.

Butchart, N., A. A. Scaife, M. Bourqui, J. de Grandpré, S. H. E. Hare, J. Kettleborough, U. Langematz, E. Manzini, F. Sassi, K. Shibata, D. Shindell, and M. Sigmond (2006), Simulations of anthropogenic change in the strength of the Brewer-Dobson circulation, *Clim. Dyn.*, 27, 727-741.

Capaldo, K., J. J. Corbett, P. Kasibhatla, P. S. Fischbeck, and S. N. Pandis (1999), Effects of ship emissions on sulphur cycling and radiative climate forcing over the ocean, *Nature*, 400, 743-746.

Charlton, A. J., and L. M. Polvani (2007), A New Look at Stratospheric Sudden Warmings. Part I: Climatology and Modeling Benchmarks, *J. Climate*, 20, 449–469, doi: 10.1175/JCLI3996.1.

Chen, G., L. G., Huey, M. Trainer, D. Nicks, J. Corbett, T. Ryerson, D. Parrish, J. A. Neuman, J. Nowak, D. Tanner, J. Holloway, C. Brock, J. Crawford, J. R. Olson, A. Sullivan, R. Weber, S. Schauffler, S. Donnelly, E. Atlas, J. Roberts, F. Flocke, G. Hubler, and F. Fehsenfeld (2005), An investigation of the chemistry of ship emission plumes during ITCT 2002, *J. Geophys. Res.*, 110, D10S90, doi:10.1029/2004JD005236.

Chipperfield, M. P., and W. Feng (2003), Comment on: "Stratospheric Ozone Depletion at northern mid-latitudes in the 21st century: The importance of future concentrations of greenhouse gases nitrous oxide and methane", *Geophys. Res. Lett.*, *30*, 1389, doi: 10.1029/2002GL016353.

Chipperfield, M. P., W. Feng, and M. Rex (2005), Arctic ozone loss and climate sensitivity: Updated three-dimensional model study, *Geophys. Res. Lett.*, 32, L11813, doi:10.1029/2005GL022674.

Cohen, A. J., H. R. Anderson, B. Ostro, K. D. Pandey, M. Krzyzanowski, N. Kunzli, K. Gutschmidt, C. A. Pope, I. Romieu, J. M. Samet, and K. R. Smith (2004), Mortality impacts of urban air pollution, In Comparative quantification of health risks: Global and regional burden of disease due to selected major risk factors, Ezzati, M.; Lopez, A. D.; Rodgers, A.; Murray, C. U. J. L., Eds. World Health Organization: Geneva, 2, 1353-1394.

Conover, J. H. (1966), Anomalous Cloud Lines, *J. Atmos. Sci.*, 23, 778-785.

Corbett, J. J., and H. W. Köhler (2003), Updated emissions from ocean shipping, *J. Geophys. Res.*, 108, doi:10.1029/2003JD003751.

Corbett, J. J., and H. W. Köhler (2004), Considering alternative input parameters in an activity-based ship fuel consumption and emis-

sions model: Reply to comment by Øyvind *Endresen et al.* on "Updated emissions from ocean shipping", *J. Geophys. Res.*, 109, D23303, doi:10.1029/2004JD005030.

Corbett, J. J., P. S. Fischbeck, and S. N. Pandis (1999), Global nitrogen and sulphur inventories for oceangoing ships, *J. Geophys. Res.*, 104(3), 3457-3470.

Davis, D. D., G. Grodzinsky, P. Kasibhatla, J. Crawford, G. Chen, S. Liu, A. Bandy, D. Thornton, H. Guan, and S. Sandholm (2001), Impact of ship emissions on marine boundary layer NO_x and SO_2 distributions over the Pacific Basin, *Geophys. Res. Lett.*, 28, 235-238.

Dentener, F., S. Kinne, T. Bond, O. Boucher, J. Cofala, S. Generoso, P. Ginoux, S. Gong, J. J. Hoelzemann, A. Ito, L. Marelli, J. E. Penner, J.-P. Putaud, C. Textor, M. Schulz, G. R. van der Werf, and J. Wilson (2006), Emissions of primary aerosol and precursor gases in the years 2000 and 1750, prescribed data-sets for AeroCom, *Atmos. Chem. Phys.*, 6, 4321-4344.

Derwent, R. G, D. S. Stevenson, R. M. Doherty, W. J. Collins, M. G. Sanderson, C. E. Johnson, J. Cofala, R. Mechler, M. Amann, and F. J. Dentener (2005), The contribution from ship emissions to air quality and acid deposition in Europe, *Ambio*, 34(1), 54-59.

Doney, S. C., N. Mahowald, I. Lima, R. A. Feely, F. T. Mackenzie, J-F. Lamarque, and P. J. Rasch (2007), Impact of anthropogenic atmospheric nitrogen and sulfur deposition on ocean acidification and the inorganic carbon system, *PNAS*, 104(37), 14580–14585.

Douglass, A. R., M. R. Schoeberl, R. S. Stolarski, J. W. Waters, J. M. Russell III, and A. E. Roche (1995), Interhemispheric differences in springtime production of HCl and $ClONO_2$ in the polar vortices, *J. Geophys. Res., 100,* 13,967-13,978.

Douglass, A., R. Stolarski, S. Strahan, and B. Polansky (2006), Sensitivity of Arctic ozone loss to polar stratospheric cloud volume and chlorine and bromine loading in a chemistry and transport model, *Geophys. Res. Lett.*, 33, L17809, doi:10.1029/2006GL026492.

Durkee, P. A., R. E. Chartier, A. Brown, E. J. Trehubenko, S. D. Rogerson, C. Skupniewicz, K. E. Nielsen, S. Platnick, and M. D. King (2000), Composite Ship Track Characteristics, *J. Atmos. Sci.*, 57, 2542-2553.

Egorova, T., E. Rozanov, V. Zubov, E. Manzini, W. Schmutz, and T. Peter (2005), Chemistry-climate model SOCOL: a validation of the present-day climatology, *Atmos. Chem. Phys.*, 5, 1557-1576.

Emmons, L. K., D. A. Hauglustaine, J.-F., Muller, M. A. Carroll, G. P. Brasseur, D. Brunner, J. Staehelin, V. Thouret, and A. Marenco (2000), Data composites of airborne observations of tropospheric ozone and its precursors, *J. Geophys. Res.,* 105, 20,497-20,538.

Endresen, Ø., E. Sørgård , J. K. Sundet, S. B. Dalsøren, I. S. A. Isaksen, T. F. Berglen, and G. Gravir (2003), Emission from international sea transportation and environmental impact, *J. Geophys. Res.,* 108, 4560, doi:10.1029/2002JD002898.

Endresen, Ø., E. Sørgård, J. Bakke, and I. S. A. Isaksen (2004), Substantiation of a lower estimate for the bunker inventory: Comment on "Updated emissions from ocean shipping" by James J. Corbett and Horst W. Koehler, *J. Geophys. Res.,* 109, D23302, doi:10.1029/2004JD004853.

Endresen, Ø., E. Sørgård, H. L. Behrens, P. O. Brett, and I. S. A. Isaksen (2007), A historical reconstruction of ships' fuel consumption and emissions, *J. Geophys. Res.,* 112, D12301, doi:10.1029/2006JD007630.

EPA (Environmental Protection Agency, U.S.A.) (2006), SPECIATE 3.2, profiles of total organic compounds and particulate matter. http://www.epa.gov/ttn/chief/software/speciate/index.html.

European Commission (2002), ENTEC UK Limited Quantification of emissions from ships associated with ship movements between ports in the European Community; FS 13881; European Commission, DG ENV.C1, Rue de la Loi, 200, B-1049: Brussels, Belgium, July 2002.

Fearnresearch (2003), Fearnleys World Bulk Trades 2003, An Analysis of 2002 With 2003 Update, Oslo.

Ferek, R. J., T. Garrett, P. V. Hobbs, S. Strader, D. Johnson, J. P. Taylor, K. Nielsen, A. S. Ackermann, Y. Kogan, Q. Liu, B. A. Albrecht, and D. Babb (2000), Drizzle Suppression in Ship Tracks, *J. Atmos. Sci.,* 57, 2707-2728.

Fioletov, V. E., G. E. Bodeker, A. J. Miller, R. D. McPeters, and R. Stolarski (2002), Global ozone and zonal total ozone variations estimated from ground-based and satellite measurements: 1964-2000, *J. Geophys. Res.,* 107, 4647, doi:10.1029/2001JD001350.

Forster, P., V. Ramaswamy, P. Artaxo, T. Berntsen, R. Betts, D. W. Fahey, J. Haywood, J. Lean, D. C. Lowe, G. Myhre, J. Nganga, R. Prinn, G. Raga, M. Schulz, and R. Van Dorland (2007), Changes in atmospheric constituents and in radiative forcing. In 'Climate Change', Fourth Assessment Report of Working Group I of the Intergovernmental Panel on Climate Change, Cambridge University Press, UK.

Froidevaux, L., N. J. Livesey, W. G. Read, R. J. Salawitch, J. W Waters, B. Drouin, I. A. MacKenzie, H. C. Pumphrey, P. Bernath, C. Boone, R. Nassar, S. Montzka, J. Elkins, D. Cunnold, and D. W. Waugh (2006), Temporal decrease in upper atmospheric chlorine, *Geophys. Res. Lett.,* 33, L23812, doi:10.1029/2006GL027600.

Garcia, R. R., D. R. Marsh, D. E. Kinnison, B. A. Boville, and F. Sassi (2007), Simulation of secular trends in the middle atmosphere, 1950–2003, *J. Geophys. Res.,* 112, D09301, doi:10.1029/2006JD007485.

Hall, T. M., D. W. Waugh, K. A. Boering, and R. A. Plumb (1999), Evaluation of transport in stratospheric models, *J. Geophys. Res.,* 104, 18,815-18,840.

Haywood, J. M., and K. P. Shine (1995), The effect of anthropogenic sulphate and soot aerosol on the clear sky planetary radiation budget, *Geophys. Res. Lett.,* 22(5), 603-606.

Huck, P. E., S. Tilmes, G. E. Bodeker, W. J. Randel, A. J. McDonald, and H. Nakajima (2007), An improved measure of ozone depletion in the Antarctic stratosphere, *J. Geophys. Res.,* 112, D11104, doi:10.1029/2006JD007860.

ICF Consulting (2005), *Best Practices in Preparing Port Emission Inventories: Draft for Review*, Prepared for Office of Policy, Economics and Innovation, United States Environmental Protection Agency: Fairfax, Virginia, p. 39.

IMO (International Maritime Organization) (1998), Regulations for the prevention of air pollution from ships and NO_x technical code, ANNEX VI of MARPOL 73/78, London.

IPCC (Intergovernmental Panel on Climate Change) (2000), Special report on emissions scenarios: a special report of Working Group III of the Intergovernmental Panel on Climate Change, 599 pp., Cambridge University Press, Cambridge, U.K.

ISL (1994), Shipping Statistics Yearbook 1994, Institute of Shipping Economics and Logistics, Bremen, Germany December.

Jöckel, P., R. Sander, A. Kerkweg, H. Tost, and J. Lelieveld (2005), Technical Note: The Modular Earth Submodel System (MESSy) – a new approach towards Earth System Modeling, *Atmos. Chem. Phys.,* 5, 433-444.

Köhler, H. W. (2003), NO_x emissions from oceangoing ships: calculation and evaluation,

Proceedings of the 2003 Spring Technical Conference of the American Society of Automotive Engineers - Internal Combustion Engine Division, ICES2003-689, Salzburg, Austria, 11-14 May.

Kokhanovsky, A. A., V. V. Rozanov, E. P. Zege, H. Bovensmann, and J. P. Burrows (2003), A semi-analytical cloud retrieval algorithm using backscattered radiation in 0.4-2.4 micrometers spectral range, *J. Geophys. Res.*, 108(D1), 4008, 10.1029/2001JD001543.

Lawrence, M. G., and P. J. Crutzen (1999), Influence of NO_x emissions from ships on tropospheric photochemistry and climate, N*ature*, 402, 167-170.

Lemmen, C., M. Dameris, R. Müller, and M. Riese (2006), Chemical ozone loss in a chemistry-climate model from 1960 to 1999, *Geophys. Res. Lett.*, 33 (15), L15820, doi:10.1029/2006GL026939.

Lin, X., M. Trainer, and S. C. Liu (1988), On the nonlinearity of the tropospheric ozone production, *J. Geophys. Res.*, 93(D12), 15879-15888, 10.1029/88JD03750.

Lloyd's Maritime Information System (LMIS) (2002), The Lloyd's Maritime Database (CD-ROM), Lloyd's Register–Fairplay Ltd., London.

Marenco, A., V. Thouret, P. Nédélec, H. Smit, M. Helten, D. Kley, F. Karcher, P. Simon, K. Law, J. Pyle, G. Poschmann, R. Von Wrede, C. Hume, and T. Cook (1998), Measurement of ozone and water vapor by Airbus in-service aircraft: The MOZAIC airborne program, An overview, *J. Geophys. Res.*, 103(D19), 25631-25642, 10.1029/98JD00977.

Mayer, B., and A. Kylling (2005), Technical note: The libRadtran software package for radiative transfer calculations, description and examples of use, *Atmos. Chem. Phys.*, 5, 1855-1877.

Miller, A. J., R. M. Nagatani, L. E. Flynn, S. Kondragunta, E. Beach, R. Stolarski, R. D. McPeters, P. K. Bhartia, M. T. Deland, C. H. Jackman, D. J. Wuebbles, K. O. Putten, and R. P. Cebula (2002), A cohesive total ozone data set from SBUV(/2) satellite system, *J. Geophys. Res.*, *107*, doi:10.1029/2001JD000853.

Montzka, S. A., J. H. Butler, B.D. Hall, D. J. Mondeel, and J. W. Elkins (2003), A decline in tropospheric bromine, *Geophys. Res. Lett.*, 30, 1826, doi:10.1029/2003GL017745.

Mote, P. W., K. H. Rosenlof, M. E. McIntyre, E. S. Carr, J. C. Gille, J. R. Holton, J. S. Kinnersley, H. C. Pumphrey, J. M. Russell III, and J.

W. Waters (1996), An atmospheric tape recorder: The imprint of tropical tropopause temperatures on stratospheric water vapor, *J. Geophys. Res.*, 101, 3989-4006, 10.1029/95JD03422.

Olivier, J. G. J. and J. A. H. W. Peters (1999), International Marine and Aviation Bunker Fuel: Trends, Ranking of Countries and Comparison with National CO_2 Emissions. RIVM.

Olivier, J. G. J., J. A. van Aardenne, F. Dentener, L. Ganzeveld, and J. A. H. W Peters (2005) Recent trends in global greenhouse gas emissions: regional trends and spatial distribution of key sources, In: "Non-CO_2 Greenhouse Gases (NCGG-4)", van Amstel, A. (coord.), 325-330, Millpress, Rotterdam, ISBN 90 5966 043 9.

Park, J. H., M. K. W. Ko, C.H. Jackman, R. A. Plumb, J. A. Kaye, and K. H. Sage (1999), Models and Measurements Intercomparison II. NASA/TM-1999-209554.

Pawson, S., K. Kodera, K. Hamilton, T. G. Shepherd, S. R. Beagley, B. A. Boville, J. D. Farrara, T. D. A. Fairlie, A. Kitoh, W. A. Lahoz, U. Langematz, E. Manzini, D. H. Rind, A. A. Scaife, K. Shibata, P. Simon, R. Swinbank, L. Takacs, R. J. Wilson, J. A. Al-Saadi, M. Amodei, M. Chiba, L. Coy, J. de Grandpré, R. S. Eckman, M. Fiorino, W. L. Grose, H. Koide, J. N. Koshyk, D. Li, J. Lerner, J. D. Mahlman, N. A. McFarlane, C. R. Mechoso, A. Molod, A. O'Neill, R. B. Pierce, W. J. Randel, R. B. Rood, and F. Wu (2000), The GCM-Reality Intercomparison Project for SPARC: Scientific Issues and Initial Results, *Bull. Am. Meteorol. Soc.*, 81, 781-796.

Petry, H., J. Hendricks, M. Mollhoff, E. Lippert, A. Meier, A. Ebel, and R. Sausen (1998), Chemical conversion of subsonic aircraft emissions in the dispersing plume: Calculation of effective emission indices, *J. Geophys. Res.*, 103, 5759 – 5772.

Platnick, S., P. A. Durkee, K. Nielsen, J. P. Taylor, S. C. Tsay, M. D. King, R. J. Ferek, P. V. Hobbs, and J. W. Rottman (2000),The Role of Background Cloud Microphysics in the Radiative Formation of Ship Tracks, *J. Atmos. Sci.*, 57, 2607-2624.

Pope, C. A.; R. T. Burnett, M. J. Thun, E. E. Calle, D. Krewski, K. Ito, and G. D. Thurston (2002), Lung cancer, cardiopulmonary mortality, and long-term exposure to fine particulate air pollution, *JAMA*, 287(9), 1132-1141.

Radke, L. F., J. A. Coakley Jr., and M. D. King (1989), Direct and Remote Sensing Observa-

tions of the Effects of Ships on Clouds, *Science*, 346, 1146-1149.

Rind, D., D. Shindell, P. Lonergan, and N. K. Balachandran (1998), Climate change and the middle atmosphere. Part III: The doubled CO_2 climate revisited, *J. Climate*, *11, 8*76-894.

Roeckner, E., R. Brokopf, M. Esch, M. Giorgetta, S. Hagemann, L. Kornblueh, E. Manzini, U. Schlese, and U. Schulzweida (2006), Sensitivity of Simulated Climate to Horizontal and Vertical Resolution in the ECHAM5 Atmosphere model, *J. Clim.*, 19, 3771-3791.

Rossow, W. B., and R. A. Schiffer (1991), ISCCP Cloud Data Products, *Bull. of American Meteor. Soc.*, 72, 2-20.

Sankey, D., and T. G. Shepherd (2003), Correlations of long-lived chemical species in a middle atmosphere general circulation model, *J. Geophys. Res.*, 108, doi:10.1029/2002JD002799.

Santee, M. L., L. Froidevaux, G. L. Manney, W. G. Read, J. W. Waters, M. P. Chipperfield, A. E. Roche, J. B. Kumer, J. L. Mergenthaler, and J. M. Russell III (1996), Chlorine deactivation in the lower stratospheric polar regions during late winter: Results from UARS, *J. Geophys. Res., 101*, 18,835-18,860.

Santer, B. D., M. F. Wehner, T. M. L. Wigley, R. Sausen, G. A. Meehl, K. E. Taylor, C. Ammann, J. Arblaster, W. M. Washington, J. S. Boyle, and W. Bruggemann (2003a), Contributions of anthropogenic and natural forcing to recent tropopause height changes, *Science*, 301, 479–483.

Santer, B. D., T. M. L. Wigley, G. A. Meehl, M. F. Wehner, C. Mears, M. Schabel, F. J. Wentz, C. Ammann, J. Arblaster, T. Bettge, W. M. Washington, K. E. Taylor, J. S. Boyle, W. Bruggemann, and C. Doutriaux (2003b), Influence of satellite data uncertainties on the detection of externally forced climate change, *Science*, 300, 1280–1284.

Sausen, R., I. S. A. Isaksen, V. Grewe, D. A. Hauglustaine, D. S. Lee, G. Myhre, M. O. Köhler, G. Pitari, U. Schumann, F. Stordal, and C. Zerefos (2005), Aviation radiative forcing in 2000: An update on IPCC (1999), *Meteorol. Z.*, 14, 555-561.

Schlager, H., R. Baumann, M. Lichtenstern, A. Petzold, F. Arnold, M. Speidel, C. Gurk, and H. Fischer (2007), Aircraft-based trace gas measurements in a primary European ship corridor, In: *Proceedings of the International Conference on Transport*, Atmosphere and Climate (TAC), Oxford, UK, 83-88.

SEDAC (Socioeconomic Data and Applications Center) (2007), Gridded Population of the World. In Columbia University.

Seinfeld, J. H., and S. N. Pandis (1998), Atmospheric Chemistry and Physics – From Air Pollution to Climate Change, John Wiley & Sons, Inc., New York.

Shepherd, T.G., and W. J. Randel (2007), Key issues arising from the 2006 WMO/UNEP Ozone Assessment, *SPARC Newsletter No. 29*, 20-22.

Sigmond, M., P.C. Siegmund, E. Manzini, and H. Kelder (2004), A simulation of the separate climate effects of middle atmospheric and tropospheric CO_2 doubling. *J. Climate*, 17, 2352-2367.

Sinha, P., P. V. Hobbs, R. J. Yokelson, T. J. Christian, T. W. Kirchstetter, and R. Bruintjes (2003), Emissions of trace gases and particles from two ships in the southern Atlantic Ocean, *Atmos. Environ.*, 37, 2139-2148.

Skjølsvik, K. O., A. B. Andersen, J. J. Corbett, and J. M. Skjelvik (2000), Study of Greenhouse Gas Emissions from Ships (MEPC 45/8 Report to International Maritime Organization on the outcome of the IMO Study on Greenhouse Gas Emissions from Ships). MARINTEK Sintef Group, Carnegie Mellon University, Center for Economic Analysis, and Det Norske Veritas: Trondheim, Norway.

Song, C. H., G. Chen, S. R. Hanna, J. Crawford, and D. D. Davis (2003), Dispersion and chemical evolution of ship plumes in the marine boundary layer: Investigation of O_3 /NO_y /HO_x chemistry version, *J. Geophys. Res.*, 108, 4143, doi:10.1029/2002JD002216.

Steinbrecht, W., B. Haßler, C. Brühl, M. Dameris, M. A. Giorgetta, V. Grewe, E. Manzini, S. Matthes, C. Schnadt, B. Steil, and P. Winkler (2006a), Interannual variation patterns of total ozone and temperature in observations and model simulations, *Atmos. Chem. Phys.*, 6, 349-374.

Steinbrecht, W., H. Claude, F. Schoenenborn, S. McDermid, T. Leblanc, S. Godin, T. Song, D. P. J. Swart, Y. J. Meijer, G. E. Bodeker, B. J. Connor, N. Kaempfer, K. Hocke, Y. Calisesi, N. Schneider, J. de la Noe, A. D. Parrish, I. S. Boyd, C. Brühl, B. Steil, M. A. Giorgetta, E. Manzini, L. W. Thomason, J. M. Zawodny, M. P. McCormick, J. M. Russell III, P. K. Bhartia, R. S. Stolarski, and S. M. Hollandsworth-Frith (2006b), Long-term evolution of upper stratospheric ozone at selected stations of the Network for the Detection of Stratospheric Change (NDSC), *J. Geophys. Res.*, 111, D10308, doi:10.1029/2005JD006454.

Stevenson, D. S., F. J., Dentener, M. G. Schulz, K. Ellingsen, T. P. C. van Noije, O. Wild, G. Zeng, M. Amann, C. S. Atherton, N. Bell, D. J. Bergmann, I. Bey, T. Butler, J. Cofala, W. J. Collins, R. G. Derwent, R. M. Doherty, J. Drevet, H. J. Eskes, A. M. Fiore, M., Gauss, D. A. Hauglustaine, L. W. Horowitz, I. S. A. Isaksen, M. C. Krol, J.-F. Lamarque, M. G. Lawrence, V. Montanaro, J.-F. Müller, G. Pitari, M. J. Prather, J. A. Pyle, S. Rast, J. M. Rodriguez, M. G. Sanderson, N. H. Savage, D. T. Shindell, S. E. Strahan, K. Sudo, and S. Szopa (2006) Multi-model ensemble simulations of present-day and near-future tropospheric ozone, *J. Geophys. Res.*, 111, D08301, doi:10.1029/2005JD006338.

Stolarski, R. S. and S. Frith (2006), Search for evidence of trend slow-down in the long-term TOMS/SBUV total ozone data record: the importance of instrument drift uncertainty, *Atmos. Chem. Phys.*, 6, 4057–4065.

Stolarski, R. S., A. R. Douglass, S. Steenrod, and S. Pawson (2006), Trends in Stratospheric Ozone: Lessons Learned from a 3D Chemical Transport Model, *J. Atmos. Sci.*, *63*, 1028-1041.

Stopford, M. (1997), Maritime Economics, 2nd ed., Routledge, London.

Struthers, H., K. Kreher, J. Austin, R. Schofield, G. E. Bodeker, P. V. Johnston, H. Shiona, and A. Thomas (2004), Past and future simulations of NO_2 from a coupled chemistry-climate model in comparison with observations, Atmos. Chem. Phys., 4, 2227–2239.Twomey, S., H. B. Howell, T. A. Wojciechowski (1968), Comments on Anomalous cloud lines, *J. Atmos. Sci.*, 25, 333-334.

Thomas, R., R. D. Lauretis, J.-P. Fontelle, N. Hill, N. Kilde, and K. Rypdal (2002), Shipping Activities, Chapter B842, in *EMEP/CORINAIR Emission Inventory Guidebook - October 2002 UPDATE*, edited by K. Lavender, G. Reynolds, A. Webster, and K. Rypdal, European Environment Agency, Copenhagen, Denmark.

Tian, W., and M. P. Chipperfield (2005), A new coupled chemistry–climate model for the stratosphere: The importance of coupling for future O_3-climate predictions, *Quart. J. Roy. Meteor. Soc.*, 131, 281–304.

Times Books (1992), The Times Atlas of the World Comprehensive Edition 9th edn, London.

Twomey, S. (1974), Pollution and the planetary albedo, *Atmosph. Environ.*, 8, 1251-1256.

Twomey, S., H. B. Howell, and T. A. Wojciechowski (1968), Comments on Anomalous cloud lines, *J. Atmos. Sci.*, 25, 333-334.

U.S. Census Bureau International Data Base (2006), IDB Data - IDB Aggregation - Table 94: Midyear Population, by Age and Sex.

U.S. Environmental Protection Agency (2005), Abt Associates BenMap: Environmental Benefits Mapping and Analysis Program, Technical Appendices; Office of Air Quality Planning and Standards, U.S. Environmental Protection Agency: Research Triangle Park, NC, May 2005, p 275.

von Glasow, R., M. G. Lawrence, R. Sander, and P. J. Crutzen (2003), Modeling the chemical effects of ship exhaust in the cloud-free marine boundary layer, *Atmos. Chem. Phys.*, 3, 233–250.

Wang, C., J. J. Corbett, and J. Firestone (2007), Improving Spatial Representation of Global Ship Emission Inventories, *Environ. Sci. Technol.*, DOI: 10.1021/es0700799.

Waugh, D. W., D. B. Considine, and E. L. Fleming (2001), Is Upper Stratospheric Chlorine Decreasing as Expected? *Geophys. Res. Lett.*, *28*, 1187-1190.

Wild, O., M. J. Prather, and H. Akimoto (2001), Indirect long-term global radiative cooling from NO_x emissions, *Geophys. Res. Lett.*, 28(9), 1719-1722.

World Health Organization (WHO) (2004), Revised Global Burden of Disease (GBD) 2002 Estimates: Mortality Data, GBD 2002: Deaths by age, sex and cause for the year 2002.

World Meteorological Organization (WMO)/United Nations Environment Programme (UNEP) (2003), Scientific Assessment of Ozone Depletion: 2002, World Meteorological Organization, Global Ozone Research and Monitoring Project, Report No. 47, Geneva, Switzerland.

World Meteorological Organization (WMO)/United Nations Environment Programme (UNEP) (2007), Scientific Assessment of Ozone Depletion: 2006, World Meteorological Organization, Global Ozone Research and Monitoring Project, Report No. 50, Geneva, Switzerland.